Multilayer graphene deposited by a filtered cathodic vacuum arc

A thesis submitted in fulfilment of the requirements for the degree of Doctor of Philosophy

Daniel Thomas Oldfield

Bachelor of Science (Applied Sciences) (Honours)

RMIT University

School of Science

College of Science, Engineering and Health

RMIT University

November 2017

“My life amounts to no more than one drop in a limitless ocean. Yet what is any ocean, but a multitude of drops?”

— David Mitchell, *Cloud Atlas*

Declaration

I certify that except where due acknowledgement has been made, the work is that of the author alone; the work has not been submitted previously, in whole or in part, to qualify for any other academic award; the content of the thesis is the result of work which has been carried out since the official commencement date of the approved research program; any editorial work, paid or unpaid, carried out by a third party is acknowledged; and, ethics procedures and guidelines have been followed.

I acknowledge the support I have received for my research through the provision of an Australian Government Research Training Program Scholarship.

Daniel Thomas Oldfield

30 January 2018

Acknowledgements

I would like to acknowledge my supervising team (Chi Huynh, Dougal McCulloch, Ludovic Dumee and Steven Hawkins), their guidance has been invaluable. The majority of the scientific research presented in this thesis was conducted at the RMIT Microscopy and Microanalysis Facility (RMMF). I would like to recognise the staff members of the RMMF (Philip Francis, Peter Rummel, Branco Cipreanu, Matthew Field, Chaitali Dekiwadia and Edwin Mayes), all of whom have never hesitated to provide assistance throughout my candidature. My time at RMIT University would not have been as enjoyable without the friendships that I formed with my fellow PhD, post-doctoral and physics staff members. I always looked forward to Monday lunch times with Billy Murdock, Kamron Ley, Nickolas McDougall and Samuel Jackson. I benefited, from evening runs around Princes Park with Cheng Tan, Jan Jeske, Lachlan Shaw, Lan Wang and Maximilian Hanlon. Additionally, I am grateful to those who joined the RMIT staff cycling team. This acknowledgements section would be incomplete without a special mention for Matthew Taylor and Masturina Kracica. Finally I would to thank my family and loved ones for their continual support during my candidature.

Preface

Throughout my candidature I have been provided with a variety of extra-curricular activities. Most notably, I become involved in science communication. At the completion of my doctorate, I will emerge a proud member of the Australian Science Communicators, who are actively involved in the community. I have detailed these activates in the proceeding front matter sections of (1) awards, (2) extra-curricular and (3) science engineering health ambassador. While it may be unusual to include an extracurricular section in a thesis, to leave it out would misrepresent my candidature.

Also detailed in the front matter of this thesis is a list of my publications, which have either appeared in the form of published journal articles, conference papers, presentations, or articles which have been submitted to general science magazines.

Awards

1. Australian Postgraduate Award, Australian Government, 2012
2. CSIRO Industrial Traineeship, CSIRO, 2013
3. Australian Nanotechnology Network (ANN) Scholarship, ANN, 2013.
4. 3 Minute Thesis Competition (3MT) Applied Science Award, 2013
5. 3MT College of Science, Engineering and Health (SEH) Semi-Final Award, 2013
6. 3MT SEH Semi-Final People's Choice Award , 2013
7. 3MT RMIT University Final Award, 2013
8. 3MT RMIT University People's Choice Award, 2013
9. 3MT Public Vote Winner at ACMM Conference, 2016
10. 3MT Competition Winner at ACMM, 2016

Extracurricular

1. 3MT School of Applied Science Competition, 2013
2. 3MT College of Science, Engineering and Health Semi-Final, 2013
3. 3MT RMIT University Final, 2013
4. 3MT Trans-Tasman Final, 2013
5. Triple RRR radio interview, 2013
6. Presented at Science Festival at Parkdale Senior Secondary, 2014
7. Presented at RMIT's My Science Day, 2014
8. Presented at RMIT's Future Students Day, 2014
9. Presented at Careers Advisers Seminar Day, 2015
10. Created the Microscopist Blog, 2015
11. Attended The Walkley Freelance Focus Conference, 2015
12. Contributed to the Uprosa Catalogue, 2015
13. 3MT at Australian Conference Microscopy and Microanalysis, 2016
14. RMIT Scientific Art Exhibition, 2016
15. Presented at Link Festival (Lightning talk), 2016
16. Presented at Link Festival (Panel talk), 2016
17. RMIT Research Microscopy Article, 2016
18. Presented at VXLab demonstration, 2016
19. RMIT Microscopy Screensavers, 2016
20. Published in Ultimate Careers magazine by the Australian Science Channel, 2017
21. Lectured at RMIT's India Summer School, 2017.

Science Engineering Health Ambassador

1. Copperfield College, 2015
2. University High School, 2015
3. St Bernard's College, 2015
4. The Hutchins School, 2015
5. Gisborne Secondary College, 2015
6. Aitken College, 2015
7. Sunbury Downs Secondary College, 2015
8. Beaconhills College, 2016
9. St Joseph's College, 2016
10. St Bernard's College, 2016
11. Hutchins School, 2016
12. St Bernard's College, 2017

Publication/Other

Journal Articles

1. D.T. Oldfield, C.P. Huynh, S.C. Hawkins, J.G. Partridge, D.G. McCulloch. Synthesis of multi-layer graphene films on silica using physical vapour deposition. Carbon, 2017. 123: p. 683-687.
2. K.S. Munir, D.T. Oldfield, and C. Wen, Role of Process Control Agent in the Synthesis of Multi-Walled Carbon Nanotubes Reinforced Titanium Metal Matrix Powder Mixtures. Advanced Engineering Materials, 2015. 18: p. 294-303.
3. D.T. Oldfield, D.G. McCulloch, C.P. Huynh, K. Sears, S.C. Hawkins, Multilayered graphene films prepared at moderate temperatures using energetic physical vapour deposition. Carbon, 2015. 94: p. 378-385.
4. K.S. Munir, M. Qian, Y. Li, D.T. Oldfield, P. Kingshott, D.M. Zhu, C. Wen, Quantitative Analyses of MWCNT-Ti Powder Mixtures using Raman Spectroscopy: The Influence of Milling Parameters on Nanostructural Evolution. Advanced Engineering Materials, 2015. 17: p. 1660-1669.
5. M. Czajka, R.A. Shanks and D.T. Oldfield, Hydrogen Reduced Low-Defect Graphene with Poly(ethylene terephthalate) Composites. Applied Polymer Composites: SI-ICAPM2013, Accepted 13 November 2014.

Conference Papers

1. D.T. Oldfield, C.P. Huynh, S.C. Hawkins, & D.G. McCulloch, Graphene Films Prepared Using Energetic Physical Vapor Deposition. MRS Advances, 2017, 2(2), 117-122.

2. M. Czajka, R. A. Shanks and D.T. Oldfield, Carbon Monoxide Reduced Low-Defect Graphene Nanocomposites with Poly(styrene-b-butadiene-b-styrene) Composites. Antec, Orlando, Florida, USA, 23-25 March 2015.
3. M. Czajka, R.A. Shanks and D.T. Oldfield, CO-Reduced Low-Defect graphene in Poly(styrene-b-butadiene-b-styrene) Composites. Antec, Orlando, Florida, USA, 23-25 March 2015.
4. M. Czajka, R. A. Shanks and D.T. Oldfield, Low Defect CO-Reduced graphene in Poly(styrene-b-butadiene-b-styrene) Composites. Nanolytica, Melbourne, Australia, 9 February 2015.
5. M. Czajka, R. A. Shanks and D.T. Oldfield, Poly(ethylene terephthalate) Composites with Low-defect Hydrogen-reduced Graphene. International Conference on Advanced Polymeric Materials, Kerala, India, 11-13 October 2013 p.68
6. M. Czajka, R. A. Shanks and D.T. Oldfield, Low Defect Hydrogen Reduced Graphene in Poly(ethylene terephthalate) Composites. OzCarbon, Melbourne, Australia, 1-3 December 2013.

Conference Presentations

1. D.T. Oldfield, D.G. McCulloch, C.P. Huynh and S.C. Hawkins, Cold synthesis routes of graphene films during device fabrication via physical vapour deposition. CSIRO Advanced Materials, Melbourne, Australia, 28 – 30 April 2014.
2. D.T. Oldfield, D.G. McCulloch, C.P. Huynh, K. Sears and S.C. Hawkins, Multilayered graphene films prepared at moderate temperatures using energetic physical vapour deposition. Recent Progress in Graphene (and Two-dimensional Materials) Research, Lorne, Australia, 25 – 29 October 2015.

3. D.T. Oldfield, D.G. McCulloch, C.P. Huynh, K. Sears and S.C. Hawkins, Multilayered graphene prepared at moderate temperatures using energetic physical vapour deposition. Australian Conference on Microscopy and Microanalysis, Melbourne, Australia, 31 – 4 February.
4. D.T. Oldfield, The pencil, fifty shades of graphene. Australian Conference on Microscopy and Microanalysis, Melbourne, Australia, 31 – 4 February.

Conference Posters

1. D.T. Oldfield, D.G. McCulloch, C.P. Huynh and S.C. Hawkins, Graphene films prepared using physical vapour deposition. OzCarbon, Melbourne, Australia, 1 – 3 December 2013.
2. D.T. Oldfield, D.G. McCulloch, C.P. Huynh and S.C. Hawkins, Graphene synthesis using filtered cathodic vacuum arc. Australian Conference on Microscopy and Microanalysis/International Conference on Nanoscience and Nanotechnology, Adelaide, Melbourne, 2 - 6 February 2014.

Science articles

1. D.T. Oldfield, The role of art in science. Australian Microscopy and Microanalysis Newsletter, Issue 121, 1 March 2014.
2. D.T. Oldfield, The lab rat amongst the journalists. SCOPE, 1 July 2015.

Contents

Abstract

Graphene is a single layer of sp^2 bonded carbon atoms; it was first practically isolated from graphite in 2004 via mechanical exfoliation and has since attracted much attention due to its remarkable properties. However, to replace existing materials in electronic and other devices, efficient methods are needed to synthesize high quality graphene directly on a range of substrates, including thermally sensitive surfaces. Although there are several methods capable of producing graphene; each technique has weaknesses, which limit their applicability.

This thesis demonstrated, for the first time, that it is possible to energetically deposit graphene films onto copper foil using physical vapour deposition (PVD) in a filtered cathodic vacuum arc (FCVA) deposition system. Raman spectroscopy and transmission electron microscopy (TEM) revealed that the graphene films were of uniform thickness of ~10 layers and that these can be deposited at moderate temperatures of 750 °C. The resulting films, which can be prepared at high deposition rates, were comparable in quality to graphene films grown at 1050 °C using conventional chemical vapour deposition (CVD). This difference in growth temperature is attributed to dynamic annealing which occurs as film grows from the energetic carbon flux present in FCVA.

The effect of processing gasses during the growth of FCVA deposited carbon films on copper foil was explored. It was shown that neither the presence of hydrogen or methane had a favourable influence on the growth of FCVA deposited graphene, with both leading to increased defects through ion bombardment. The growth of graphene by CVD requires the removal of the native oxide layer on the copper substrate aided by the presence of

hydrogen gas. It was found that the energetic C^+ ions in FCVA remove the oxide layer by sputtering without the need for any hydrogen gas.

This thesis also explored the deposition of graphene on other substrates. In the case of nickel substrates, it was found that graphene films can also be prepared at moderate substrate temperatures. Much higher carbon doses were required to produce graphene films on nickel due to the solubility of carbon in this substrate. This indicates that the growth mode differs between substrates as observed in CVD grown graphene. The films deposited onto nickel were also found not to be uniform in thickness, demonstrating that the grain structure of the nickel substrate influenced the growth of graphene layers.

The growth of a film by CVD is dependent on a reaction between the substrate and the processing gas. In PVD, a film can be energetically deposited onto almost any type of substrate. Hence, the possibility of depositing graphene onto hexagonal boron nitride (BN), yttrium stabilised zirconia (YSZ) and silicon carbide (SiC) was explored. It was found that carbon films deposited at 750 ^{o}C on BN adopted a graphene microstructure. However, no evidence of graphene was found when films were deposited at 750 ^{o}C on YSC and SiC.

Interest in the properties of junctions between semiconductor materials and carbon allotropes is growing. Carbon films with high sp^2 fractions were energetically deposited onto copper template-layers. These copper template-layers were subsequently sacrificially etched to leave carbon films supported directly on either silicon or silica. On silicon, ordered growth was inhibited by the formation of copper silicide. However, on silica, large areas of ~ 10 graphene layers were formed with orientation parallel to the substrate. Both the copper template-layers and the carbon films were energetically deposited in the same FCVA deposition system. The energetic deposition process provides dense, high quality <111>

copper and conditions suitable for producing graphene layers at lower growth temperatures than those required for conventional CVD grown graphene.

1 Introduction

This chapter provides the background to this thesis, including the motivations and aims. An outline of the structure of the thesis is also provided.

1.1 Materials in history

The history of human technological advancement has been dominated by a relatively small range of materials: stone, wood, iron, copper, bronze, steel, aluminium, plastic and silicon. The genesis of each new individual material throughout history has heralded a technology breakthrough which has allowed us to reach for things which were once impossible. With stone tools we hunted fearsome prey. On wooden boats we traversed the globe in search of new lands. The twentieth century was a time of unprecedented advancement in materials. In the 1900s we developed steel, which gave rise to sky scrapers and modern cities. During the 1950s silicon based electronics were invented and subsequently gave rise to the computer. Man left earth in the 1960s on the back of an aluminium space craft. The development of plastics and carbon fibre composites in the 1980s and early 2000s led to light weight building materials with properties superior to steel. Of these materials which have been listed, perhaps silicon has had the most profound influence on human society. Today the use of silicon in electronic devices has totally revolutionised the way that society functions.

Despite the technological advances that each material has enabled, there are limitations. For examples, metals are generally conductive but not transparent, while plastics can be transparent but are generally poor conductors. Thus scientists continue to conduct research in search of new materials which could potentially further innovate the way that we live.

In 2004 scientists, Kostya Novoselov and his supervisor Andre Geim first isolated a material called graphene using mechanical exfoliation. Up until then scientists knew that a one atom thick, two-dimensional (2D) crystal of carbon atoms existed, however no-one had ever successfully extracted it from graphite. The carbon atoms in a graphene sheet are sp^2 bonded together in a hexagonal honeycomb lattice. The discovery of graphene, earned both Kostya Novoselov and Andre Geim the 2010 noble prize for physics. Graphene has a range of remarkable properties, which make it an ideal candidate for a variety of applications.

The isolation of graphene sparked research into many other 2D materials, some of which have been exfoliated from bulk materials. These other 2D materials include boron nitride [1], niobium disulfide [2], molybdenum disulfide [3-5], fluorographene, tungsten disulfide [6], bismuth selenide [7] and black phosphorus [8]. As these 2D materials all have promising physical and electronic properties [9, 10], several research groups are investigating layering different 2D materials in order to produce high performance devices.

1.2 The properties of graphene

Since graphene was discovered it has attracted the attention of the broader scientific community due to its remarkable properties [11, 12]. First it should be noted that in an ideal graphene sheet free of defects, electrons behave like massless Dirac-Fermions [12]. This means that the electrons travel through the carbon lattice at relativistic speeds. Therefore it is not surprising that graphene has a mobility of 120 000 $cm^2V^{-1}S^{-1}$ at room temperature [13], which is higher than any known semiconductor. Even higher values for mobility (200 000 $cm^2V^{-1}S^{-1}$) have been recorded for graphene suspended in liquid [14]. Graphene also has a low optical absorbance 2.3% absorbance per layer over a 400 – 7000 nm range [15]. Additionally a suspended single layer of graphene has been shown to have a

thermal conductivity of 5.3 kW/mK [16]. Mechanically, graphene has a tensile strength of 130 GPa and a young's modulus of 1 TPa [17].

1.3 Potential applications for graphene

The outstanding properties of graphene make it a potential candidate for a range of applications as outlined below.

1.3.1 Batteries:

As the demand for electric powered vehicles grows, the demand for better battery technology also grows. Furthermore countries around the globe, like the Australian Government, are committed to increasing the production of electricity from renewable resources. With the earth's climate delivering an intermittent energy supply, it is important to carefully consider how to store and distribute energy. Battery technology is an important part in the solution to storing power, from intermittent energy sources.

Lithium (Li) ion batteries, which were first introduced into the market in 1991 by Sony [18], are todays leading commercially available battery technology. Today Li ion batteries are used in a range of applications including electric cars and for the storage of renewable energy. The key parameters for Li ion batteries include the energy and power density, cyclability, rate capability, safety and dependence from temperature and cost of production [19]. The cathode material is the second most heaviest and expensive material in Li ion battery. The conductivity and electro chemical properties of the cathode material can be tailored by doping, modifying the pore size and shape of the cathode material [20, 21]. Currently common cathode materials include carbon black, carbon coatings [20, 21], carbon nanotubes [22, 23] and other materials. Recently, scientists have been exploring the potential for graphene as a conducting material in the cathode with promising results [24].

Graphene is a promising replacement for other carbon materials in Li ion battery cathodes for the following reasons. Conventional carbon materials such as carbon black are relatively poor conductors when compared against more crystalline forms of carbon such as graphene. For carbon black, only the outer surface of the material is in contact with the active material. Hence, only the outer surface of the carbon black is able to conduct electricity [25]. Thus carbon materials with larger surface/mass ratios are highly desirable. Graphene has a very large surface to mass ratio and has one of the highest electron conductivities every recorded [26]. Therefore graphene could be ideal conducting additive in Li ion battery cathodes.

1.3.2 Optoelectronics

Optoelectronics is a branch of technology concerned with the combination of electronics and light. Optoelectronic devices exploit the photoelectric, photovoltaic, photoconductivity or stimulated emission in order to source, detect and control light. In this context, light often includes the invisible forms of radiation such as gamma rays, X-rays, ultraviolet and infrared, in addition to visible light. Optoelectronic devices, include but are not limited to photodiodes (including solar cells), phototransistors, photomultipliers, optoisolators, integrated optical circuit (IOC) elements, photoresistors and light-emitting diodes or LEDs.

Traditionally indium tin oxide (ITO) and fluorine tin oxide (FTO) have been used as window electrodes in optoelectronic devices. However there are several drawbacks with these materials. Indium is considered to be a rare metal, with some people predicting known reserves of indium to be depleted within the next 10 to 20 years. Both ITO and FTO are unstable in presence of an acid or base. Furthermore, they are both susceptible to ion diffusion into polymer layers [27]. Additionally they have a limited transparency in the near

infrared region. Finally, FTO can suffer from current leakage caused by structural defects. Because of these limitations for ITO and FTO, scientists are searching for novel electrode materials with good stability, high transparency and excellent conductivity which can improve the performance of optoelectronics [28].

Graphene has the potential to make a great window electrode because it is made from cheap and abundant carbon resources (graphite oxide) and is produced by a simple fabrication process (exfoliated graphite oxide, followed by thermal reduction) [29]. Furthermore the exfoliated graphene has a whole host of desirable traits. Graphene has excellent conductivity, is transparent in the visible and near-infrared regions, is atomically smooth, the wettability can be tuned, is chemically and thermally stable, can be transferred between substrates and is flexible [29]. The properties make graphene a desirable material for window electrodes in solar cells and other optoelectrodes.

In particular the flexibility of graphene is exciting, as it allows for the production of flexible window electrodes. Traditionally solar cells made from doped silicon are hard and ridged. Organic solar cells which incorporated a graphene window electrode are flexible. Because of the flexible nature of these solar cells, they can be made using a printer. This drastically brings down the cost of production and means that one day you could print your own solar cells at home.

1.3.3 Filtration of water

In the coming decade, the lack of clean water is a formidable challenge because of urbanisation, rapid population growth, extended droughts and fast growing demands [30]. In order to address the issue of water security scientists have investigated filtration and desalination of water. Historically methods used to filter and desalinate underground and

sea water have been expensive. Methods to clean water include, ion exchange, reverse osmosis, and distillation [31]. These methods are not great as they can self-contaminate, they require a lot of power, need a lot of resources; thus these methods are economically unfavourable.

Hence, a method which can purify and desalinate which is cheap, energy efficient and does not self-contaminate is required. Nanotechnology has resulted in new materials which could be potentially used for water purification and could result in a cheap and energy efficient method. For example, scientists have explored the use of carbon nanotube membranes and zeolite structures for the purification of water [32, 33]. Unfortunately carbon nanotubes, were shown to have a low salt rejection, whilst zeolites where shown to have a low water permeability.

Due to the short comings in the nanomaterial's outlined above, the search for the perfect material continues. Graphene has been shown to have a salt rejection and water permeability; it could potentially outperform the best desalination techniques. Furthermore, due to graphene's high thermal and electrical conductivity as well as hard structure, graphene could be a suitable candidate for water purification. Nanoporous graphene has been shown to perform exceptionally well. The advantages of a nanoporous graphene membrane include: it can be used in low pressures and it is more power efficient, and by modifying the size of the pores in the membrane, you can control which minerals are filtered out of the water. Note that by adding pores into the graphene sheet, the mechanical properties can be affected.

1.3.4 Nano electronics

Perhaps the most promising application area for graphene is in electronics. The outstanding properties of 2D materials such as graphene, hold great promise to be incorporated in conventional electronics (as discussed previously (batteries/solar cells)) but could also be used in the emerging field of nanotechnology. Currently a range of 2D materials are available which fall into different categories: conductors, semiconductors, insulators. Flexible nanoelectronics will probably benefit the most in the short term from 2D materials. 2D materials have unique device physics and device mechanics which remain active on soft polymeric or plastic substrates after being transferred [34, 35]. It is hoped that the construction of nanoelectrons from 2D materials will enable large area high performance electronic devices. Up until now flexible electronics has been a niche area of technology with only few items being flexible, such as radio frequency identification tags, and sensors. It is likely that with the advent of 2D materials we will see the development of flexible electronics like integrated nano systems, which preform similar functions to today's silicon devices counter parts [36].

1.4 Graphene synthesis

In order to replace existing materials in electronic and other devices, efficient methods are needed to synthesize high quality graphene directly on a range of substrates, including thermally sensitive surfaces. In this section, a summary of the existing techniques which are used to produce graphene is provided (see *Figure 1*). Each method for graphene production has individual strengths and weakness. The different production methods also produce varying quantities and qualities of graphene.

There are reports showing attempts to synthesis graphene as early as 1975 [37]. B. Lang et al. grew a combination of mono and multi-layered graphite using thermal decomposition on Pt substrates. Due to the variation in the number of sheets and the subsequent electrical properties of the carbon films, this method was not widely studied by the broader scientific community. Further attempts to synthesis graphene occurred in 1999 [38] and 2001 [39], however it is Novoselov et al. who is commonly credited with the successful isolation of graphene in 2004. Novoselov et al. method of exfoliation showed the first consistently repeatable method for producing graphene, hence revealing the unique electrical properties of graphene.

A range of methods are currently being employed to produce graphene, such as the unzipping of nanotubes [40, 41], sonication of thermally expanded graphite (as graphene oxide) [42-44], epitaxial growth on silicon carbide [45, 46], exfoliation [47, 48], CVD [49, 50] and plasma enhanced CVD (PECVD) [51]. CVD is considered to produce the highest quality large-area sheets of graphene at the lowest cost [52]. However CVD is very sensitive to growth conditions (eg, gas concentration, deposition time, temperature and substrate) [53, 54] and a transfer process is required post-deposition in order to relocate graphene to a desirable substrate [55, 56].

A less studied technique to produce graphene is physical vapour deposition (PVD). Despite it being widely used to produce carbon materials such as ‘tetrahedral amorphous carbon’ [57, 58], ‘diamond like carbon’ [59] and a range of nanostructured graphitic materials [60], there is relatively little published on graphene synthesis [61-63]. These previous works on graphene only consider nickel substrates and employed a post deposition annealing process in order to obtain graphene. PVD is both controllable and scalable and is already used in

industry to create coatings with specific hard wearing, corrosion resistant, optical and biocompatible properties [64]. The subsequent sections of this chapter will now focus on the different methods used to produce graphene and the potential to physically deposit graphene using PVD in a filtered cathodic vacuum arc (FCVA) system.

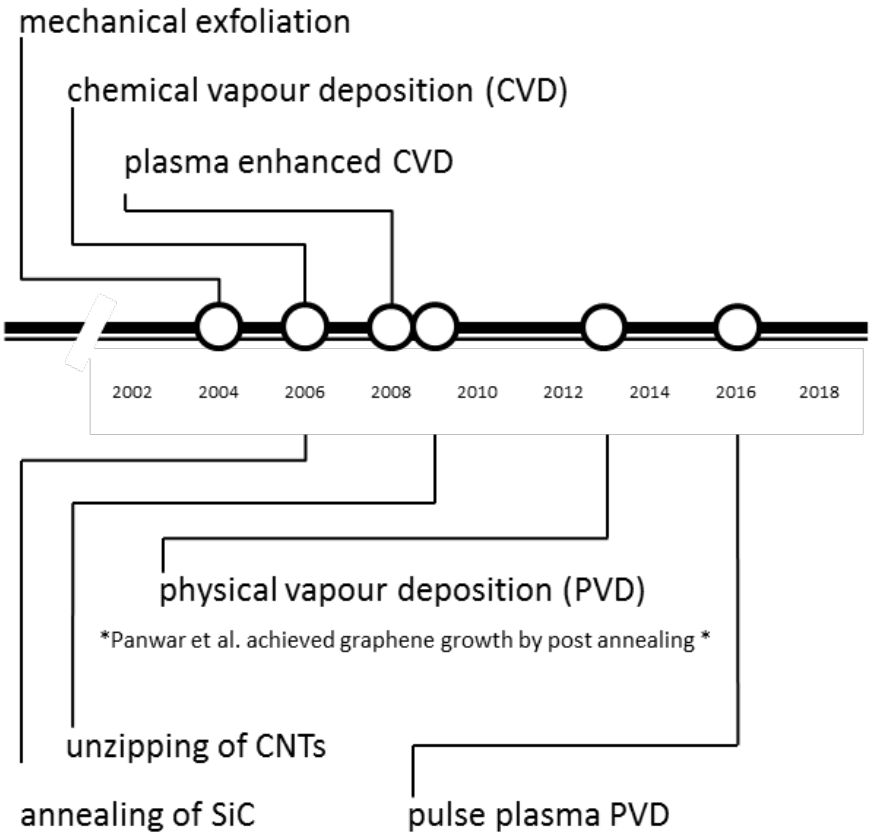

Figure 1: Timeline for new synthesis techniques for the production of graphene [11, 40, 51, 61, 65-69].

1.4.1 Exfoliation and cleavage

Graphite is comprised of a stack of graphene sheets bonded together by Van der Waal forces. Therefore, in principle, if the Van der Waal forces between layers could be broken than graphite could be separated into its individual sheets. Exfoliation and cleavage using mechanical or chemical energy have been used to isolate single sheets of graphene from

graphite. One of the first attempts to exfoliate and cleave graphite is documented in a paper by Viculis et al. in 2003 [70]. In this study, the group used an exothermic reaction between intercalated potassium and graphite; and then exfoliated with ethanol in order to explore whether scrolling of graphite could lead to nanotube-like structures. The resulting carbon nanoscrolls were found to occupy a volume six times greater than that of the original sample of graphite. Furthermore, transmission electron microscopy (TEM) analysis showed that the exfoliated carbon nanoscrolls consisted of 40 ± 15 layers. In this paper, the author noted that carbon nanoscrolls could be used to adsorb and retain solvents in a similar manner to activated carbons and therefore could potentially be used for hydrogen storage. While unsuccessful at separating single sheets of graphene, this process showed that it was plausible to separate layers of graphene from graphite through exfoliation.

In 2004, in perhaps one of the most heavily cited papers in recent times, Novoselov et al. refined the technique of exfoliating graphite [11]. Graphene films were prepared by mechanical exfoliation of highly orient pyrolytic graphite (HOPG). This was achieved by etching the HOPG in oxygen plasma to form mesas which were 5 μm deep with an area varying between 0.4 to 4 mm^2. Photoresist was baked onto the back of the mesas and scotch tape was used to peel of layers off graphite. Acetone was used to release single to few layer sheets of graphene from the photoresist. The films were then transferred to a silicon substrate. Since then this method has been used to isolated other 2D materials, including single layers of boron nitride and molybdenum disulphide [71]. While mechanical techniques such as exfoliation and cleavage are capable of producing high quality sheets of graphene, these methods are unsuitable for large scale production. Both methods produce uneven films, are labour intensive and are only capable of producing millimetre sized films.

1.4.2 Thermal chemical vapour deposition

In order to address some of the concerns surrounding the production of graphene by mechanical exfoliation, several groups investigated the potential to produce graphene by CVD. The first report on CVD synthesis of graphene was by Somani et al in 2006 [65]. Realising that graphene could bring about an electronic revolution similar to conducting polymers and conducting nanotubes, this group set about looking for a new technique to synthesize graphene which was economical and reproducible. In this work graphene was grown on nickel foil through a two-step process. In a quartz tube, camphor was evaporated at 180 ^{o}C and then pyrolysed in a second chamber at temperatures between 700 and 800 ^{o}C, with an argon carrier gas. The sample was then allowed to cool to room temperature. Upon cooling to room temperature the formation of graphene on the nickel foil was observed. The carbon material was collected by scraping the nickel foil with a sharp blade and was imaged with high resolution TEM. The collected sample was identified as being comprised of 35 sheets. Being the first study of its kind, it opened up a new processing route for the synthesis of graphene, albeit with several issue remaining to be solved, such as controlling the number of layers and minimizing the number of defects due to the transfer of graphene.

Other groups also perused the use of CVD to grow graphene films, often citing that that mechanical cleaved graphene samples were too small for industrial application and only suitable for scientific studies. It was believed that CVD could enable the growth of extended films practical applications. However, studies up to that point had been unsuccessful in producing few layer graphene, instead growing thick films of graphite. A paper published in the following year by Obraztsov et al. [72], showed that it is possible to grow few layer graphene in the order of 1 to 2 nm thick on nickel foil. A precursor gas mixture of hydrogen

(H_2) and methane (CH_4) at a ratio of 92 to 8 with a total gas pressure of 80 Torr activated by a DC discharge, all contained in a glass furnace held at 950 ^{o}C, was employed. Scanning electron microscopy (SEM) analysis of the resulting film showed smooth region graphene interrupted by ridges, at the time the formation of ridges in the carbon foil were proposed to be due the different thermal expansion coefficients of nickel and graphite. In this paper the growth mechanism of the film was attributed to heteroepitaxy.

A study published in 2008 which also used a mixture of CH_4 to H_2 by Yu et al. managed to reduce the number of graphene to 3 to 4 layers of graphene [73]. This paper highlighted that controlling the cooling rate is critical for producing graphene films on nickel which are less than 10 layers. The study showed that moderate cooling rates of 10 °C/s were ideal for the formation of graphene and that cooling faster than 20 °C/s or slower than 0.1 °C/s was detrimental. The difference in the quality of the graphene due to the change in the cooling rate was attributed to the segregation of carbon from the nickel substrate. At the slowest cooling rate the carbon of 0.1 °C/s, no carbon peak was observed in the Raman spectrum. The lack of a carbon in the Raman spectrum was justified saying that this indicated that few carbon atoms segregated to the surface and that most of the atoms had diffused into the bulk of the nickel substrate.

The Raman spectrum of the carbon film grown with a medium cooling rate displayed two peaks located at 1583 and 2704 cm^{-1}, commonly referred to as the G and 2D bands. The intensity of the 2D peak to the G peak for this film indicated the growth of few layer graphene. In contrast the Raman spectrum for the film grown with the fastest cooling rate had G peak much greater than the 2D and displayed a D peak located at 1360 cm^{-1}. The change in the Raman spectrum as a result of the cooling rate, was explained to indicated

that the faster cooling rate prevented the migration of carbon from the surface in the bulk of the substrate and thus enhanced the migration of carbon to the surface of the nickel substrate. The appearance of the D peak in the Raman spectrum for this film grown with the faster cooling rate demonstrated that the segregated carbon had an insufficient time to form a crystalline state with few defects.

Having understood how to control the precipitation of graphene in nickel, the problem remained on how to grow large areas of graphene with constant number of sheets. Published in 2009 by Reina et al. [74], another study showed that graphene films could be grown on polycrystalline nickel films with CVD. Nickel films, 500 nm thick, were e-beam evaporated onto SiO_2/Si substrates. The nickel films were thermal annealed before the growth of graphene. The annealing created single-crystalline grains of sizes between 1 µm to 20 µm. It was noted that the surface of grains were atomically flat. A mixture of H_2 and CH_4 was used to grow graphene on the nickel grains. After cooling the sample, the graphene film was coated in poly(methyl methacrylate) (PMMA) and the nickel film was etch with hydrogen chloride (HCl). The graphene film was transferred to a range of different substrates and the PMMA was removed. Observation made before and after the transfer of the graphene film showed that the microstructure of the transferred graphene film closely resembled that of the nickel film. The location of large nickel grains corresponded the site of large uniform graphene. Thus the group came to the conclusion that the individual nickel grains affect the thickness of graphene films. Furthermore, their observations suggested that multilayer grown graphene commonly occurred at grain boundaries. This was justified, stating that at a grain boundaries there are potential nucleation sites.

Another metal of interest is copper. In a study by Li et al., large areas of graphene up to 1 cm^2 were grown on copper foil at 1000 ^oC using a mixture of CH_4 and H_2. The growth of graphene on cupper is considered to be self-limiting due to the low solubility of carbon in copper. Unlike the growth of graphene on nickel through precipitation, it is understood that graphene grows on copper via a surface catalytic effect [75].

CVD has proven to be capable of producing large quantities of high quality graphene, however there are several drawbacks. Conventional CVD entails high temperatures (~1000 °C), the method is substrate dependent, it is not compatible with complementary metal oxide semiconductor (CMOS) fabrication, and requires a transfer process in order to relocate graphene to a desirable substrate.

1.4.3 Plasma enhanced chemical vapour deposition

In order to keep producing large quantities of high quality graphene but hopefully at lower growth temperatures, scientists have explored PECVD. One of the earliest studies on PECVD for nanostructured graphite was by Obraztsov et al., which managed to grow nanostructured graphite onions [72]. The group studied the effects of gas composition and pressure on the carbon films grown in CVD reactor. The gas mixture had a pressure between 10 to 150 Torr with the CH_4 concentration varying between 0 to 25%. Several different types of substrates were used, for example Si, Ni, W and Mo. The substrates were located on the water cooled anode. The group found that graphite-like films formed at temperatures between 1050 – 1100 ^oC with a CH_4 gas concentration between 5 – 10 % at a total gas pressure between 60 – 100 Torr [76].

Future studies further explored the growth of carbon films using PECVD. In two studies published by Wang et al. in 2004 vertically orientated few layer graphene grown by PECVD

was reported [77]. The growth of graphene was achieved on variety of substrates, Si, W, Mo, Zr, Ti, Hf, Nb, Ta, Cr, stainless steel, SiO_2 and Al_2O_3. The sheets were produced with H_2 and CH_4 at a total pressure of 12 Pa. The menthene concentration varied between 5 to 100% and a power 900 W and a temperature of 680 ^oC was employed.

The mechanism for growth of graphene sheets orientated perpendicular to the substrate was investigated in a reported by Zhu et al. The study stated that the graphene sheets were a product of the surface diffusion of carbon from the precursor gas and the etching of atomic hydrogen, similar to what had already been observed for CVD. The study went on to further explain the vertical orientation of the graphene sheets. Films were grown over deposition times varying from 30 second to 8 minutes, in order to investigate the nucleation of the graphene films. The study showed that between the 2 to 4 minute period the growth is planar to the substrate, with film thickness growing up to 15 nm. Eventually enough force develops at the grain boundary of the substrate to cause the leading of the top sheet of graphene to curl up. After the top layer has curled up it becomes aligned with the plasma sheath. As a result of high mobility of the carbon ions, and the induced polarization of the graphene, the sheets of graphene grow higher rather than thicker. Vertical orientated graphene sheets are ideal for sensing applications as the entire surface of the graphene sheet is accessible [78].

PECVD is advantageous over conventional CVD as it requires slightly lower growth temperatures. However, PECVD is still substrate dependent, and requires a transfer process in order to relocate graphene to a desirable substrate.

1.4.4 Cold wall chemical vapour deposition

As stated previously, graphene is commonly grown by thermal CVD, which is known as a hot wall system. The output of this system is limited by the long heating and cooling times, which can take several hours. Therefore cold wall CVD is becoming increasing popular. Cold wall CVD selectively heats the catalytic substrate. There are several types of cold wall CVD systems which can be employed to grow graphene such as magnetic induction heating CVD [79], rapid thermal annealing CVD using halogen lamp heating [80], Joule heating CVD [81], and resistively heated stage CVD [82]. A study by Bointon et al. showed that the growth of graphene using resistive-heating cold-wall CVD is 100 times faster and 99% lower cost than standard CVD [83]. The drawback to this technique is that it still substrate dependent and requires high local temperatures of ~1000 ^{o}C. There is also no strong evidence that cold walled CVD grown graphene is of significantly different quality to that grown using conventional CVD.

1.4.5 Thermal decomposition

Graphene has also been grown through the decomposition of several types of materials. Graphene can be grown on by the thermal decomposition of Si on 6H-SiC at temperatures around 1250 to 1450 ^{o}C. This technique is attractive for the semiconductor industry. Albeit some issues remain around the repeatability, the of size graphene sheet and the number of layers. The decomposition of other metals such as Ru [84], Ir, Ni, Co, Pt which had previously absorbed carbon has also been used to grown graphene. The downside to this method is that it requires extremely high growth temperatures.

1.4.6 Un-zipping of carbon nanotubes

Graphene can also be grown by opening multi walled nanotubes as shown in a study by Cano-Ma´rquez [85]. The paper claimed that multi-walled nanotubes MWNTs can be opened longitudinally by intercalation of lithium and ammonia followed by exfoliation. The process resulted in the creation of multilayered flat graphitic structures, partially open MWNTs and graphene. Evidently, this method only produces very small sheets of graphene.

1.4.7 Pulsed laser deposition

Pulsed laser deposition (PLD) can be used to grow graphene. Graphene is deposited through the ablation of particles/ions. The high kinetic energy of the particles allows for the deposition of graphene at lower growth temperatures when compared to other techniques. Studies have shown that is possible to grow graphene onto a range of substrates using PLD [86, 87]. In fact a study by Kumar et al. demonstrates that it is possible to deposit multilayer graphene on silica by PLD without the need for a catalyst at 700 ^{o}C [88]. The ability to deposit graphene directly onto silica is a promising result. However, it should be not that the grown under these conditions is highly defective.

1.5 Physical vapour deposition

As stated above, there are limitations in current graphene synthesis methods. Exfoliation produces high quality graphene but is unsuitable for large scale production. Both CVD and PECVD produce large quantities of high quality graphene however both methods are substrate dependent, and requires a transfer process in order to relocate graphene to a desirable substrate. Thermal decomposition only produces small amount of graphene and requires extremely high growth temperatures.

Hence, this study seeks to find out if graphene can be grown by PVD in a FCVA system. PVD allows the deposition of films at room temperature, from a pure carbon source of ions. Films produced by PVD are commonly used to improve hardness, wear resistance and oxidation resistance; such films are used in a variety of commercial applications: aerospace, automotive, medical instruments, cutting tools and firearms. Despite PVD being widely used to produce carbon materials such as tetrahedral amorphous carbon [57, 58], diamond like carbon [59] and a range of nanostructured graphitic materials [60], there is relatively little published on graphene synthesis.

Previous to this current study, the only published work demonstrated that is possible to grow graphene by annealing (750 and 800 °C) amorphous carbon (a-C) film, approximately between 3 to 6 nm on nickel films grown on SiO_2/Si substrates [61-63]. The films were allowed to cool naturally in vacuum to room temperature and underwent a phase change from a-C to graphene. Field effect transistor (FET) where made from the PVD fabricated graphene. The transmittance, sheet resistance and mobility of graphene films are in the range of 85.5–89.3%, 540–720 Ω/□ and ~725 cm^2 V^{-1} s^{-1}, respectively. The graphene derived from a-C films of 3 nm thickness showed minimum sheet resistance, maximum transmittance accompanied with the high mobility of FET. These previous works only considered nickel growth surfaces and involved the conversion of a carbon film using annealing. It remains a challenge to deposit graphene directly using a PVD technique.

1.6 Aims

The aims of this research were to:

- Determine whether it is possible to deposit graphene using the PVD technique FCVA.

- Investigate what substrate types can be used to successfully synthesize graphene using PVD.

- Explore the role of important deposition parameters such as temperature, landing energy and hydrogen background gas on the quality of the graphene.

- Develop a new efficient graphene transfer method by depositing any required underlying growth material and graphene in the same thin film deposition system.

1.7 Outline for thesis

This thesis is broken into the following sections:

Chapter 2 starts by discussing in detail the equipment and procedure for the synthesis of graphene by CVD and the growth of carbon films by PVD. It then explains the methodology used to transfer graphene off the metallic substrate in order to perform characterisation, which is subsequently discussed.

Chapter 3 presents a detailed investigation into the synthesis of graphene on bulk copper. It first reviews the initial conditions suitable for depositing graphene by a FCVA system. It then presents a detailed examination of the microstructure and properties of FCVA grown graphene. Additionally, we explore the effect of a processing gas such as H_2 and CH_4 on the quality of FCVA grown graphene. The chapter then concludes by proposing a model to explain the formation of graphene by FCVA deposition.

Chapter 4 investigates the potential to deposit graphene onto a variety of alternative substrates with PVD. As discussed in the literature review, graphene has been grown on a variety of substrates with a range of different synthesis methods. CVD has been used to grow graphene not only on copper but also nickel and a few other types of substrates.

Additionally, graphene has been grown by the thermal decomposition of Si on 6H-SiC at temperatures around 1250 to 1450 ^{o}C. Furthermore, YSZ has been used to template copper films for the growth of graphene by chemical vapour deposition. While graphene has not been directly deposited onto hBN, several research groups have successfully transfer graphene onto hBN which is considered to be an atomically compatible substrate.

Chapter 5 discusses the synthesis of graphene on copper films, both grown by PVD. This chapter begins with the investigation of Cu films grown using FCVA with the aim of making suitable growth surfaces for graphene synthesis. Then the results of the growth of graphene and its transfer to the underlying substrate are presented.

Finally, in chapter 6 a short conclusion is presented.

2 Methods

This chapter outlines the main experimental methods used in this thesis. Described are the two fabrication methods used to grow graphene which are CVD and PVD in a FCVA system. Also detailed are the techniques used to assess the growth and quality of the graphene.

2.1 Fabrication methods

Two main methods were employed in this thesis to prepare graphene. As discussed in chapter 1, CVD is a well-established method for preparing graphene. In this thesis graphene deposited by CVD was compared against graphene films grown by PVD in a FCVA system.

2.1.1 Chemical vapour deposition

Copper foil substrates were cut to an appropriate sized, placed on quartz holders and then loaded into the CVD system. After loading the copper substrates the reactor was sealed by tightening the inlet and outlet valves. The CVD system was then purged several times by flushing with 1200 cc of argon (Ar) gas. After the third flush, Ar gas was allowed to flow through the CVD system to the outlet valve for 10 minutes. With 3 minutes left, 100 cc of H_2 gas was directed in the CVD system. With 1 minute left the Ar gas was turned off. Once the 10 minute period had elapsed the furnace was allowed to heat up to its set value of 1050 ^{o}C. Samples were annealed in the hydrogen rich environment for one hour. 5 minutes prior to the conclusion of the 1 hour annealing period, 200 cc of Ar gas were directed into the reactor. After 1 hour of annealing, 15 cc of CH_4 gas were directed into the reactor. When the desired reaction time has passed, the CH_4 gas and the heating element were turned off. The reactor was then fan forced cooled to room temperature. The inlet valve was opened and the Ar and H_2 gas were turned off before retrieving graphene samples.

2.1.2 Filtered cathodic vacuum arc

Carbon films were deposited using a FCVA system (*Figure 2*a) equipped with a double bend magnetic filter to minimise the deposition of macroparticles [64] which can be ejected from the carbon cathode (99.999% C, Nano Film International, Singapore). A 60 A current was used to generate a carbon plasma and films were deposited after a base pressure of 10^{-6}mTorr was reached. The plasma which consists of ~100% C^+ ions [64] and electrons, was initiated using an earthed graphite tipped striker. During a deposition, gas can be introduced into the chamber through the gas inlet connected to the sample chamber and the flow controlled by a mass flow controller.

The kinetic energy of the impinging carbon ions can be controlled by applying a negative potential on the substrate. The ion energy is given by the equation below,

$$E_{ion} = qV + E_o \tag{2.1}$$

q is the charge state of the carbon ion; V is any substrate voltage; E_o is the natural ion energy of the plasma. Previous work has shown that for a vacuum arc operating under similar conditions, more than 95 % of the ions are singly ionised (q = +1) with the remainder doubly ionized [89]. A previous study, measured E_o of carbon plasma in the FCVA system used in this work to be 20 V [60]. The substrate bias (V) at floating condition has been measured for C in our FCVA system and found to be -20 eV [90].

A paper by André Anders proposes a zone diagram for the growth of thin films by energetic deposition that typically occurs in FCVA and high power impulse magnetron sputtering (HiPIMS), this diagram can be seen in *Figure 2*b [91]. In this zone diagram for growth of films is characterised by three axes: generalized homologous temperature (T*), normalized

kinetic energy flux (E*), and net film thickness (t*). The diagram shows that the use of energetic deposition may allow microstructures to be formed at lower growth temperatures than low energy deposition methods. While in this diagram the growth of films is only defined in terms of three axes, the author stresses that there are a myriad of other physical factors which could affect the growth of films, such as substrate type.

In this thesis, the amount of carbon deposited was expressed in terms of dose (atoms/cm^2) for two reasons. (1) Measuring the film thickness of a thin carbon film presents a significant challenge; (2) carbon is soluble in some substrates.

The dose of the deposited carbon was calculated using the following procedure. First the thickness of a carbon film deposited on silicon (in which C is insoluble). The carbon film used was significantly thicker than a single layer of graphene. The film was measured and used to calculate the volume deposited over a 1 cm^2 area using

$$volume = film\ thickness \times area. \tag{2.2}$$

The mass of the carbon deposited was then obtained using,

$$mass = density\ \times volume \tag{2.3}$$

where the density was assumed to be that of graphite (2.27 g/cm^3). The number of carbon atoms within a 1 cm^2 area by

$$dose = \ mass\ \times \frac{Na}{atomic\ mass}\ (\frac{atoms}{cm^2}) \tag{2.4}$$

where N_a is Avogadro's number and the atomic mass of carbon is 12. The dose rate was calculated by dividing the dose by the deposition time,

$$dose\ rate = \frac{dose}{time}. \tag{2.5}$$

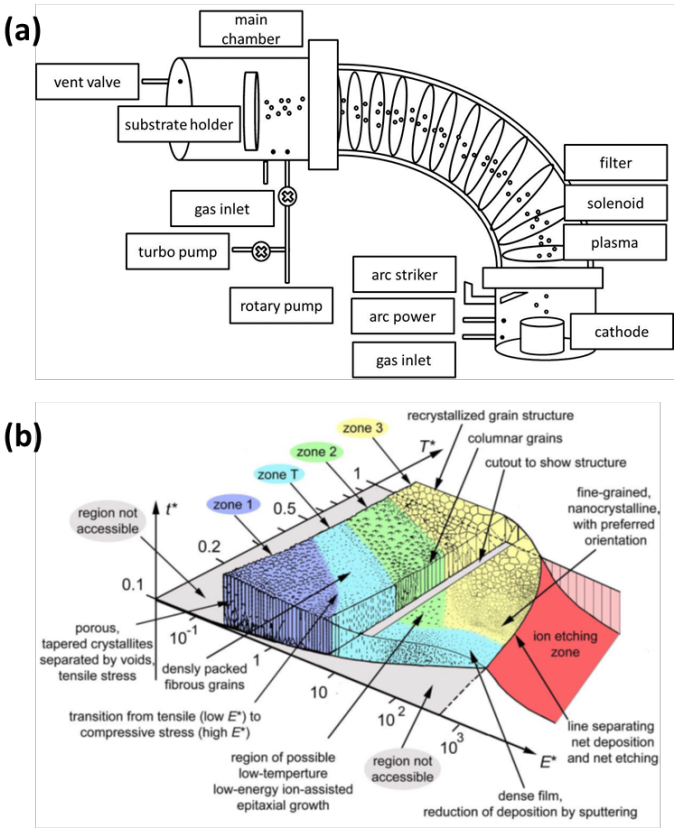

Figure 2: (a) Schematic diagram (not to scale) of the FCVA system. (b) Structure zone diagram for films deposited by energetic deposition. The axes are in terms of temperature (T), kinetic energy flux (E*), and thickness (t*) [91].*

2.1.3 Transfer

Graphene was transferred from the growth substrate to glass slides using a polymer-support method. A PMMA solution (40 mg of PMMA in 1 ml of anisole) was spin coated onto the deposited graphene films and air dried to leave a ~500 nm thick support film. The PMMA/graphene/Cu sample was then floated on a solution of ammonium persulfate ($(NH_4)_2S_2O_8$, 0.1 M) to etch away the copper. After the copper was completely etched away, the remaining PMMA/graphene film was rinsed thoroughly with milli-Q deionized water then collected graphene-side down on an ozone-treated glass slide. Graphene deposited onto nickel was etched and transferred in a similar manner except that a 0.35 M solution of

iron chloride ($FeCl_3 \cdot 6H_2O$) was used as the etchant. The PMMA was removed from the graphene sheets by repeatedly dipping in fresh dichloromethane until free of polymer.

2.2 Characterisation

A range of characterisation methods, which are detailed below, were employed to investigate and access the quality of the FCVA deposited carbon films.

2.2.1 Raman spectroscopy

The spectroscopic technique, known as Raman spectroscopy, is used to observe the vibrational states of phonons in materials. This technique is commonly used in chemistry; as the detected vibrational states of the phonon can be used as a fingerprint to identify a range of molecules and materials. This method operates by illuminating the sample with a monochromatic light source and relies on Raman scattering, which is the inelastic scattering of photons off the sample. The inelastic scattering of photons occurs by the interaction between the vibrations of phonons and other excitation states within the system. This interaction results in the energy of the photons being shifted up or down. By measuring the shift in the photon energy, scientists are able to conclude information about the vibrational modes of the sample. Raman spectroscopy was performed using a Renishaw Raman system 100 with a 514 nm Ar^+ laser and 50 µm spot. The intensity of the D peak (~1350 cm^{-1}) relative to the G peak was used to indicate the amount of defects in the carbon films (defect ratio). The intensity of the G to the 2D peak (~2700 cm^{-1}) can be used to indicate the number of graphene layers (intensity ratio). The equations which describe the intensity and defect ratio described below. *Figure 3* shows a comparison between the Raman spectra of single, double and triple layer graphene.

$$Defect\ ratio = \frac{I_G}{I_D} \tag{2.6}$$

$$Intensity\ ratio = \frac{I_{2D}}{I_G} \tag{2.7}$$

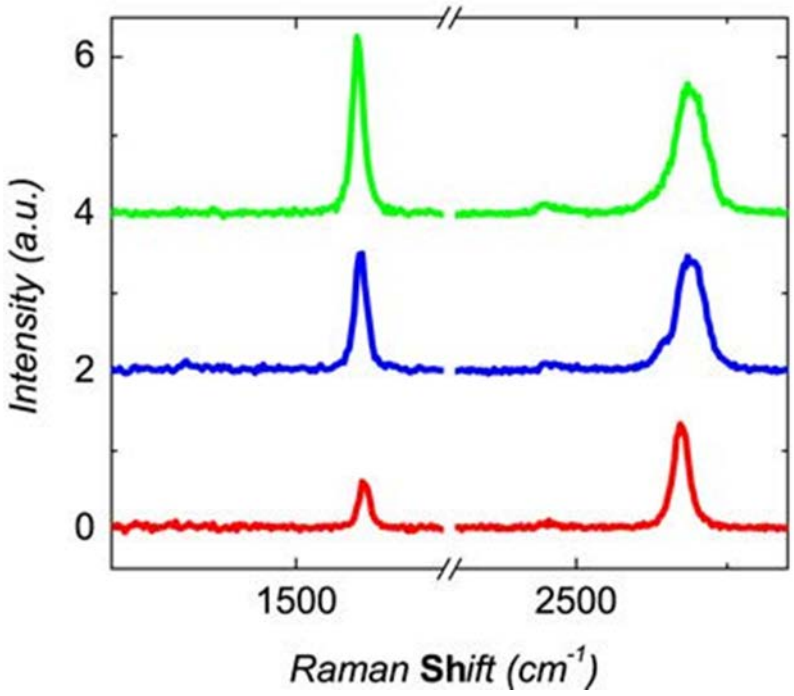

Figure 3: Comparison of Raman spectra of (red) 1, (blue) 2 and (green) 3 layer graphene [92].

2.2.2 Scanning electron microscopy

SEMs are similar to optical microscopes; however instead of using visible light, a SEM uses a beam of electrons. An image is generated by scanning the sample with the electron beam in a raster pattern. The use of electrons, enables SEMs to achieve a resolution of better than 1 nm, which is much higher than that of a light microscope which is limited by the wavelength of visible light. Furthermore, the use of electrons in a SEM provides both topography and compositional information. Additionally, the use of electrons also affects the depth of field and provides a greater depth of field than optical microscopes. Electrons also provide information about the samples composition as well as the crystallographic, magnetic and electrical characteristics. There are several drawbacks to using SEMs. A SEM must operate under vacuum. Furthermore the sample must be conductive. Often a sample

will be coated with a thin film of carbon or metal in order to become conductive. Fortunately, graphene is conductive. Secondary electron images from SEM analysis of the surface morphology of the carbon films were collected using a FEI Nova NanoSEM. Images were collected in high vacuum mode with a spot size of 3.5 and an accelerating voltage of 3 kV. Additionally, images of the transferred graphene film on SiO_2 and the boron nitride on copper were collected with the FEI Verios 460L SEM operating with an accelerating voltage of 500 V.

2.2.3 X-ray diffraction

X-ray diffraction (XRD) is an analytical technique used to identify the phase of crystalline materials such as thin films, ceramics, metals, minerals and pharmaceuticals. This method works by measuring the angles and intensities of x-rays which are diffracted by the atomic structure of the crystalline material. The diffraction of the x-rays is specific to the crystal structure of the material, as well as the chemical bonds and disorder within the material. Crystal restructuring in copper and nickel foils, and copper films on silicon and silica wafers as a result of the deposition of carbon were studied using D4 Endeavour XRD.

2.2.4 Atomic force microscopy

Atomic force microscopy (AFM) can be used to create three dimensional images which reveal information about the height and roughness of a sample. An AFM creates these three dimensional images by tracing a fine needle across the surface of the sample and measuring the deflection of needle. The Root Mean Squared (RMS) roughness and surface morphology of copper films before and after the deposition of carbon films was assessed with a Veeco Dimension 3100 AFM operated in tapping mode over an area of 10 nm x 10 µm.

2.2.5 Focused ion beam

Cross-sectional TEM samples of graphene on copper and nickel foil were prepared using a FEI Scios duel beam SEM / Focused Ion Beam (FIB). The setup of a FIB is very similar to a SEM with the exception of being equipped with an ion beam. The most recent models of FIBs are equipped with both an ion beam and an electron beam. The ion beam can be used deposit and ablate materials. Historically FIBs have been used in the semiconductor industry to make devices and have also been used for site specific analysis of biological samples. Additionally, FIB have also proved themselves useful for TEM preparation.

2.2.6 Transmission electron microscopy

TEM generates an image by detecting electrons transmitted through a very thin specimen. The electrons interact with the specimen as they pass through it and thus provide information about the internal structure of the sample. For example, TEM can be used to generate an image of the individual components within a cell, such as the cell membrane, vacuole, nucleus and mitochondria. Cross-sectional TEM specimens were prepared using a FIB. These specimens were analysed using JEOL 2100F TEM at 80 kV. TEM of the cross sectional allows for the microstructure of the carbon film to thoroughly explored.

2.2.7 Ultraviolet – visible absorption spectroscopy

White light is comprised of electrometric radiation with a broad range of wavelengths; from ultraviolet through to visible light and up to infrared. When white light is either transmitted through or reflected off an object a portion of wavelengths are absorbed. Ultraviolet–visible absorption spectroscopy measures the absorption of light in the ultraviolet-visible spectral region, which is transmitted through an object. The transparency of the graphene films between 400 nm to 700 nm was measured using a Cary UV-Vis Spectrophotometer. The

optical transmittance of a graphene film varies in a log-linear fashion with the thickness, with a single graphene layer conventionally quoted as absorbing about 2.3% of incident light [15].

2.2.8 Resistivity

Resistivity quantifies how strongly a given material opposes the flow of electric current. Materials with a low resistivity allow for the flow of electricity with minimal lose in energy. The four point probe apparatus is a common tool used to measure the resistivity of a material. A four point probe consists of four thin collinearly placed tungsten wires probes. The method works by bringing the four probes into contact with the sample. A current is emitted from the outer probes, and the voltage is measured between the two inner probes. The resistivity of the graphene films was measured using two techniques. The sheet resistance was measured using a four point probe and a two point probe with silver contacts.

2.2.9 X-ray absorption near edge structure

Absorption spectroscopy was conducted at the soft x-ray beam line at the Australian Synchrotron. X-ray absorption near edge structure (XANES) was developed in 1980s. This technique is particular sensitive to molecules comprised of atoms with a low atomic number, i.e. hydrogen, carbon, nitrogen, oxygen and fluorine. XANES can identify individual elements through its K-edge and probes the intra-molecular and extra molecular neighbours [93]. In particular this method is useful in accessing the structure of bonded molecules. For example it can identify specific bonds, i.e. C-C, C=C, C≡C and C-H bonds. Simplistically this technique works by measuring the separation of a core electron from the absorption of x-rays.

An example of XANES from glassy carbon, a 100 % sp^2 bonded material is shown in Figure 4. XANES is sensitive to the degree of layering in anisotropic materials. For glassy carbon, XANES can be characterised by three regions, by specific resonance energies: π* peak at 285 eV, the C=O peak at 288.5 eV and the σ* doublet located between 290 eV – 315 eV.

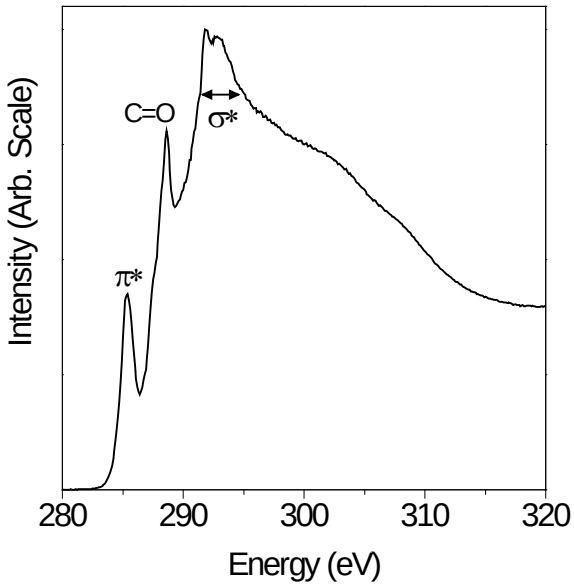

Figure 4: XANES of glassy carbon.

*Figure 5*a is a schematic of the atomic bonding of an aromatic ring which could be found in a benzene, Pyridine or graphite. A molecule can be divided into different classes, depending on whether the π* or σ* orbitals point in a specific direction (vector type) or if they span a plane (plane type). The angular resonance intensities for vector and plane type molecules are described by two different theoretical expressions. For an aromatic ring, the atoms are arranged in a plane. Thus the σ* orbitals can be represented by a plane. However, the π* can be represented by vectors which are perpendicular to the plane. Hence for an aromatic ring, the intensity of angular dependence resonance needs to be considered for two cases π* and σ* as i) vectors and as ii) planes.

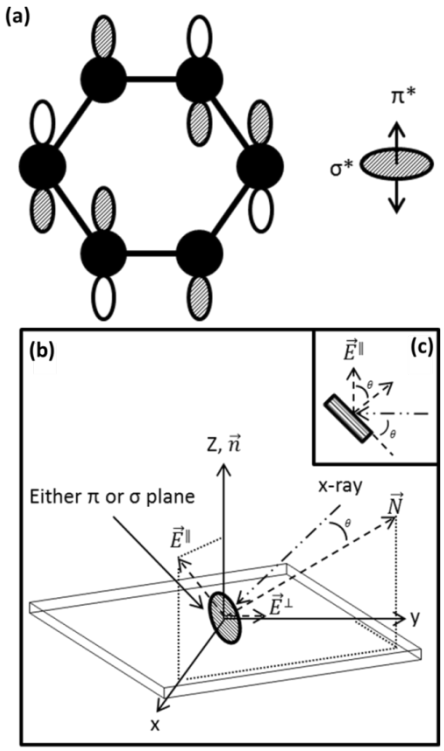

Figure 5: (a) Spatial orientation of π and σ* orbitals for an aromatic ring. (b) Coordinate system defining the geometry of σ* or π* vector orbital on the surface. (c) Inset showing a simplified diagram.*

A good example of strong angular dependence of resonance and proof of the theory is provided by the angle dependent NEXAFS spectra of highly orientated pyrolytic graphite [93]. As described before, graphite is composed of six membered rings of carbon atoms which all lie in parallel planes to the surface of the crystal. The π* orbitals can be described as vectors which are perpendicular to the basal plane, along the c axis. The π* orbital exhibits a sharp resonance near 285 eV, which corresponds to a transition to the first empty π* state. The resonance of this peak is strong at a grazing x-ray angle when the electric field vector has a large projection along the direction of the π* orbital. The increase in the intensity of the π* resonance should be proportional to the change in $\cos^2\theta$.

3 Graphene synthesis on copper

In this chapter, the conditions under which graphene grows on copper by PVD in a FCVA system is presented. It includes a detailed investigation of the microstructure and properties of the resulting graphene. The effect of the processing gases such as H_2 and CH_4 on the quality of FCVA grown graphene is also explored. Finally, a model is proposed to explain the formation of graphene by FCVA deposition.

** Aspects of this chapter have been discussed in the following published papers:*

- *D.T. Oldfield, C.P. Huynh, S.C. Hawkins, & D.G. McCulloch, Graphene Films Prepared Using Energetic Physical Vapor Deposition. MRS Advances, 2017, 2(2), 117-122.*
- *D.T. Oldfield, D.G. McCulloch, C.P. Huynh, K. Sears, S.C. Hawkins, Multilayered graphene films prepared at moderate temperatures using energetic physical vapour deposition. Carbon, 2015. 94: p. 378-385.*

3.1 Introduction

The numerous and remarkable properties of graphene have earmarked it as a potential material to be incorporated in electronic devices. In order to integrate graphene into electronic devices, methods are required to deposit wafer scale graphene that can be processed using existing or post CMOS fabrication techniques. In order to meet this need scientists have been exploring new methods capable of controlling the deposition of large area, high quality uniform films.

As discussed in chapter 1, graphene obtained by mechanical cleavage from highly oriented pyroltyic graphite has had the best structural integrity [11]. While mechanical cleavage is capable of producing graphene with low amounts of structural defects; the method itself

lacks control over the size, location and number of graphene sheets. Multiple methods have been developed in order to achieve reproducible graphene growth. Of these methods CVD is considered to hold the most promise and is capable of growing graphene on several different transition metal substrates such Ni [94], Pd [95], Ru [96], Ir [97] or Cu [98]. In particular, copper is proving to be a promising substrate for the growth of CVD graphene. With copper as a substrate, researchers have achieved the growth of uniform single layer graphene over large areas [98, 99]. Compared to some of the other substrates previously mentioned, the growth on copper is relatively straightforward. Additionally, the deposition of large area graphene can be transferred by etching away the copper substrate. In this introduction, I will provide a summary of some of the key aspects of graphene growth on copper by CVD.

Interestingly, copper has been historically used as a catalyse for the growth of several carbon allotropes such as graphite [100], diamond [101], carbon nanotubes [102] and most recently graphene [98]. Furthermore the growth of graphite, multilayer graphene, was first unintentionally discovered in 1991 [100, 103] in experiments aimed at growing diamond by CVD. Today, graphene growth on copper by CVD typically involves the decomposition of CH_4 gas over a copper substrate held at approximately 1000 °C

Studies have found that the growth of graphene on copper foil by CVD is self-limiting and thus the deposition parameters do not greatly influence the physical and electrical properties of as-grown graphene on copper. However, the pre-treatment of the copper foils has been found to be important in obtaining large graphene domains [98, 99]. It is important to remove the native oxide layer on the copper foil (which consists of CuO, Cu_2O) [104], as the oxide layer reduces the catalytic activity. In order to remove the oxide layer it

is common to anneal the copper substrate in a hydrogen atmosphere at 1000 °C [105]. Subsequently, this annealing step has a further benefit of increasing the copper grain size and rearranging the surface morphology.

As the deposition time is increased, the graphene domains grow until they coalesce into a single layer [106]. The density of the nucleation sites can be controlled by the pre-treatment conditions and by the gas ratio during deposition. Additionally, the growth of graphene domains are influenced by the crystal structure of the copper substrate. Furthermore, after the graphene domains coalesce into a continuous graphene sheet, the growth of the graphene film will cease. Commonly the graphene film will grow over the boundaries of the copper foil. A study by Ruoff group [107] using isotopic labelling of the CH_4 precursor gas illuminated the mechanism of growth. The growth mechanism on copper has been shown to be surface related and not due to the diffusion of carbon from the substrate.

Graphene films grown on copper are then typically transferred in order to assess the quality of the deposited film. Properties such as carrier mobility and optical transparency are commonly needed to assess the quality of graphene film. The transfer is typically done by coating the graphene film with a protective polymer layer [Polydimethylsiloxane (PDMS) or PMMA]. The under lying copper substrate is then removed by etching with iron chloride, nitric acid, ammonia persulfate. Iron chloride is widely used [108] because it slowly and effectively etches the copper without forming gaseous products or precipitates. In contrast, reactions during etching of copper with nitric acid leads to the formation of H_2 bubbles which causes cracking in the graphene film and nitric acid can also degrade the carbon sp^2 network. Hydrogen chloride releases corrosive vapor and the etching rate of copper is

very slow. Once transfer is completed, the polymer is removed (by dissolving with acetone, for the case of PMMA). The transfer of graphene films from the copper to insulating substrates inevitably leads to cracking.

3.2 The growth of graphene by filtered cathodic vacuum arc

Previous to this study, there were no reports of graphene directly deposited onto copper by FCVA. Therefore, a variety of deposition parameters were varied to determine the conditions for synthesising graphene. Films were prepared using the FCVA system outline in section 2.1.2 with the sample under floating bias conditions (giving a deposition energy of ~ 40 eV), with a deposition rate of 2.3×10^{15} atoms/cm^2 s. Temperatures in the range of 700 ^{o}C to 1100 ^{o}C are commonly reported for CVD growth of graphene using volatile organic carbon compounds [49, 50]. The effect of growth temperature was studied by coating substrates held at different temperatures with a dose (calculated using the method outlined in section 2.1.2) of 4.6×10^{16} atoms/cm^2, equivalent to a fully dense layer approximately 4 nm or 12 atoms thick [68].

Two substrate types were chosen for this initial study, 99.999 % pure copper foil and silicon wafer (polished and cleaned in ethanol). The Raman spectrum for a film deposited on silicon at 25 ^{o}C (Figure *6*a) shows a broad asymmetric peak at ~1500 cm^{-1}, characteristic of amorphous carbon [109]. This peak is broadened at a deposition temperature of 400 ^{o}C, and resolved at 750 ^{o}C into two peaks at ~1350 cm^{-1} and ~1580 cm^{-1}. These peaks are often observed in nano and micro crystalline graphitic materials and are referred to as the D and G peaks, and can be attributed to the 'defective' edges and defect-free centre of graphene layers respectively [92]. This indicates that the elevated growth temperature has allowed the carbon atoms to adopt the sp^2 bonding configuration resulting in a nano-crystalline

graphitic material. However there is no 2D (G') peak at ~2700 cm^{-1} in these films, which together with the large D peak indicates that the films do not contain significant amounts of single or organised multi-layer graphene [92].

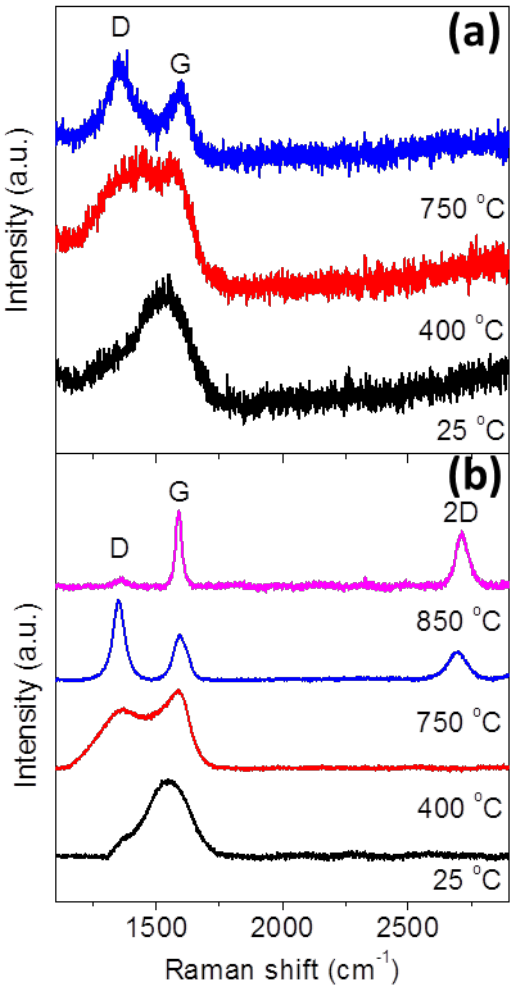

Figure 6: Raman spectra showing the effect of temperature on carbon films deposited on (a) silicon and (b) 99.99% copper foil at a dose of 4.6x10^{16} atoms/cm^2 using a deposition rate of 2.3x10^{15} atoms/cm^2.s.

A carbon dose of 4.6x10^{16} atoms/cm^2 deposited on copper at 25 °C or 400 °C gives similar Raman spectra to silicon under the same conditions (Figure *6*). However at 750 °C a clear difference is observed. The D and G peaks are fully resolved and, most importantly, a 2D

peak appears at ~2700 cm^{-1} when using a copper substrate. This Raman spectra is typically observed from defective multilayer graphene and confirms that the substrate material has a critical effect on the structure of the deposited carbon at 750 ^{o}C. At 850 ^{o}C, the intensity of the D has decreased relative to the G peak, indicating few defects. The intensity of the G peak is slightly greater than the 2D peak, indicating multiple layers of graphene.

The effect of the copper substrate purity was investigated on the deposited carbon film (Figure 7). Raman spectroscopy was used to examine carbon films deposited on low purity (99.8%) and high purity (99.99%) copper foil. Compared to the Raman spectra observed for films deposited on high purity copper foil, the formation of the 2D peak is greatly reduced on copper foil which is less pure. As outlined in in section 2.2.1 the presence of a small 2D peak relative to the G peak indicates an increase in the number of graphene layers, impurities in the copper foil can inhibit graphene growth. For this reason, all subsequent growth was performed on high purity 99.99% copper foil.

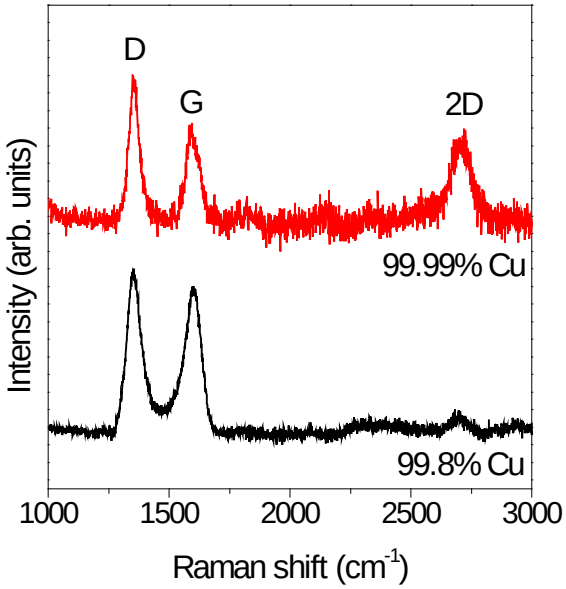

Figure 7: Raman spectra of carbon films grown on 99.8% and 99.99% copper foil at 750 ^{o}C.

In order to investigate the effect of a more carbon energetic flux on the carbon films, films were deposited with substrate biases of up to 100 V at 750 ^{o}C. As shown in Figure 8, the additional energy of the carbon flux (~ 70 eV at 50 V, calculated using equation 1) has resulted in a highly defective (amorphous) carbon film resulting from ion damage during film growth.

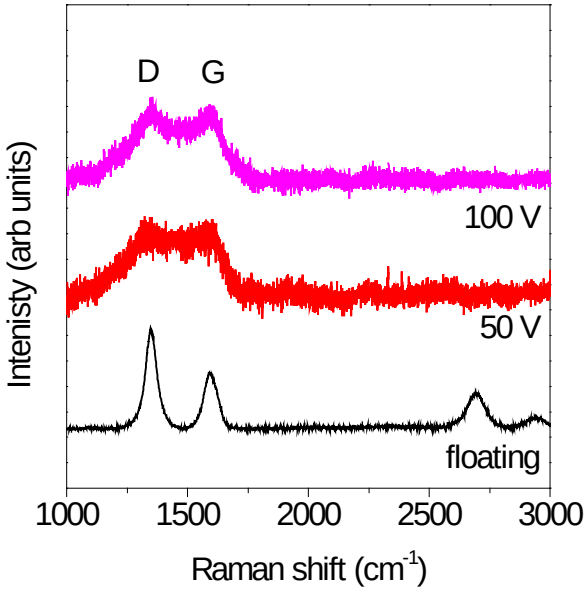

Figure 8: Raman spectra demonstrating that an applied bias prevents the formation of graphene layers in carbon films deposited at 750 ^{o}C.

The deposition rate was adjusted by changing the current in the double bend filter as shown in *Figure 9*a. At higher currents, the filter focuses the flux increasing the deposition rate. As shown in *Figure 9*b, the reduction in flux by an order of magnitude makes little difference to the quality of the graphene. This suggests that the flux of 2.3x10^{15} atoms/cm^{2}.s is sufficiently low to create an environment with a low nucleation density for optimum graphene growth at a temperature of 750 ^{o}C.

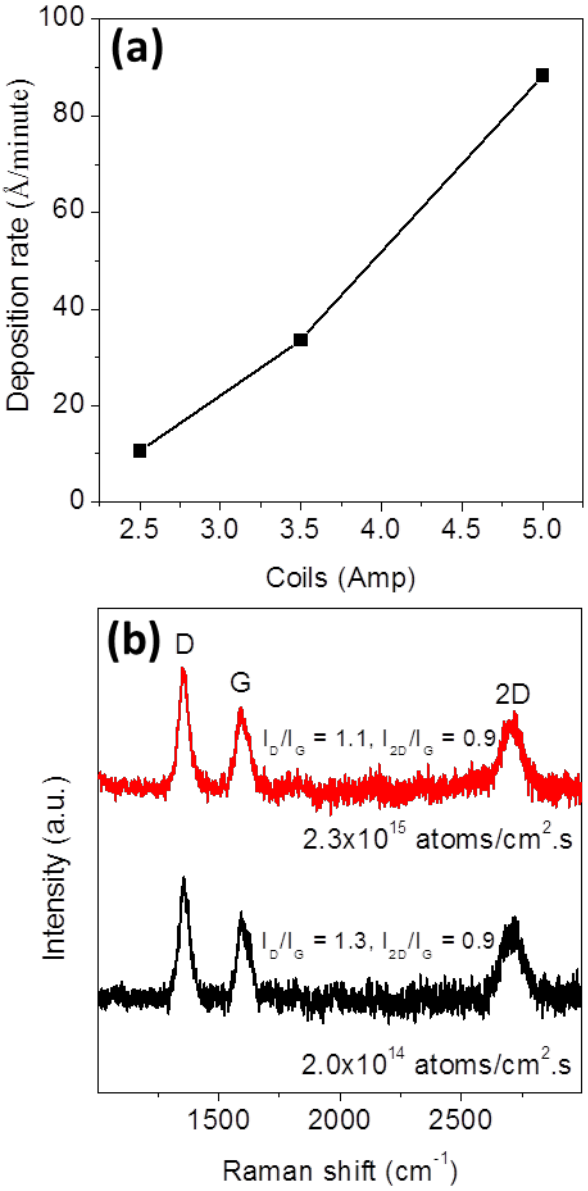

Figure 9: a) The effect of double bend filter coil current on the deposition rate of carbon in our FCVA. b) Raman spectra showing the effect of flux on the carbon films deposited on copper foil to a dose of ~3.4x10^{16} atoms/cm^2 at 750 ^{o}C. The spectra are almost identical.

In order to confirm that graphene layers form during the energetic deposition onto copper rather than being formed after the deposition by annealing; a film deposited at 25 ^{o}C was annealed to 750 ^{o}C. *Figure 10* compares the Raman spectra before and after annealing and demonstrates that annealing alone is insufficient to convert an amorphous carbon film into

graphene layers. The absence of a 2D peak indicates graphene was not formed after annealing the substrates. Therefore, the growth of graphene on substrates held at 750 ^{o}C can be directly attributed to the presence of an energetic carbon source.

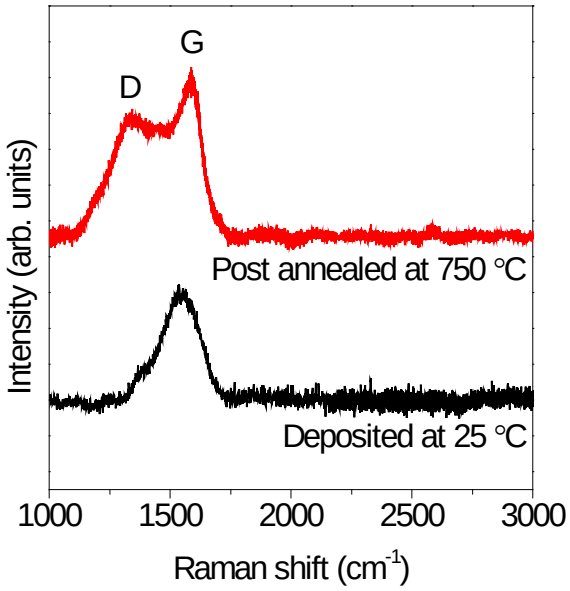

Figure 10: Raman spectra demonstrating that a post annealing temperature of 750 ^{o}C is insufficient to convert an amorphous carbon film on copper foil into graphene layers.

The total carbon dose, applied at a constant carbon flux of 2.3 × 10^{15} atoms/cm^2 s and a substrate temperature of 750 ^{o}C, was also found to have a significant effect on the carbon film microstructure (Figure *11*a). At the lowest dose of 2.3x10^{16} atoms/cm^2 (approximately equivalent to a layer 2 nm or 6 atoms thick assuming no loss of carbon atoms from the film) the Raman spectrum consists of a relatively sharp G peak and weak 2D peak indicating significant graphitic bonding. However, the large D peak indicates that the film contains a large proportion of defects possibly due to discontinuities such as graphene sheet edges.

At 3.4x10^{16} atoms/cm^2 (~ 3 nm or 9 atoms thick), the G peak is now larger than the D peak and narrower than before. This, combined with a more intense 2D peak indicates a relative

reduction in the defective (edge) component and an increase in the number, extent and order of the graphitic layers [92]. The spectrum indicates good coverage and a low defect density and is very similar to that from CVD grown graphene prepared at 1050 ^{o}C (Figure *11*a, top spectrum). The ratio of the 2D to the G peak can be used to estimate the number of graphene layers [110]. For this film, this ratio of 0.7 indicates ~ 10 layers, about the same as that for the CVD-grown graphene. To confirm that a 2D to G peak ratio of ~ 0.7 does indicates ~ 10 layers, a cross-sectional TEM specimen was made from the CVD sample. As shown in Figure *11*b, there are ~ 10 layers on the copper substrate.

The main difference between the FCVA deposited film and that grown using CVD is the width of the G peak, suggesting that the higher deposition temperature in the case of CVD has resulted in higher crystallinity. Note that the FCVA film was deposited in ~10 s, whereas the CVD graphene is grown over a period of 10 minutes.

At the highest doses of 4.6×10^{16} and 5.7×10^{16} atoms/cm^2 the Raman spectra still exhibit D, G and 2D peaks but the intensity of the D peak is now much higher than the G peak indicating an increase in the number of defects. We attribute this increase in defects either to a gradual accumulation of disordered carbon that the Raman is looking through; to increased damage caused by ion bombardment at these higher doses; and/or to decreased ordering due to the diminishing influence of the copper substrate with film thickness. The intensity of the 2D peak is low compared to the G peak, indicating the presence of many layers consistent with an increase in film thickness.

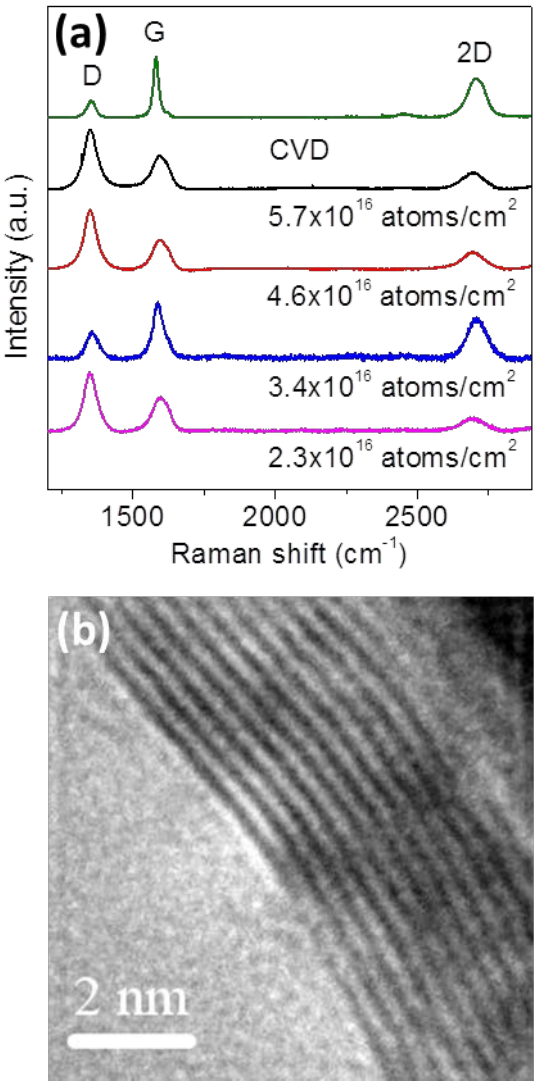

Figure 11: (a) Raman spectra showing the effect of dose on carbon films deposited onto copper foil at 750 °C. Also shown for comparison is a carbon film deposited onto the same type of copper foil by CVD at 1050 °C. (b) TEM image of CVD grown film showing ~10 graphene layers.

The films formed with different carbon doses on copper at 750 ^{o}C were transferred to glass slides using the process outlined in section 2.1.3 and were studied by SEM (Figure 12). The morphology of the films correlates well with the Raman results. For the smallest dose ($2.3x10^{16}$ atoms/cm^2, Figure 12a) a large number of folds/wrinkles and possibly cracks

(bright lines with ~100 nm width) are observed, and possibly the underlying texture of the copper foil is visible.

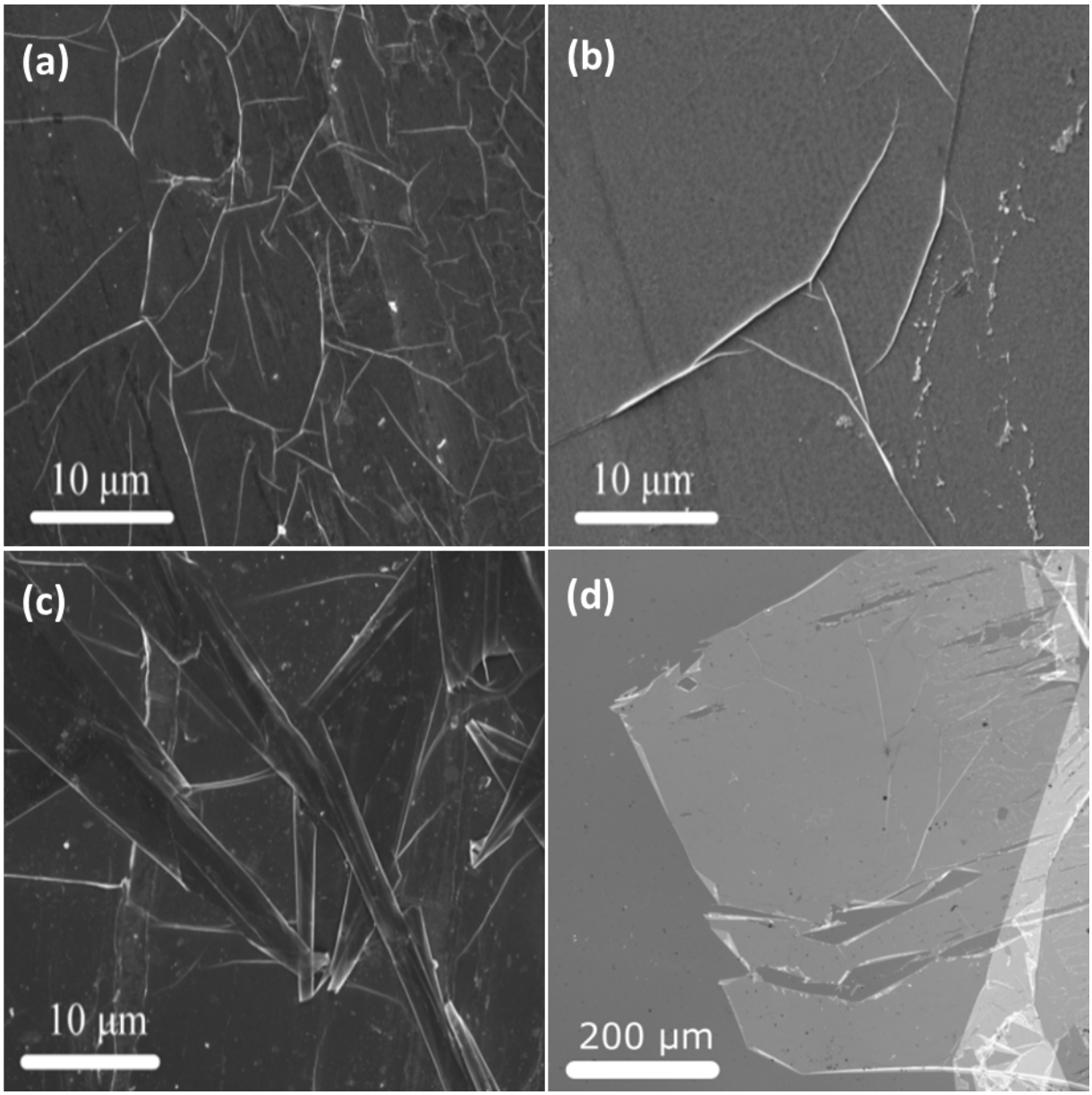

Figure 12: SEM images of graphene films grown on a copper foil with doses of (a) 2.3x10^{16}, (b) 3.4x10^{16} and (c) 5.7x10^{16} atoms/cm^2.(d) Optical microscopy of the graphene film grown with a dose of 3.4x10^{16} atoms/cm^2.

Folds/wrinkles are commonly observed for transferred graphene and can, for example, represent copper grain boundaries. During growth, the graphene follows the underlying metal surface which may have steps and grooves due to grain edges or machine marks. This

often leads to folds when the graphene is transferred to the very smooth glass [111, 112]. Wrinkles can also occur due to the strain induced by thermal mismatch between the graphene and substrates [113]. At the higher dose of $3.4x10^{16}$ atoms/cm^2 (Figure 12b), the film appears highly uniform with few cracks/folds but at the largest dose ($5.7x10^{16}$ atoms/cm^2, Figure 12c) the images shows mulitple sheets some of which have curled up into cones or cylinders. The transition in the microstructure of these films with dose is consistent with the Raman spectra which indicated fewer defects for the film deposited with a dose of $3.4x10^{16}$ atoms/cm^2 compared to the lower and higher doses. Optical microscopy of the graphene film grown with a dose of $3.4x10^{16}$ atoms/cm^2 (Figure 12d) consists of domains 200 μm in size. The lateral size of this transferred graphene film was ~2 cm.

Figure 13 shows the XANES collected from carbon films grown at a dose of $3.4x10^{16}$ atoms/cm^2 on copper foil at 750, 400 and 25 ^{o}C. The XANES were collected with the sample orientated at angles of 20, 55 and 90^{o} to the x-ray beam. *Figure 13*a reveals the XANES measured for the film grown at 750 ^{o}C. The XANES of graphene films grown at these temperatures can be characterised by three regions by specific resonance energies: π* peak at 285 eV, the C=O peak at 288.5 eV and the σ* doublet located between 290 eV – 315 eV [114]. The σ* doublet is similar to that observed in graphite [115]. The presence of the small C=O peaks indicates that some O is present in the films, likely bonded at the defect sites. Angular dependence of the π* and σ* peaks are typical of XANES collected from oriented graphene.

The XANES spectrum for the carbon film deposited with a dose of $3.4x10^{16}$ atoms/cm^2 at 400 ^{o}C is shown in *Figure 13*b. As seen previously in the spectrum for the film grown at the

higher deposition temperature of 750 ^{o}C, the π* and C=O peaks can be observed in the spectrum for the film grown at 400 ^{o}C. However, the σ* doublet is no longer present in the spectrum for the film grown at a lower deposition temperature of 400 ^{o}C. This absence of the σ* doublet indicates a change in the atomic arrangement of the carbon atoms in the film towards one with more in-plane graphitic disorder. The XANES spectrum for the film grown at 400 ^{o}C agrees favourably with the Raman spectrum for this film. The Raman spectrum for this film comprised of a broad G peak with shoulder, which is typical of nanocrystalline graphite.

Lastly, the XANES spectrum for the film grown at the lowest deposition temperature (25 ^{o}C) can be seen in *Figure 13*c. For this film the σ* doublet is absent and the C=O has almost disappeared. This result is consistent with the Raman spectra for this sample, which indicated the presence of amorphous carbon.

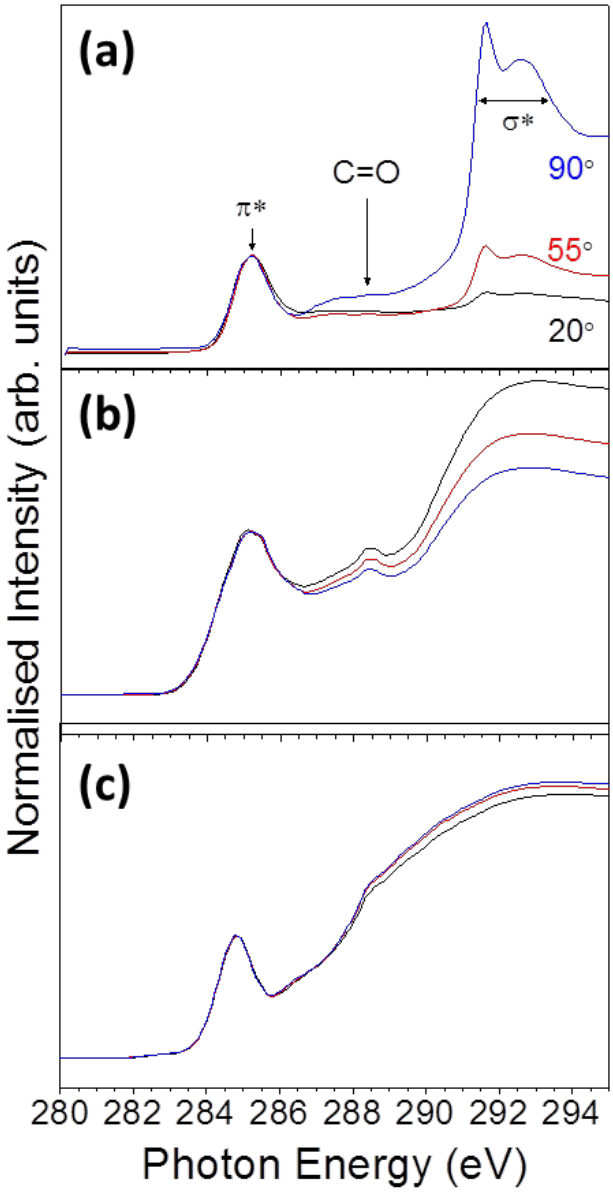

Figure 13: XANES spectrum of FCVA deposited carbon films grown at a) 750, b) 400 and c) 25 ^{o}C at a dose of 3.4x10^{16} atoms/cm^{2} on copper.

Figure 14 shows the XANES collected from carbon films grown at different doses on copper foil at 750 ^{o}C. As seen previously, three distinct peaks (π*, C=O, σ* doublet) can be observed in these spectra. However, the angular dependence of the π* and σ* peaks can be seen to significantly increase as the deposition dose is lowered to 3.4x10^{16} atoms/cm^{2}. The increase in the angular dependence is likely to be the result of an improvement in the orientation for

the carbon film grown at lower doses. Increased orientation for the carbon films as indicated by XANES is supported by Raman spectroscopy. Raman spectroscopy indicated an improvement in the defect ratio and the intensity ratio as the deposition dose was lowered from $2.3x10^{17}$ to $3.4x10^{16}$ atoms/cm^2. This was attributed to a decrease in the templating effect of the copper substrate of the carbon film became thicker.

It is possible that if the deposition dose had been lowered further, the lack of carbon atoms is likely to have led to the growth of a discontinuous film and resulted in deterioration of the angular dependence of the π* and σ* resonances. This theory is supported by the previously collected Raman spectroscopy (*Figure 11*a). The defect ratio from the Raman spectrum for films grown with a dose lower than $3.4x10^{16}$ atoms/cm^2 had a high defect ratio indicating a high number of defects; additionally, a weak 2D peak was observed indicating little parallel orientation.

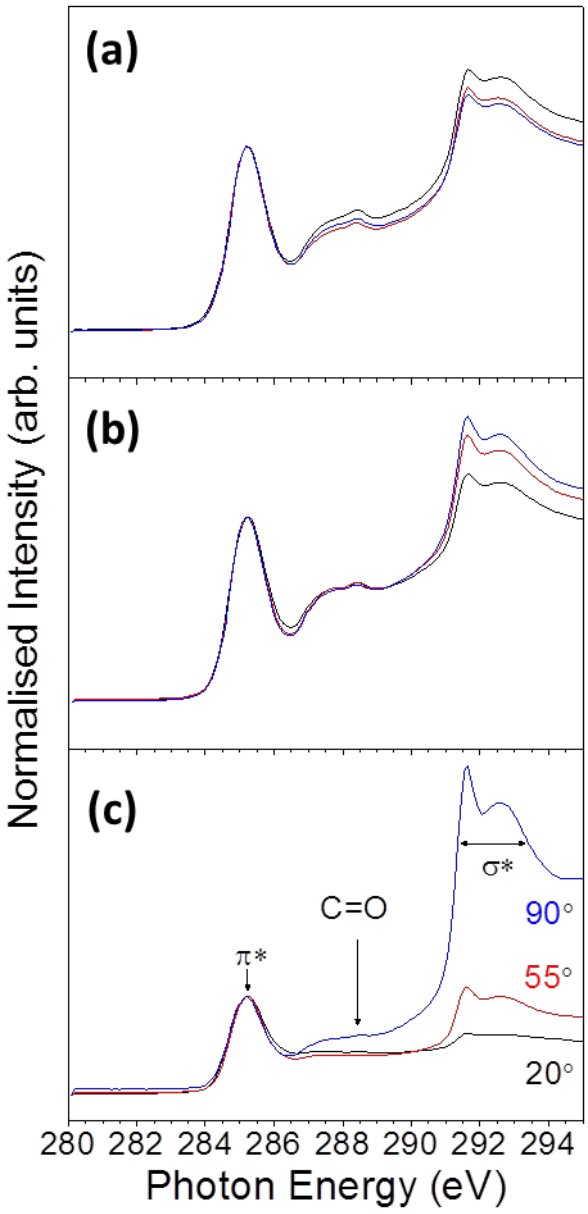

Figure 14: XANES spectrum a FCVA deposited carbon films grown at 750 ^{o}C on Cu at a dose of (a) 5.7x10^{16}, (b) 4.6x10^{16} and (c) 3.4x10^{16} atoms/cm^{2}.

Cross-sectional TEM analysis of the sample prepared at 750 ^{o}C to a dose of 3.4x10^{16} atoms/cm^{2} (Figure 15a) shows well-formed graphene layers between the copper substrate (right side of image) and the platinum protective layer used during the FIB sample preparation (left side of the image). The number of graphene layers compares well with that predicted from the intensity ratio between the 2D and G peaks of 0.7 of the sample *Figure*

11 which is ~ 10 carbon layers. The total thickness of the film of ~ 3nm is also what is expected at this dose. This implies that most or all of the carbon falling on the substrate, at least up to this level, is being incorporated into a relatively ordered structure.

Whereas CVD depends upon high temperatures of ~1000 ˚C [98] and labile organic gases to ensure correct arrangement of the carbon, the PVD process achieves this at a lower temperature using carbon ions alone. This outcome is attributed to dynamic annealing which occurs during the energetic deposition of carbon. In the case of a floating substrate holder the incoming carbon ions will have an average energy of ~40 eV [58]. This energy enables the carbon atoms to rearrange into lower energy bonding configurations and the formation of graphene layers [116] templated by the underlying copper.

A cross-sectional TEM image of the film prepared on copper at the highest dose ($5.7x10^{16}$ atoms/cm^2) shows randomly orientated graphitic sheets (*Figure 15*b). This is consistent with the Raman spectrum from this film (*Figure 11*a). The breakdown of the graphene layers at higher doses is attributed to a loss in the templating effect of the copper substrate as the film thickness increases. For thicker films, ion damage from the energetic flux would also cause damage resulting in a breakup of the graphene microstructure. Large intrinsic stresses are often observed in films prepares using energetic deposition [60]. As the film increases in thickness, theses stress may also constitute to a breakup of the graphene microstructure.

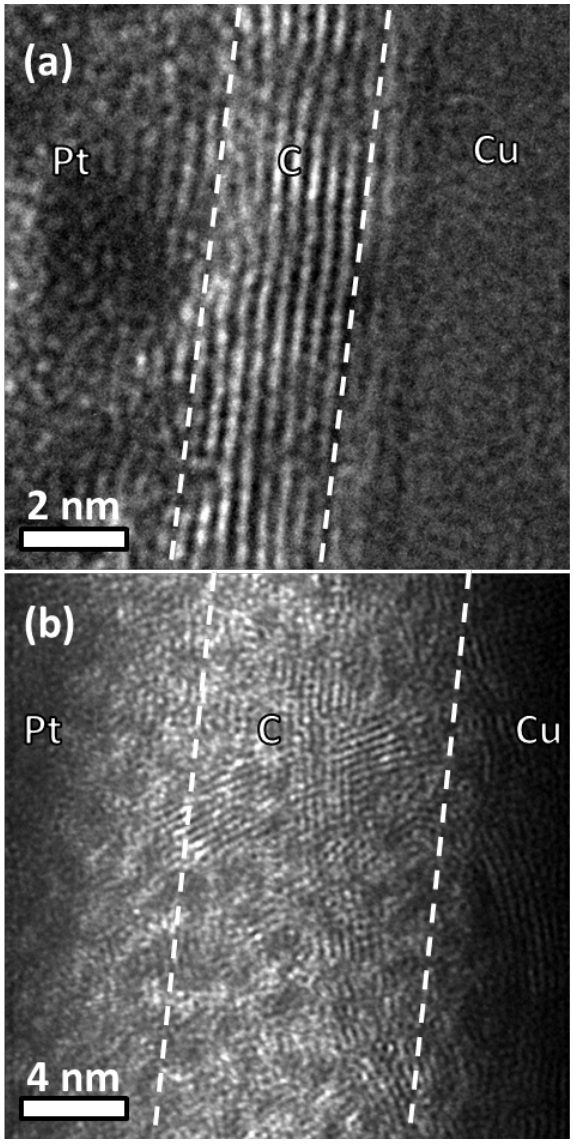

Figure 15: Cross sectional TEM images of graphene deposited on copper foil with a dose of (a) 3.4x10^{16} and (b) 5.7x10^{16} atoms/cm^2 using FCVA. The copper substrate is on the right. Both films have a platinum protection later on the left.

For many applications, the optical transparency and sheet resistance of graphene are important properties and can give insight into its quality. For films deposited on copper (*Figure 16*) the sheet resistance, as measured by four point probe (4PP) and by two point probe (2PP) with silver-paint contacts, initially decreases as the dose is increased from 2.3x10^{16} to 3.4x10^{16} atoms/cm^2. However at the larger doses of 4.6x10^{16} and 5.7x10^{16} atoms/cm^2 the resistivity increases again where the sample film is heavily disrupted

(Figure 12c). The low resistance of the film deposited at a dose of 3.4x10^{16} atoms/cm^2 can be attributed to its better microstructure. Raman spectroscopy showed that this film was the least defective (Figure *11*a) while SEM showed it to be highly uniform with few folds/cracks (Figure 12b).

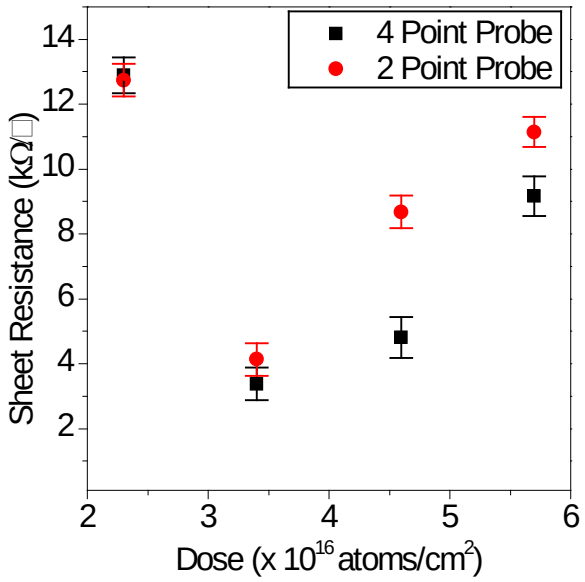

Figure 16: Sheet resistance of graphene etched off copper. The sheet resistance of CVD graphene as measured by 4 point probe is represented by an asterisk.

The optical transmittance of a graphene film varies in a log-linear fashion with the thickness, with a single graphene layer conventionally quoted as absorbing about 2.3% of incident light [15] although a recent analysis of multilayer graphene finds a value of 2.6% (ie a transmittance of 97.4%) and a more complex non-linear negative exponential relationship [117]. The optical transmittance of the multilayer films deposited by FCVA PVD on copper at 750 ^{o}C together with a film of 6 to 7 graphene layers produced by CVD was plotted from 400 to 800 nm and measured for reference at 550 nm (*Figure 17*), showing a range of 80-90%. Much lower transmission (34-60%) is observed for the nickel samples (*Figure 17*b) compared

to the copper ones (80-90%), consistent with the much larger carbon doses used and higher number of layers evidenced by TEM.

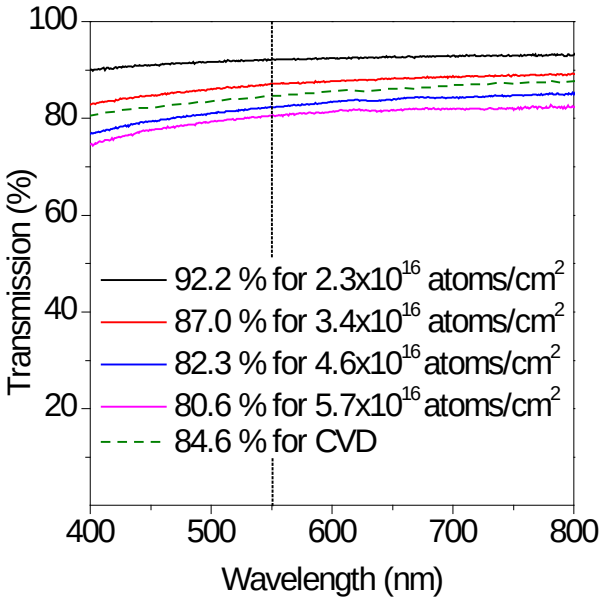

Figure 17: Transmittance of graphene films transferred from copper substrates.

The number of graphene layers estimated from the optical absorbance [117] is compared with the number equivalent calculated from the carbon dose (*Table 1*). Thus the 3.4×10^{16} atom/cm^2 dose on copper appears by TEM to comprise about 10 graphene layers (*Figure 15*a) in good agreement with the number of about 9 estimated from the dose. However the optical transmittance of 87% is consistent [117] with a film of just 5.5 graphene layers and other layers are similarly lower than calculated from the dose.

The lower than predicted optical density, and hence number of graphene layers, suggests that the layers are somewhat thinner than anticipated, possibly due to sputtering of some deposited carbon atoms off the surface, or incomplete transfer of the layer. The CVD graphene film is shown by TEM (*Figure 11*b) to have about 10 layers whereas optical measurement (*Table 1*) suggests about 6.75. This is qualitatively consistent with it having a

lower sheet resistance (*Figure 16*a) than the $3.4x10^{16}$ atoms/cm^2 film on copper, estimated optically to be 5.6. Both sheet resistance and the optical transmittance are extensive measures of average properties and require minimal sample preparation whereas the TEM is only from one point and also entails considerable sample manipulation.

Table 1: Dose equivalent thickness in graphene layers compared with calculated number from measured optical transmittance.

	Carbon Dose atoms /cm^2 x 10^{16}	**Equivalent thickness nm**	**Equivalent no of Graphene layers**	**Measured Transmittance %**	**Calculated no of Graphene layers [38a]**
Graphene on copper	2.3	2.0	6.0	92.2	3.2
	3.4	3.0	8.8	87	5.6
	4.6	4.1	11.9	82.3	7.9
	5.7	5.0	14.8	80.6	8.8
CVD Graphene				84.6	6.75

3.3 Graphene synthesis on copper with a process gasses.

This section examines the effect of CH_4 and H_2 gas on the deposition of graphene in a FCVA system. CH_4 and H_2 are essential components in the production of graphene by CVD. Hydrogen plays an important role in CVD graphene growth. Therefore the addition of these gasses during film growth in FCVA could potentially improve the quality of the graphene grown.

Carbon films were deposited at room temperature, 400 ^oC and 750 ^oC onto copper foil. Once the substrate had reached the desired temperature, the samples were annealed for 1 minute in a hydrogen rich environment prior to the deposition of the carbon film. The

processing gas was left on during the deposition of carbon film and was only turned off after the sample has sufficiently cooled. Films were deposited at chamber pressures of 0.25, 0.5 and 1 mTorr.

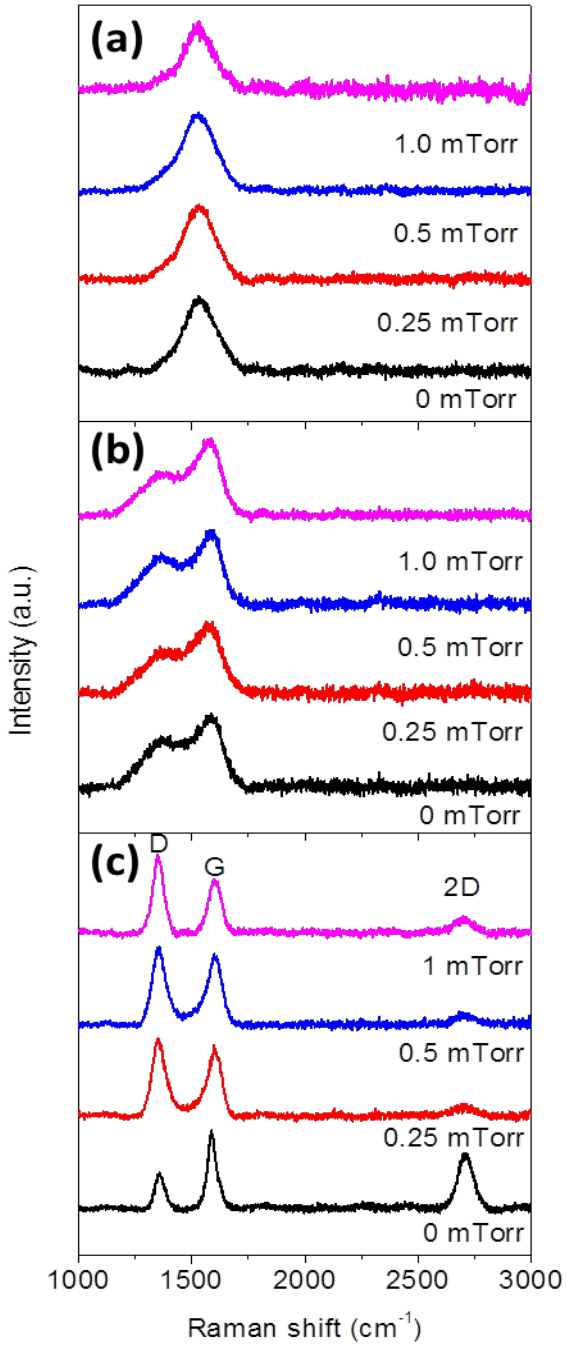

Figure 18: Raman spectra of carbon films deposited at (a) room temperature,(b) 400 ^{o}C and (c) 750 ^{o}C with hydrogen.

There was a negligible effect on the Raman spectra for films with a H_2 processing gas, prepared at room temperature (*Figure 18*a) and 400 ^{o}C (*Figure 18*b). In the case of the 750 ^{o}C growth temperature the addition of the H_2 caused the films to become more defective (increase in the D peak intensity) and lead to the loss of the 2D peak (*Figure 18*c). This indicates that the addition of H_2 has resulted in damage to the film. This is likely due to the H ion bombardment, which occurs as H_2 gas is ionised in the plasma stream.

To investigate whether graphene can grow in a background ground gas of CH_4 and in the absence of a carbon plasma, copper foil was placed in the FCVA and pumped down to a base pressure of 10^{-6} mTorr. Then 2 mTorr of CH_4 was introduced into the chamber for 1 minute. This process was conducted with the copper held at room temperature and 750 ^{o}C. The Raman spectra from the two samples can be seen in Figure 19.

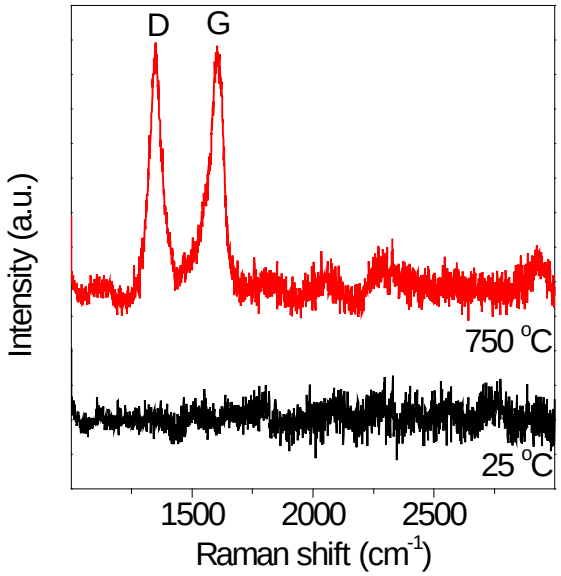

Figure 19: Raman spectra of copper foil held at room temperature and 750 ^{o}C in the presence of CH_4 without any carbon plasma.

The Raman spectra of the film which was grown on copper substrate held at 750 ^{o}C (Figure 19), shows a D peak located at 1350 cm^{-1} and a peak G at 1500 cm^{-1}, indicating that a carbon film has been created. This result is not surprising, when the condition used is compared to those employed in CVD. In these experiments the much lower pressure of CH_4 (2 mTorr compared to ~760 Torr) and lower growth temperatures (750 ^{o}C compared to ~1000 ^{o}C) is unlikely to result in graphene growth.

Figure 20 compares the Raman spectra of carbon films deposited on copper at room temperature for different background gas pressures of CH_4. Previously, it was shown that FCVA deposited carbons films grown at room temperature onto copper foil were amorphous (Figure *6*b). The amorphous nature of the carbon film is indicated by the broad G peak situated at 1500 cm^{-1}. A similar spectra is seen for the film deposited at 0 mTorr. With the elevation in the CH_4 gas pressure to 0.25 mTorr the intensity of the G peak is observed to dramatically decrease. This is a consequence of the CH_4 gas molecules impeding the carbon ions in the plasma, resulting in fewer carbon ions being deposited on the surface of the copper substrate. At a CH_4 pressure of 1 mTorr, a G peak can no longer be observed in the Raman spectra indicating that few carbon atoms made it to the surface of the copper substrate resulting in no film.

The Raman spectra of carbon films deposited on copper at 750 ^{o}C in the presence of CH_4 is shown in *Figure 21*. All these films were deposited with a dose of 3.4x10^{16} atoms/cm^{2}, Raman spectra of the films grown at a temperature of 750 ^{o}C, reveal a graphite-like microstructure as indicated by the presence of the D, G and 2D peak. Unfortunately, neither the defect or intensity ratio improved favourably in the presence of CH_4 from 0.25 mTorr to

1 mTorr. Instead, the D peak intensity increased and the 2D peak intensity reduced, indicating a deduction in ideal graphene layers.

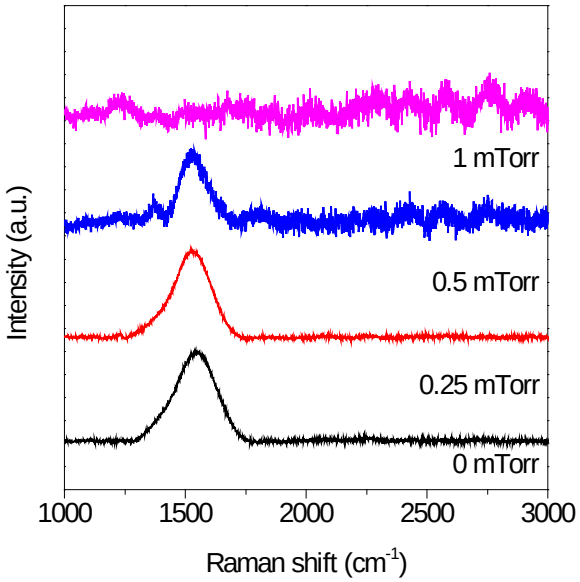

Figure 20: Raman spectra of carbon films deposited at room temperature with background CH_4, pressures values indicated.

In *Figure 20*, it was observed that an increase in the CH_4 pressure to 1 mTorr prevented the growth of carbon film at room temperature. The intensity of the peaks for films deposited at 750 ^{o}C with 1 mTorr suggests that the film growth is occurring regardless of the increase in the CH_4 gas pressure. Therefore the higher growth temperature is assisting in the formation of a film. These results demonstrate that unlike CVD, where the addition of H containing molecules assists the growth of graphene, the addition of these gasses during film growth using FCVA results in a degradation of film quality. The reason is likely due to the increased bombardment of the film by the energetic flux causing damage.

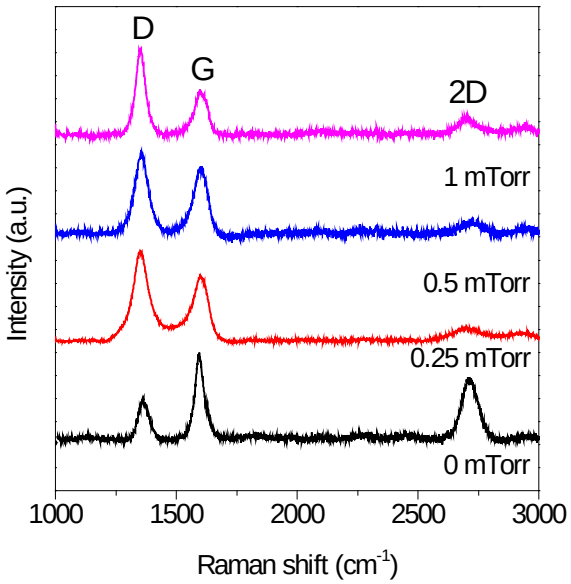

Figure 21: Raman spectra of carbon films deposited at 750 ^{o}C in the presence of CH_4.

3.4 Model for the growth of filtered cathodic vacuum arc graphene on copper

In this chapter, we have shown that it is possible to physically deposit graphene onto copper foil at 750 ^{o}C using a carbon plasma generated by FCVA [68]. This thesis has remarked on the similarities and difference between the growth mode of FCVA and CVD deposited graphene. We now propose a growth mechanism for the formation of FCVA deposited graphene.

*Figure 22*a shows a schematic of the graphene growth process by CVD. (1) Hydrogen gas acts as an etchant, removing oxygen from the surface copper. (2) Graphene is grown from a hydrocarbon source, such as CH_4 gas. (3) At temperatures around 1000 ^{o}C, the hydrocarbon is split and the carbon is adsorbed onto the copper surface via catalytic reaction. Furthermore, hydrogen helps to prevent oxygen from bonding to the carbon, which would result in defects in the graphene sheet. (4) The growth of graphene films is dependent on

the reaction between the substrate and the hydrocarbon, thus is self-limiting as the graphene becomes thick. The morphology of the graphene film is influenced by the formation domains in the copper substrate which occurs as result of the high deposition temperature.

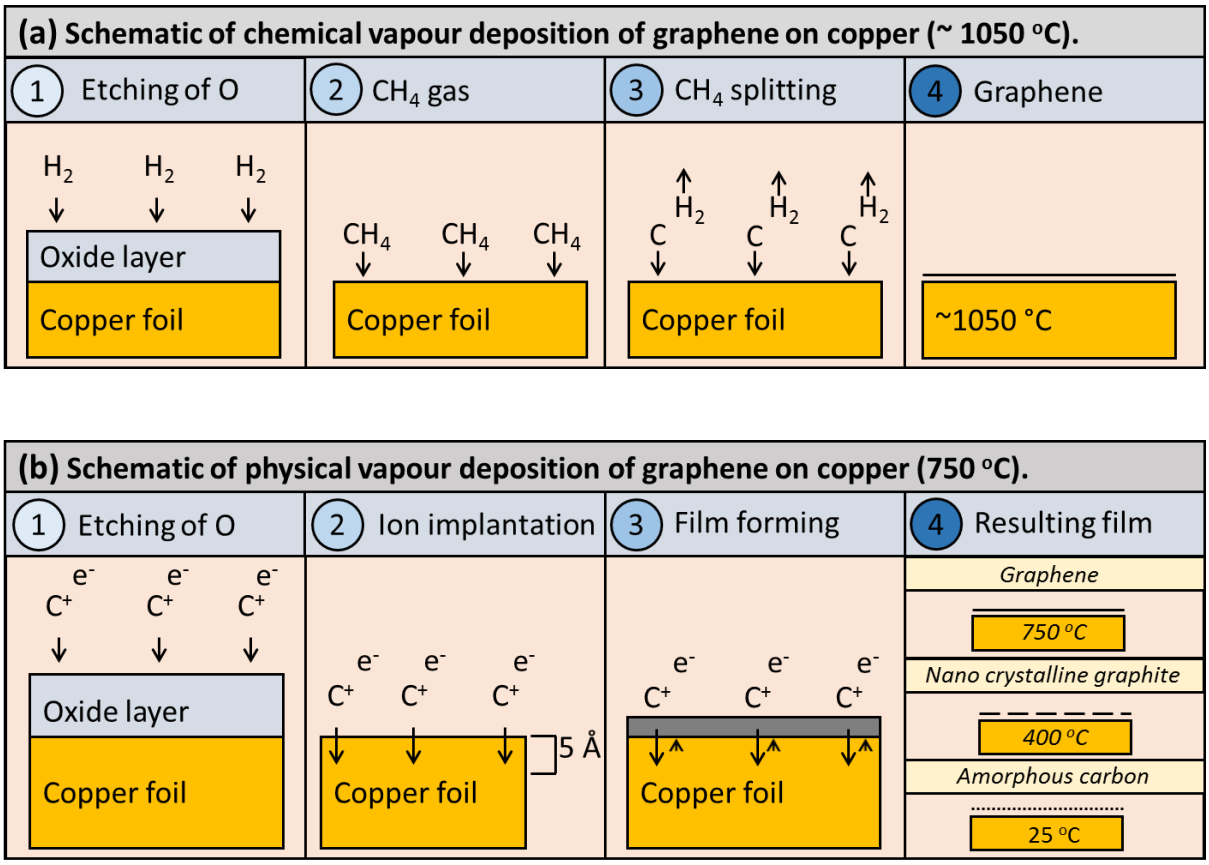

Figure 22: Growth mechanism for (a) CVD and (b) PVD grown graphene on copper foil.

*Figure 22*b shows a schematic of the graphene growth process by PVD. (1) The energetic carbon ions remove oxygen from the surface copper. (2) Stopping and Range of Ions in Matter calculations showed that the energetic carbon ions from the plasma have an average implantation depth of 5 Å. (3) As the carbon ions come to rest on the copper substrate a film is formed. (4) A carbon film can be deposited from carbon ions contained within an energetic plasma at room temperature. As the substrate temperature is elevated from room

temperature to 750 ^{o}C the structure of the deposited carbon changes from amorphous carbon to graphene. At 750 ^{o}C the deposited carbon ions are templated by the surface of the copper foil. Unlike CVD the thickness of the carbon film is not limited by the reaction between the carbon source and the copper foil. As the growth occurs, the thickness increases and the templating effect of the copper substrate reduces leading to a loss of well-ordered graphene layers. As the film becomes thicker ion damage also contributes to a breaking up of the graphene layers. Internal stress in the film may also be a factor disrupting graphene growth as the film becomes thicker.

3.5 Conclusion

This research demonstrates the synthesis of multilayer graphene on both copper substrates at moderate temperature using the PVD method in a FCVA system. These films were characterised for their morphology (SEM and TEM), electrical resistivity and optical transmission. This revealed that good quality multilayer graphene can be synthesised on copper at temperatures of 750 °C**,** with comparable properties to a film grown using CVD at the higher temperature of 1050 °C. The lower temperature required to synthesis graphene using FCVA can be attributed to dynamic annealing which occurs as the film grows from the energetic carbon flux. Furthermore, unlike CVD, the use of a processing gas limits the growth of a graphene and has no positive benefits.

4 Graphene synthesis onto other substrates

After the successfully deposition of multilayer graphene onto copper foil by FCVA in Chapter 3, this chapter will investigate the potential to physically deposit graphene by FCVA onto a variety of alternative substrates.

** Aspects of this chapter have been discussed in the published paper:*

- *D.T. Oldfield, D.G. McCulloch, C.P. Huynh, K. Sears, S.C. Hawkins, Multilayered graphene films prepared at moderate temperatures using energetic physical vapour deposition. Carbon, 2015. 94: p. 378-385.*

4.1 Introduction

It is desirable to develop a method which is capable of depositing graphene on to a range of substrates. The freedom to deposit graphene directly onto any substrate is beneficial for multiple reasons. Such a method would enable graphene to be grown on materials which could be immediately incorporated into device manufacturing. Growing graphene on a desirable substrate removes the need for a transfer process. Transfer processes have been cited by the broader scientific community as being time intensive and costly, as well as capable of inducing damage to the graphene film. For example, CVD grown graphene is commonly removed from the copper substrate by etching with solutions of iron nitrate [98], iron chloride [94] or and ammonium persulfate [99]. While these etchants effectively dissolve the copper substrate, the commonly leave behind oxidized metal particles which contaminate the graphene films. These contaminates are often trapped between the graphene film and the new substrate, resulting in the degradation of the carrier transport proprieties and subsequently leading to a determination the performance of the device. For

these reasons, we will now consider if it is possible to deposit graphene by PVD onto substrates other than copper.

Other than copper, graphene is commonly deposited by CVD onto nickel. A paper published by Obraztsov et al. [72] showed that it is possible to grow few layer graphene of the order of 1 to 2 nm thick on nickel foil with a combination of H_2 and CH_4 at a temperature of 950 ^{o}C. The morphology of the CVD grown graphene is heavily influenced by the morphology of the nickel substrate and the different thermal expansion coefficients of nickel and graphite. This study stated that the growth mechanism of the film was attributed to heteroepitaxy. Later studies would paint a slightly more detailed description of the growth mechanism.

A study published in 2008 which also used a mixture of CH_4 to H_2 by Yu et al. managed to reduce the number of graphene to 3 to 4 layers of graphene [73]. This paper highlighted that controlling the cooling rate is critical for producing graphene films on nickel which are less than 10 layers. The study showed that moderate cooling rates of 10 °C/s were ideal for the formation of graphene and that cooling were faster (20 °C/s) or slower 0.1 °C/s were detrimental. The difference in the quality of the graphene due to the change in the cooling rate was attributed to the segregation of carbon from the nickel substrate. At the slowest cooling rate the carbon of 0.1 °C/s, no carbon peak was observed in the Raman spectrum. The lack of a carbon in the Raman spectrum was justified saying that this indicated that few carbon atoms segregated to the surface and that most of the atoms had diffused into the bulk of the nickel substrate.

The successful isolation of the atomically thin material graphene and it miraculous properties, has inspired scientists to investigate the potential of other 2D atomic crystals, such as isolated mono- and few- layers of boron nitride, molybdenum disulphide, other

dichalcogenides and layered oxides. In turn, the research into other 2D atomic crystals has led to emergence of a new research field concerned with the layering of 2D crystals in order to form heterostructures [118]. While the strong covalent bonds in plane provide stability to the 2D crystal; the relatively weak Van der Waals forces bind the 2D crystals together. Recently several groups have constructed Van der Waals heterostructures. The possibility of making multilayer Van der Waals heterostructures has recently been demonstrated [6, 119-123]. These heterostructures are made by layer 2D atomic crystals with a transfer process. As stated previously, transfer processes are time intensive and costly, and capable of inducing damage. We will now consider the possibility of depositing graphene directly onto boron nitride. Previously, work by Haigh et al. showed that it is possible to stack 2D atomic crystals on top of each other. In this study they created a multilayer heterostructure from graphene and boron nitride layers [121].

Alternatively, some researchers have investigated growth of graphene on thin metallic films. For economic reasons, the synthesis of graphene onto thin metal films is highly desirable. In order to grow defect free graphene, thin metals films should be monocrystalline with minimum mosaic spread and without small angle grain boundaries. Moncystalline rhodium [124] and iridium [125] have been deposited onto a silicon wafers with an yttria-stabilized zirconia (YSZ) buffer layer. The lattice of the YSZ buffer layer templates the metallic film which assists the growth of graphene. Further studied have explored the deposition of carbon films directly onto YSZ using molecular beam expitaxy [126]. The resultant films were described as mainly sp^2 amorphous carbon. Here we consider the YSZ as a growth substrate for the PVD growth of graphene

The preparation of graphene by the thermal decomposition of silicon carbide negates the need for a transfer process and has been suggested as a possible route to wafers sized graphene sheets for electronic applications [127, 128]. Previous investigations have shown that graphene can be grown by sublimating silicon from silicon carbide by annealing at temperatures between ~1000 ^{o}C to 2000 ^{o}C [45, 127, 129]. However a major drawback to this technique is the lack of continuity and uniformity of the grown graphene film. The graphene domains have been found to varying in size on silicon and carbon terminated basal planes from 30 – 100 nm to ~ 200 nm respectively [129]. Furthermore the thermal decomposition of silicon carbide is not a self a limiting process [130].

4.2 Graphene growth on chemical vapour deposited graphene

4.2.1 Introduction

In this section, the growth of graphene onto CVD deposited is investigated. Before considering other substrates, it is important to consider if it is possible to grow graphene directly on graphene.

4.2.2 Experimental

Depositions were performed at floating substrate potential with a constant flux of 2.3x10^{15} atoms/cm^{2}.s at ambient temperature (~ 25 °C), 400 °C and 750 °C to a dose of 3.4x10^{16} atoms/cm^{2}. Carbon films were deposited onto CVD grown graphene on copper. The synthesis of CVD grown graphene is described in section 2.1.1 of this thesis.

4.2.3 Results and discussion

Figure 23 shows the Raman spectra of carbon films deposited in the FCVA system onto CVD grown graphene. Raman spectroscopy of the initial substrate (CVD grown graphene on copper foil) shows the formation of a D, G and 2D peak. The D peak is relatively small

indicating few defects, while the G and 2D peak are approximately the same size indicating multiple layers of graphene. The Raman spectrum of the film deposited at 25 ^{o}C, still displays a D, G, and 2D peak. However, the G peak now has a broad shoulder, which is likely to be contributed from an amorphous carbon layer. The Raman spectrum of the film deposited at 400 ^{o}C also has the D, G and 2D peak. Now however, the D and G is are strongly linked, most likely due a nano crystalline of carbon. The Raman spectrum of the film deposited of the 750 ^{o}C, closely matches that of the substrate. However, the D peak is slightly larger. The increase in the D peak indicates that the energetic flux is damaging the graphene layers. The G peak is slightly broader, and the 2D peak appears slightly shorter indicating more layers of graphene. However, it is clear that it is not possible to grow well ordered graphene on graphene using FCVA. This is due to the loss of the templating effect of the copper substrate and the ion damage from the energetic flux.

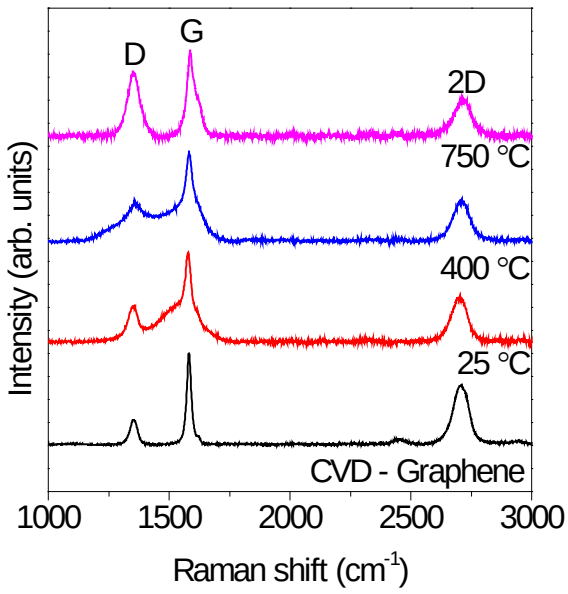

Figure 23: Raman spectroscopy of carbon films deposited on a CVD grown graphene. Also shown is the spectra of the CVD substrate.

4.3 Graphene synthesis onto nickel

4.3.1 Introduction

In this section, the deposition of graphene on nickel using the FCVA is investigated. As outlined above, nickel has been used to successfully grow graphene using CVD.

4.3.2 Experimental

Depositions were performed at floating substrate potential with a constant flux of $2.3x10^{15}$ atoms/cm^2.s at ambient temperature (~ 25 °C), 400 °C and 750 °C. In this study two substrates were used, silicon wafer <100> (bearing a native oxide layer of ~3 nm) and nickel (99.95%) foil. The silicon substrate was used as a control.

4.3.3 Results and discussion

Figure 24a shows the Raman spectra of carbon films deposited onto Nickel at 750 ^{o}C as a function of dose. A carbon dose of $5.7x10^{16}$ atoms/cm^2 shows no Raman signal (Figure 24a), indicating that no carbon film is present. This is despite the fact that this dose is sufficient to produce a carbon film on copper (*Figure 11*a). A dose around ten-fold higher than that used for copper is required to give a similar Raman signal. The difference is attributed to the high solubility of carbon in nickel [73], leading to little carbon on the surface of the nickel.

In the case of CVD growth of graphene it is known that the nickel substrate cools, carbon solubility decreases and graphene precipitates at the surface. This is in contrast to graphene formation on copper, in which carbon is insoluble, involves an epitaxial process. The results of Figure 24a suggests that the growth process of graphene on nickel by CVD and FVCA share some similarities. As the dose is increased, the Raman spectra follow a similar trend to that observed for copper. A Raman signal is observed for a dose of $2.3x10^{17}$ atoms/cm^2 but has a large D to G peak ratio indicating high disorder. As the dose is further increased

($4.6x10^{17}$ atoms/cm^2), a strong, sharp G peak, a relatively small D peak and a G to 2D peak ratio of 0.7 is observed, indicative of multilayer graphene. With a further increase in dose ($5.7x10^{17}$ atoms/cm^2) the D/G peak ratio increases again indicating that greater disorder is introduced into the film. These results suggest either that the nickel reaches a saturation level and some disordered carbon accumulates on the surface, or that the excessive concentration of dissolved carbon precipitates too quickly and hence chaotically.

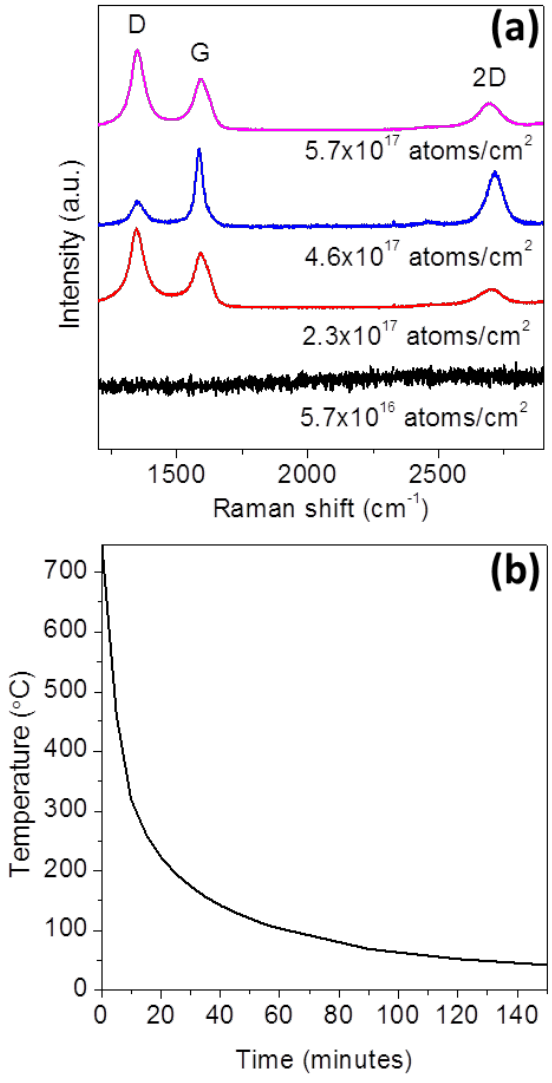

Figure 24: (a) Raman spectra showing the effect of dose on carbon films deposited onto nickel at 750 °C. (b) Cooling rate of films grown in the FCVA.

It has been well documented that the rate at which the nickel substrate cools affects the growth of graphene by CVD [131]. Cooling too fast reduces the mobility of the carbon atoms before they can diffuse, thus limiting the amount of carbon atoms which precipitate at the surface. An appropriate cooling rate of ~10 °C/s leads to the growth of multilayer graphene. Too slow a cooling rate of 0.1 °C/s prevents carbon atoms from oversaturating and precipitating at the surface as they have enough time to diffuse deeper into the nickel substrate [73]. The cooling rate of our system (Figure 24b) in the initial stage is approximately 1 °C/s which is within the favourable range reported in the literature [73, 131] and supports the proposition that the growth mode in FCVA is similar to CVD.

The Raman spectra for films deposited at a dose of 2.3×10^{17} atoms/cm^2 on silicon at different temperatures (Figure 25a) show a similar development to the films deposited with a dose of 4.6×10^{16} atoms/cm^2 (Figure *6*a) but with a considerably stronger signal and also with some indication of improved graphitisation at the highest temperature. Deposition of 2.3×10^{17} atoms/cm^2 on nickel at different substrate temperatures (Figure 25b) follows a similar pattern to that for 4.6×10^{16} atoms/cm^2 on copper (Figure *6*b) with the lowest temperature (25 ^{o}C) giving a broad asymmetric Raman peak which is split into D and G peaks at 400 ^{o}C and fully resolved at 750 ^{o}C. These results suggest that as with copper, a 750 ^{o}C substrate temperature is required for the growth conditions to be suitable for graphene growth.

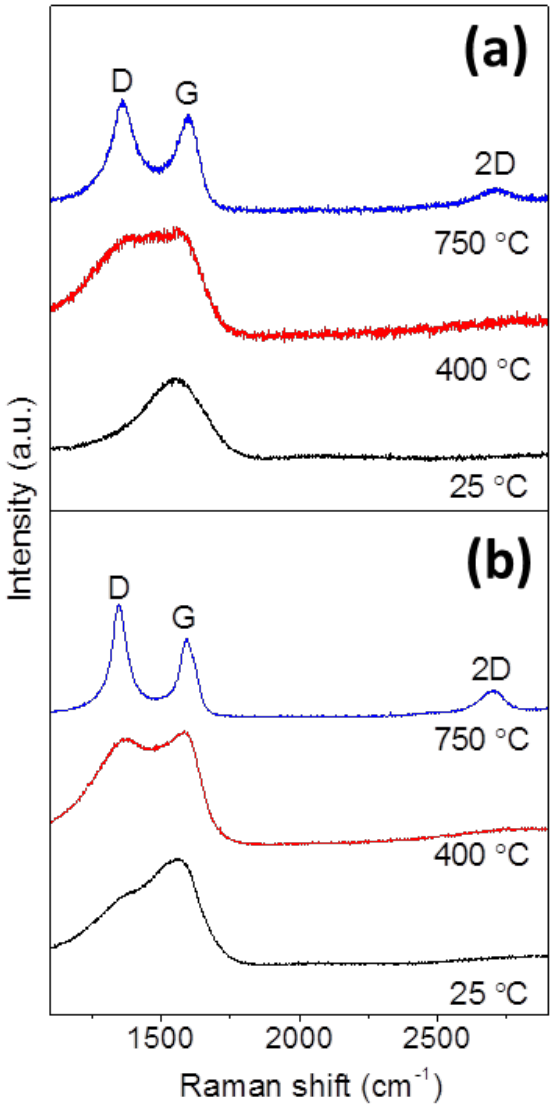

Figure 25: Raman spectra showing the effect of temperature on carbon films deposited on to (a) silicon and (b) nickel with a dose of 2.3x10^{17} atoms/cm^2.

All the films deposited on nickel are much rougher than those grown on copper. This roughness likely originates from the finer grain structure of nickel compared to copper (as revealed by SEM images, which are not shown here). The SEM images show a clear change in morphology with dose (Figure 26). The most uniform film is achieved at the intermediate dose of 4.6x10^{17} atoms/cm^2, in agreement with the Raman measurements which showed this film to be the least defective. At the lower dose (2.3x10^{17} atoms/cm^2), the surface is

more fragmented with what appear to be fine particles across the surface, while at the higher dose ($5.7x10^{17}$ atoms/cm^2), there appears to be a thick over-coating of disordered material. Optical microscopy of the graphene film grown with a dose of $4.6x10^{17}$ atoms/cm^2 (*Figure 26*d) displays domains which are less than 10 µm in size.

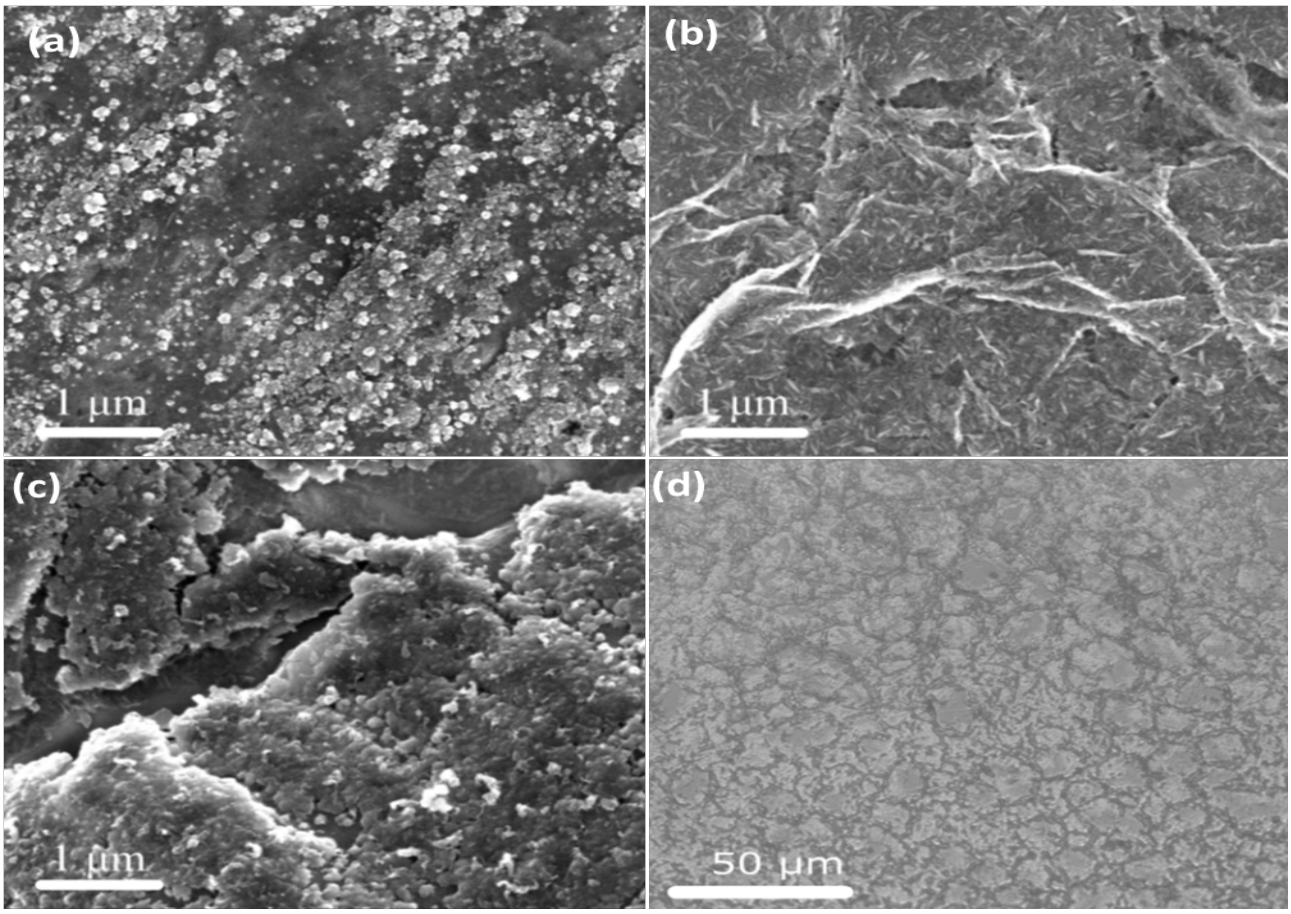

Figure 26: SEM showing graphene etched off the nickel substrate deposited with a dose of (a) $2.3x10^{17}$, (b) $4.6x10^{17}$ and (c) $5.7x10^{17}$ atoms/cm^2 grown at 750 ^oC. (d) Optical microscopy of the graphene film grown with a dose of $4.6x10^{17}$ atoms/cm^2

Figure 27 shows the XANES collected from carbon films grown at a dose of $2.3x10^{17}$ atoms/cm^2 on nickel foil at 750, 400 and 25 ^oC. The XANES were collected with the sample orientated at angles of 20, 55 and 90^o to the x-ray beam. *Figure 27*a shows the XANES measured for the film grown at 750 ^oC. As previously discussed; the XANES of

graphene films grown at these temperatures can be characterised by three regions by specific resonance energies: π* peak at 285 eV, the C=O peak at 288.5 eV and the σ* doublet located between 290 eV – 315 eV. Angular dependence between the π* and σ* peaks are typical of XANES collected of oriented graphene. However there is less angular dependence evident in the spectra, likely a result of increased surface roughness.

The XANES for the carbon film deposited with a dose of 2.3×10^{17} atoms/cm^2 at 400 ^{o}C is shown in *Figure 27*b. The σ* doublet is no longer present, which indicates a change in the atomic arrangement of the carbon atoms in the film to one with more in-plane graphitic disorder. The XANES for the film grown at 400 ^{o}C agrees favourably with the Raman spectrum for this film. The Raman spectrum for this film comprised of a broad G peak with shoulder, which is typical of nanocrystalline graphite.

Lastly, the XANES spectrum for the film grown at the lowest deposition temperature (25 ^{o}C) can be seen in *Figure 27*c. For this film the σ* doublet is absent and the C=O has almost disappeared indicating the presence of amorphous carbon, as seen in the Raman results for this film (*Figure 25*).

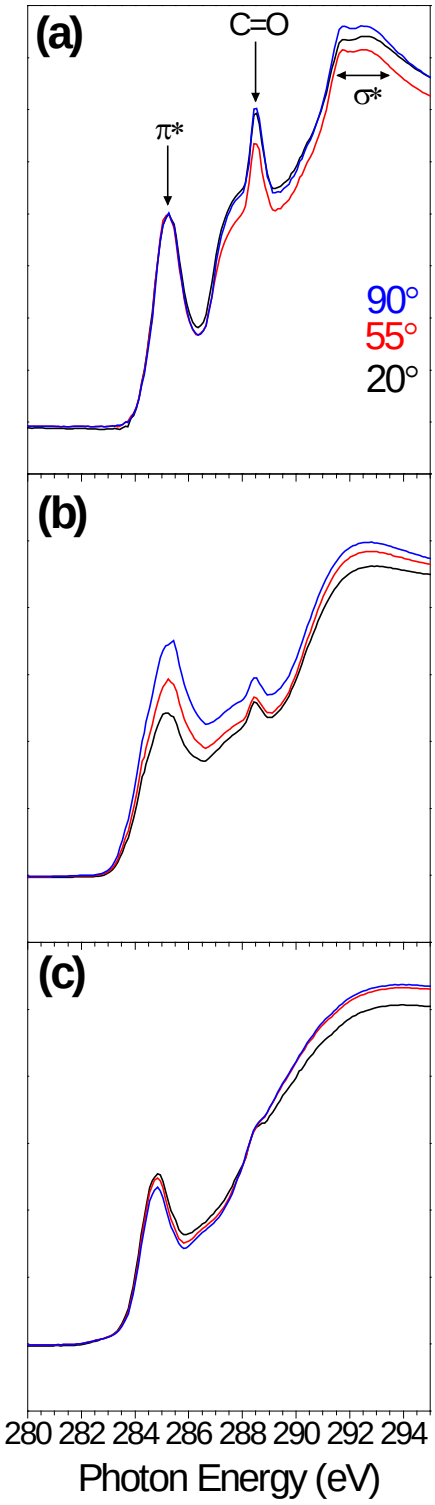

Figure 27: XANES spectrum of FCVA deposited carbon films grown on Ni at (a) 750, (b) 400 and (c) 25 ^{o}C at a dose of 2.3x10^{17} atoms/cm^{2}.

Figure 28 shows the XANES collected from carbon films grown at different doses on nickel foil at 750 ^{o}C. The XANES were collected with the sample orientated at angles of 55 and 90^{o} to the x-ray beam. Figure 28a shows the XANES measured for the films grown at a dose of 4.6x10^{17} atoms/cm^{2}. The strong angular dependence of the π* and σ* peaks are typical of XANES collected from oriented graphene layers.

The XANES spectra for the carbon films deposited with a lower dose of 2.3x10^{17} atoms/cm^{2} are shown in Figure 28b. The angular dependence of the π* and σ* peaks has been significantly reduced compared to the film prepared at 4.6x10^{17} atoms/cm^{2}. The decrease in the angular dependence is a result of a reduction in orientation for this carbon film as the lower dose has led to the growth of a discontinuous film. Furthermore the poor angular dependence is supported by the previously collected Raman spectroscopy. The defect ratio from the Raman for this film indicates a high number of defects; additionally a weak 2D peak was observed indicating little evidence of stacked graphene layers.

Finally, the XANES spectrum for the film grown with smallest dose of carbon (5.7x10^{16} atoms/cm^{2}) can be seen in Figure 28c. For this film the σ* doublet is almost completely absent, indicating no in plane graphitic order. This result is consistent with the Raman spectra for this sample, which was absent of peaks. The strong C=O peak indicates that this film contains a significant amount of oxygen. At this low dose, it is likely that the XANES, which is highly surface sensitive is probing a thin surface amorphous layer.

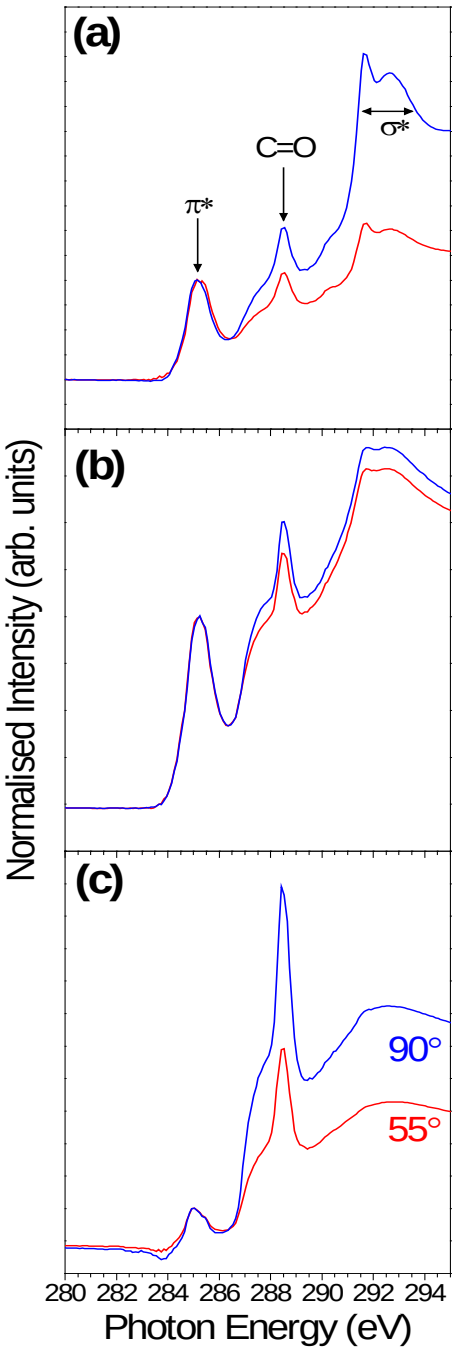

Figure 28: XANES spectrum a FCVA deposited carbon films grown at 750 ^{o}C on Ni at a dose of (a) 4.6x10^{17}, (b) 2.3x10^{17} and (c) 5.7x10^{16} atoms/cm^{2}.

Figure 29 shows a low magnification cross-sectional TEM image of the film grown on nickel to a dose of 4.6x10^{17} atoms/cm^{2} grown at 750 ^{o}C. The image shows there is a variation in the carbon film thickness which may correlate with the underling nickel grain structure.

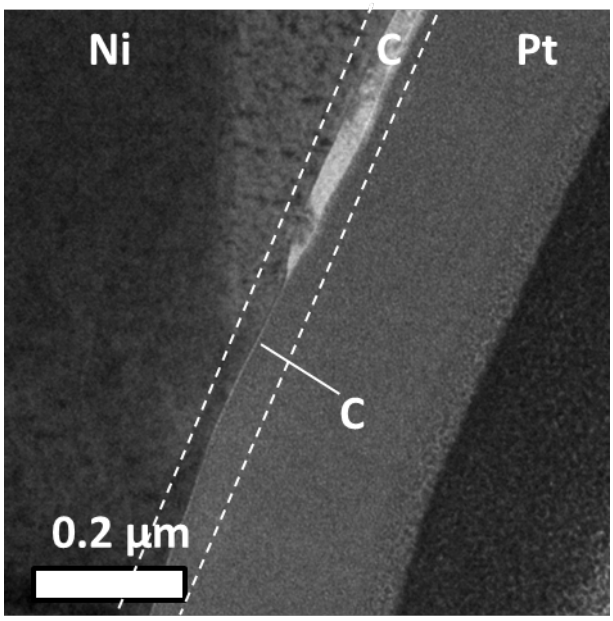

Figure 29: Low magnification cross-sectional TEM image of the film grown on nickel to a dose of $4.6x10^{17}$ atoms/cm^2 grown at 750 ^oC, showing a variation in the carbon film thickness.

Figure 30 shows cross-sectional TEM images from different regions of a film grown on nickel to a dose of $4.6x10^{17}$ atoms/cm^2, grown at 750 ^oC. In contrast to films grown on copper (Figure 15), the TEM images of the film grown on nickel is highly non-uniform with the number of graphene layers ranging from around 5 (Figure 30a) to 80 (Figure 30c) depending on the location. In the case of CVD grown graphene on nickel, variations in the film thickness have been observed and attributed to differences in the growth rates depending on the orientation of nickel grains [74]. Therefore, given their low spatial resolution both the Raman and XANES analysis in the previous sections will only provide an average of all the different thicknesses present.

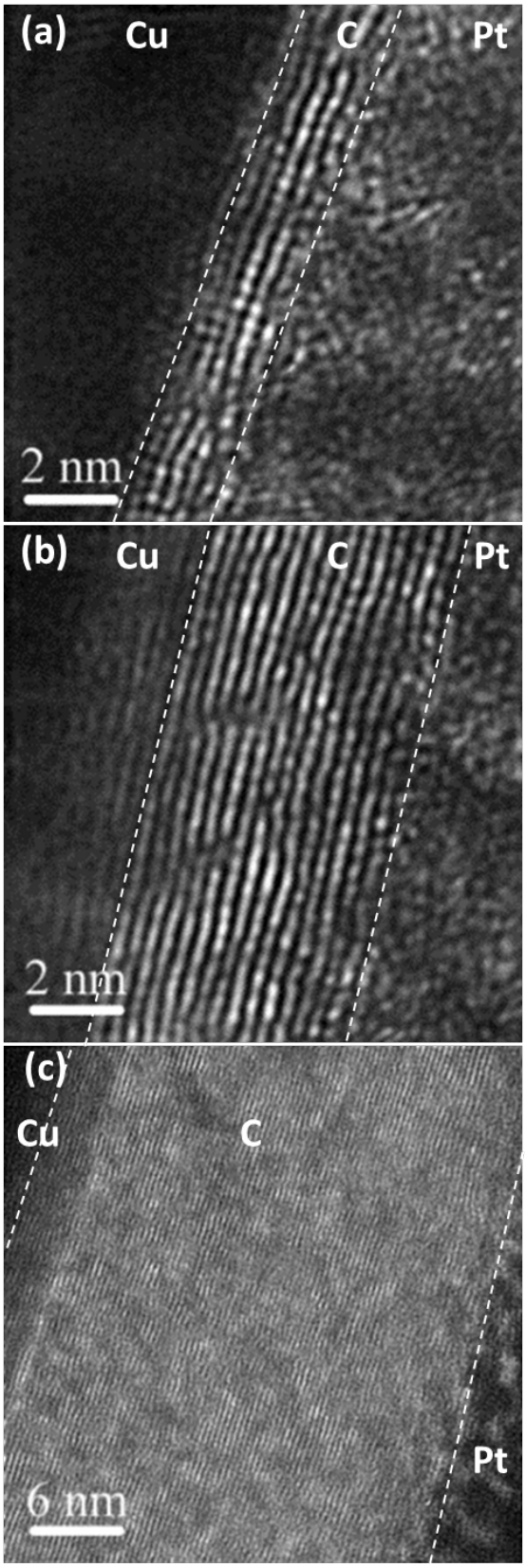

Figure 30: TEM images of three different regions of the film grown on nickel to a dose of 4.6x10^{17} atoms/cm^2 grown at 750 ^{o}C, showing (a) ~ 5, (b) ~ 15 and (c) ~ 80 layer graphene.

The sheet resistance as measured by 4PP and by 2PP for the films grown on copper (*Figure 16*) are in fair agreement, but diverge markedly for all films on nickel (*Figure 31*), with the 4PP being consistently higher. The number of graphene sheets on nickel is not uniform (*Figure 30*) and thus it is likely that the four point probe will only form a contact with the graphene high points. Whereas the silver-paint contacts used in the 2PP method will cover all the exposed sheets of graphene thus providing a more reliable contact and measuring lower resistivity values.

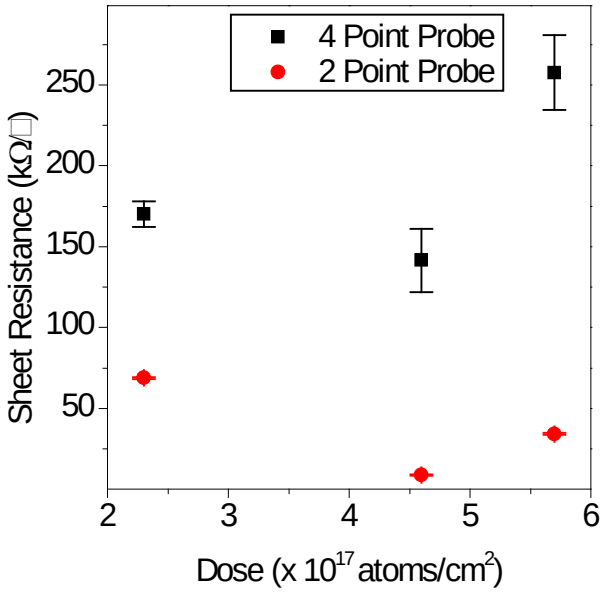

Figure 31: Sheet resistance of graphene etched off nickel substrates grown at 750 °C to the doses indicated.

Figure 32 shows the transmittance of films grown on nickel at 750 °C. Much lower transmission (34-60%) is observed for the nickel samples (*Figure 32*) compared to the copper ones (80-90%) (*Figure 17*), consistent with the large variation in the number of layers evidenced by TEM.

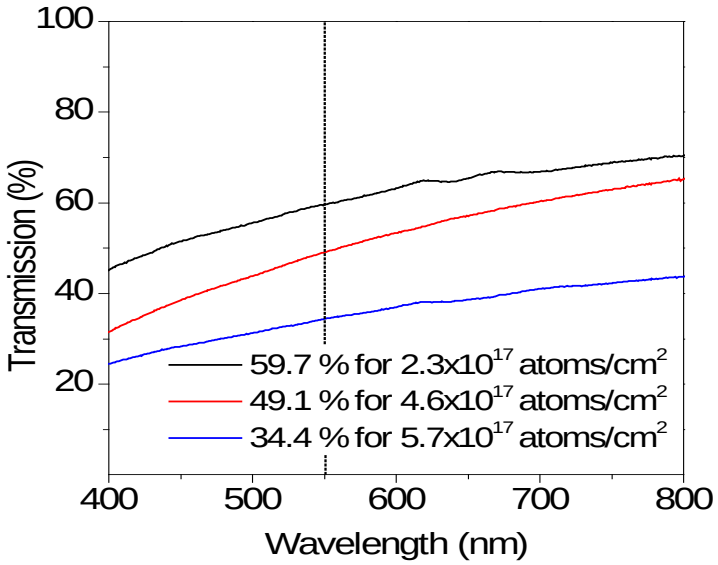

Figure 32: Transmittance of graphene films grown on nickel substrates at a temperature of 750 ^{o}C, to the doses indicated.

The number of graphene layers estimated from the optical absorbance [117] is compared with the number equivalent calculated from the carbon dose (*Table 2*). Thus the 4.6x10^{17} atom dose on nickel appears by TEM to comprise of a number of graphene sheets ranging between 5 to 80 layers (*Figure 30*). The optical transmittance of 49.1% is consistent [117] with an average film thickness of 23 graphene layers which falls within this range.

Table 2: Dose equivalent thickness in graphene layers compared with calculated number from measured optical transmittance.

	Carbon Dose Atoms /cm^2 x 10^{16}	**Equivalent thickness nm**	**Equivalent no of Graphene layers**	**Measured Transmittance %**	**Calculated no of Graphene layers [38a]**
Graphene on nickel	23	20.3	59.7	59.7	23
	46	40.6	119.4	49.1	33
	57	50.3	147.9	34.4	54

4.3.4 Model for the growth of filtered cathodic vacuum arc graphene on nickel

In this chapter, we have shown that it is possible to physically deposit graphene onto nickel foil at 750 ^{o}C using a carbon plasma generated by FCVA. We will now compare the growth model for graphene on nickel by CVD against our proposed growth model for the formation of FCVA deposited graphene on nickel.

*Figure 33*a shows a schematic of the graphene growth process by CVD on nickel. (1) Free hydrogen gas molecules act as an etchant, capable of removing oxygen from the nickel surface. (2) Similar to the growth of graphene on copper foil, CH_4 is commonly used as the hydrocarbon precursor to grow graphene on nickel via CVD. At temperatures around 1000 ^{o}C the hydrocarbon is split and the (3) carbon atoms are absorbed into the nickel substrate. (4) Over a period of time, the annealed sample is allowed to cool and the absorbed carbon atoms precipitate back to the surface during this cooling phase. (5) The precipitation of the carbon atoms is strongly influence by the rate of cooling. Different cooling rates lead to different segregation behaviours, which consequently affect the thickness and quality of the graphene film. An extremely fast cooling rate results in the carbon atoms losing their mobility before they are able to diffuse to the surface. A medium cooling rate allows for a finite amount of carbon atoms to segregate to the surface of the nickel substrate, ideal for growing graphene with 10 or less sheets. A slow cooling rate allows the carbon atoms diffuse deep into the bulk of the substrate, resulting in few carbon atoms segregating to the surface of the substrate. Additionally the graphene film is strongly influenced by the morphology of the nickel substrate. The annealing of the nickel foil leads to the formation of domains. At the grain boundaries of the nickel substrate, a higher rate of carbon atom precipitation is commonly observed, resulting in the formation of thicker graphene films.

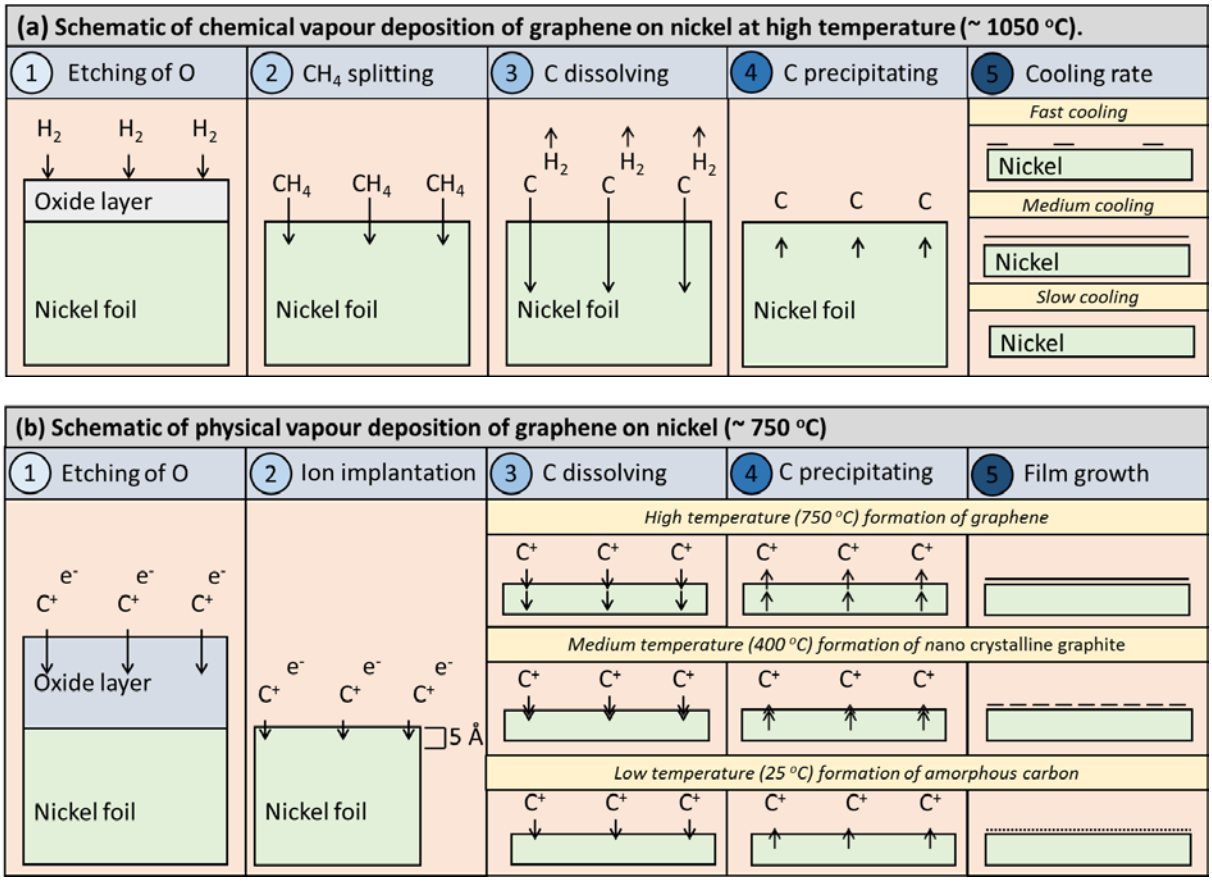

Figure 33: Growth mechanism for (a) CVD and (b) PVD grown graphene on nickel.

*Figure 33*b shows a schematic of the graphene growth process by FCVA on nickel. (1) The energetic carbon ions remove oxygen from the nickel surface. (2) SRIM calculations have shown that the carbon ions have an average implantation depth of 5 Å. (3) The carbon atoms are absorbed into the nickel substrate. The carbon solubility in nickel increases as a function of temperature [132]. (4) Upon cooling the carbon atoms precipitate back to the surface. A change in deposited dose was found to affect the amount of carbon atoms which precipitated to the surface, in a similar fashion to how the cooling rate in CVD influences precipitation rate. (5) In FCVA carbon deposition can lead to the growth of a film on nickel at room temperature, but this film has an amorphous structure as indicated by the Raman spectroscopy (*Figure 25*) and XANES (*Figure 27*). As the temperature of the substrate is

elevated to 750 ^{o}C the precipitated carbon film has a graphene microstructure. The morphology of nickel substrate was found to affect the precipitation of the carbon atoms as shown by TEM (Figure 29 and *Figure 30*), resulting in a variation in the thickness of the graphene film.

4.4 Deposition of carbon film on hexagonal boron nitride

4.4.1 Introduction

In this section, the growth of graphene on hBN is investigated. The growth of graphene onto BN, would be beneficial for the production of heterostructures made from 2D crystals.

4.4.2 Experimental

Depositions were performed at floating substrate potential with a constant flux of 2.3x10^{15} atoms/cm^{2}.s at ambient temperature (~ 25 °C), 400 °C and 750 °C to a dose of 3.4x10^{16} atoms/cm^{2}. Substrates of hBN were used for the growth of graphene, and were supplied by Roland Yingjie Tay from the School of Electrical and Electronic Engineering at Nanyang Technological University Singapore. These hBN flakes were grown using the method described in a study by Tay et al. [133].

4.4.3 Results and discussion

A carbon film was deposited by FCVA at 750 ^{o}C onto CVD grown hBN still sitting on copper foil. SEM micrographs (Figure *34*) shows that the hBN flakes are still present after the deposition of the graphene film. Furthermore, it is worth noting that the size and density of the asymmetric hBN flakes is much greater than the triangular flakes. On average, the triangular boron nitride flakes are approximately 2 μm whereas the asymmetric hexagons boron nitride flakes are approximately 4 μm.

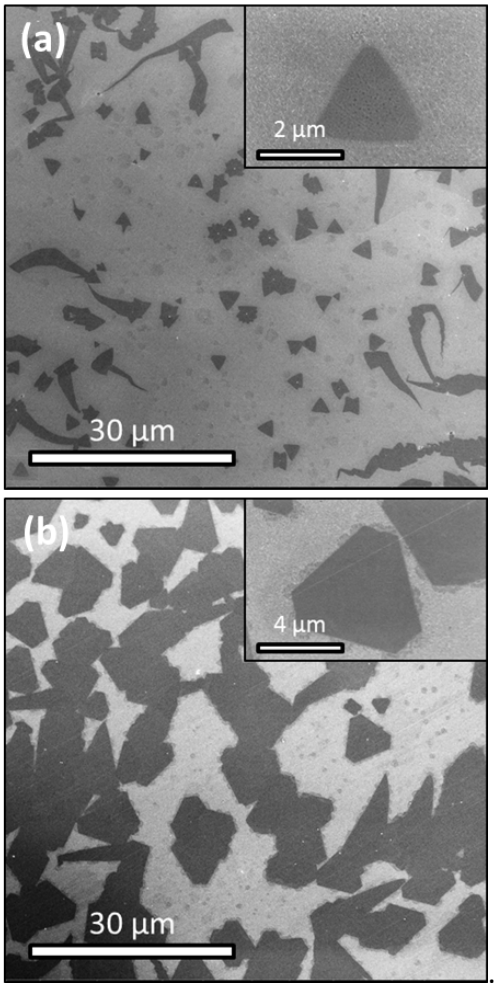

Figure 34: SEM micrographs of the (a) triangle and (b) asymmetric hBN flakes on copper foil. The insets show the boron nitride flakes after the deposition of graphene.

Raman spectra were collected from regions of high populations of either triangular or hexagon hBN. *Figure 35* shows the Raman spectra of carbon films deposited at 25 ^{o}C or 400 °C and 750 ^{o}C, grown with a dose of 3.4x10^{16} atoms/cm^{2} on hBN. The Raman spectrum for a film deposited on silicon at 25 ^{o}C shows a broad asymmetric peak at ~1500 cm^{-1}, representing amorphous carbon. This peak is broadened at a deposition temperature of 400 ^{o}C, and resolved at 750 ^{o}C into two peaks at ~1350 cm^{-1} and ~1580 cm^{-1}. At a growth temperature of 750 ^{o}C a 2D peak is observed at ~2700 cm^{-1}. The presence of the D and G peaks, with the 2D peak indicates the presence of graphene.

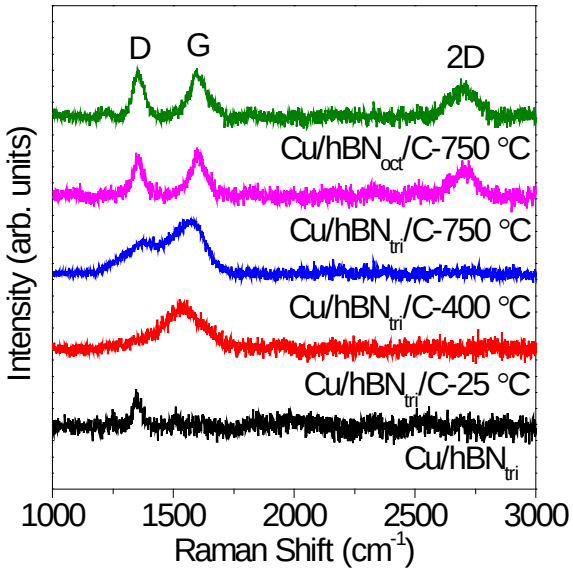

Figure 35: Raman spectroscopy of carbon films grown at temperatures between room temperature and 750 ^{o}C, on copper foil with triangular flakes of boron nitride. Also included is a Raman spectrum of a carbon film deposited at 750 ^{o}C onto copper foil with hexagonal boron nitride.

Raman spectra were collected from carbon films deposited at 750 ^{o}C onto copper foil with hexagonal flakes of hBN. The Raman spectra of the deposited carbon films is compared against the spectra from the triangular flakes. The Raman spectra for the substrate, shows a peak at ~1366 cm^{-1} which can be attributed to hBN [134]. For the deposited films, the D (1350 cm $^{-1}$), G (1580 cm^{-1}) and 2D (2700 cm^{-1}) peak are all present indicating that graphene is present. The defect ratio and intensity ratio for the carbon film deposited onto triangular boron nitride flakes is similar to that of the film grown on the asymmetric hexagons boron nitride flakes. These results suggest that it may be possible to grow graphene directly onto hBN using FCVA. At the time that this thesis was completed, further work was underway to explore the nature of the graphene / hBN material using TEM.

4.5 Deposition of carbon film on onto yttria-stabilized zirconia and silicon carbide

4.5.1 Introduction

In this section, the growth of graphene on YSZ and SiC by PVD is investigated. As discussed earlier, both YSZ and SiC have been previously used to growth graphene. YSZ has been used to template copper films used for the growth of graphene. It would be of interest if YSZ could directly provide a template for carbon ions to form a graphene film, without the need for a catalytic layer. Graphene has been successfully grown by thermal decomposition of silicon carbide.

4.5.2 Experimental

Depositions were performed at floating substrate potential with a constant flux of $2.3x10^{15}$ atoms/cm^2.s at ambient temperature (~ 25 °C), 400 °C and 750 °C to a dose of $3.4x10^{16}$ atoms/cm^2. Carbon films were deposited onto YSZ from MTI corporation; and onto SiC substrates from University Wafer.

4.5.3 Results and discussion

The growth of a film by CVD is dependent on a reaction between the substrate and the processing gas. In PVD, a film can be energetically deposited onto any type of substrate. Hence, we explored the possibility of depositing graphene onto yttrium stabilised zirconia and silicon carbide. Figure 36 shows the Raman spectra of carbon films deposited onto YSZ and SiC at a growth temperature of 750 ^{o}C. The Raman spectra of the YSZ and SiC substrate before the deposition, is also included in the Figure 36.

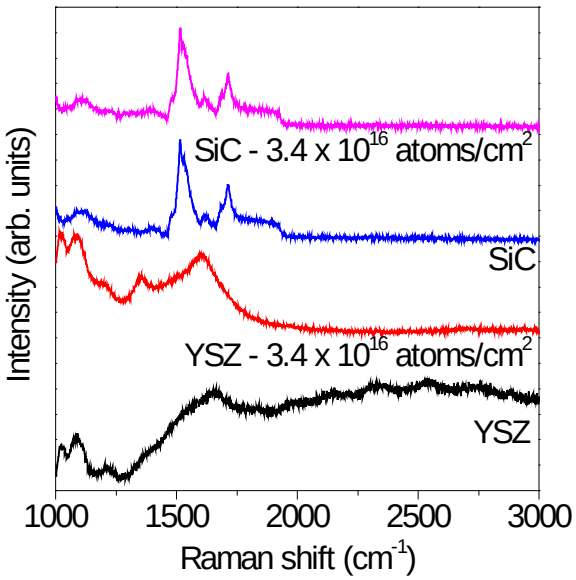

Figure 36: Raman spectra of carbon films deposited on YSZ and SiC substrates at growth temperatures of 750 ^{o}C at a dose of 3.4 x 10^{16} atoms/cm^2. Also show is the Raman spectra of the substrates prior to the deposition.

Two key changes can be seen in the Raman spectra of the carbon films deposited on YSZ. The spectra left of 1500 cm^{-1} is slightly elevated when compared against that of the substrate. The elevation in spectra is likely due a contribution in counts from the carbon film. For the films grown at 750 ^{o}C on YSZ an extra peak can be observed at 1350 cm^{-1} (D peak). Furthermore the peak seems slightly sharper at ~1550 cm^{-1} which is the location of the G peak. A strong 2D peak is not observed at 2700 cm^{-1}. These Raman spectra suggest some graphitic bonding, indicating that there is a polycrystalline coating rather than graphene. No observable difference was observed in the Raman spectra of carbon films deposited onto SiC. It is possible that higher temperatures are required to deposited graphene by physical vapour deposition onto SiC.

4.6 Conclusion

In this chapter the growth of graphene on graphene, nickel, hBN, YSZ and SiC was investigated. The results showed that is not possible to grow graphene with few defects by FCVA on CVD grown graphene at 750 ^{o}C as the energetic flux introduces defects in the film. This research demonstrated the synthesis of multilayer graphene on nickel substrates at moderate temperature using FCVA. Higher carbon doses were required to produce graphene layers compared to that required for growth on a copper substrate. This result is due to a change in the growth mode, which occurs by precipitation from the nickel substrate. These films are found to be non-uniform in thickness, indicating that the grain structure of the nickel substrate influenced the growth of graphene layers. Promising results were present for the growth of graphene on hBN at 750 ^{o}C using FCVA. The presence of the D and G peaks, with the 2D peak indicates the presence of multilayer graphene, however further work is required to confirm this result. No evidence for graphene was found on YSZ and SiC substrates following depositions at 750 ^{o}C using FCVA.

5 Graphene synthesis on copper film

In this chapter, the result for the synthesis of graphene on copper films by FCVA is presented. Included are the deposition of suitable Cu films to act as growth surfaces for graphene and the transfer of graphene on the underlying substrate.

** Aspects of this chapter have been discussed in the published paper:*

- *D.T. Oldfield, C.P. Huynh, S.C. Hawkins, J.G. Partridge, D.G. McCulloch. Synthesis of multi-layer graphene films on silica using physical vapour deposition. Carbon, 2017. 123: p. 683-687.*

5.1 Introduction

The synthesis of graphene device layers on CMOS compatible substrates is advantageous for an increasing number of applications, including dye-sensitized solar cells [135], super capacitors [136], biosensors [137], nano-electronics [138] and batteries [139]. Large areas of graphene (up to 1 cm^2) have been grown on metallic templating surfaces such as copper [98]. Whilst it has been demonstrated that large area graphene can be grown on silica directly without the need for a catalyst [140] and in atmospheric pressure CVD systems [141], the growth rates achieved are so low that the growth processes take many hours to complete. A motivation for this work was to deposit graphene at moderate temperatures in short periods (minutes or less) using a scalable method. With regard to the latter, FCVA is a proven method for large scale deposition of high quality carbonaceous films [142]. Furthermore, this method would enable transfer to a wide range of substrates, requires no toxic gases and is achieved with low system cost.

Several authors have reported methods for the transfer of graphene from metallic template layers to other substrates such as silica [111, 143]. An alternative approach is to grow graphene on copper films deposited onto silicon or silica [54, 144]. Subsequent sacrificial etching of the copper film then enables transfer of the graphene directly onto the underlying substrate. This method of transfer reduces the probability of damage to the graphene when compared with transfer from a separate metallic foil substrate [144]. Transfer of CVD grown graphene to an underlying substrate has been demonstrated using evaporated and/or sputtered copper under-layers [54, 144]. However, further simplification of the process would be achieved if the graphene and copper films could be deposited in a single vacuum system.

In chapter 3 and 4, we showed that it is possible to grow graphene films on copper and nickel foils using the carbon plasma generated by a FCVA [68]. Our results showed that the energetic carbon flux enabled graphene to grow at higher rates and lower temperatures (~750 ^{o}C) than typical for conventional CVD. The FCVA technique can also produce other high quality films, including a range of metals, nitrides and oxides [145, 146]. In particular, it is possible to prepare low roughness copper films with the preferred crystallographic orientation suitable for graphene growth [147]. Here, FCVA is used to prepare both copper under-layers and carbon over-layers with varying microstructures including that of graphene.

5.1.1 Graphene grown on copper films

A study by Tao et al. (2012) investigated the deposition of CVD grown graphene on evaporated copper films [54]. The report claims up until their work the quality of graphene on evaporated copper has been poor compared to graphene grown on copper foil. They

attribute the difference in the quality of deposited graphene to the difference in the thermal, chemical and physical growth characteristics of evaporated copper and copper foil.

The study [54] reported the growth of CVD graphene at 900 ^{o}C with CH_4 but without the presence of H_2 gas on evaporated copper. The study claims that the reason they did not require H_2 gas stemmed from the preferred crystal orientation of the evaporated copper films and the subsequent interaction with the carbon precursor. For this study, the group used an electron beam to evaporate copper film 0.5 – to 1 μm thick, onto a silicon wafer with a 300 nm thick oxide layer. Their procedure involved annealing the copper films with H_2 gas, and then growing graphene by introducing an ultra-high purity CH_4 gas. It was observed that with an increase in the thickness of the copper film, the minimum temperature required to grow graphene increased. Secondly, it was noted that intensity of the D-peak decreased as the H_2 to CH_4 ratio decrease. For films grown without the addition of H_2 gas, the D-peak in the subsequent carbon films was not measurable. Finally the reported pointed out that the graphene closely followed the grains of the copper films, whereas traditionally on copper foil the graphene film will traverse the boundary.

The paper made the following postulate as to why the use of H_2 gas during the growth phase was detrimental. The adsorption of hydrogen for (111) and (110) is higher than that of (200) copper face [148, 149]. Hence, during the annealing phase the (111) surface of the copper film adsorbed large amount of hydrogen which diffused back out to the surface during the growth phase and helped to promote the growth of monolayer graphene. Whereas, the (200) surface of the copper foil did not show a difference in hydrogen content as a result of annealing in H_2 gas.

5.1.2 Graphene grown on nickel films

Graphene has also been grown on nickel films. In a study by Juang et al. published in 2009 [46], the group presented a method for growing millimetre scale graphene films on SiC. Electron beam evaporated nickel film, 200 nm thick, was deposited onto SiC, which under rapid heating extracted the carbon from the SiC substrate. During the cooling phase, carbon atoms precipitated to the free side of the nickel film and formed single and few layer graphene. The nickel coated SiC was placed in a vacuum chamber which was held at a pressure of 10^{-7} Torr. The sample was brought to a temperature of 750 ^{o}C at a rate of 25 ^{o}C/s heating rate and then was immediately cooled at a rate 10-20 ^{o}C/s.

In a study published in 2010 by Lahiri et al., a novel method for the formation of graphene on nickel on silicon carbide [150] was discovered. At temperatures below 460 ^{o}C, the hydrocarbon ethylene was unable to dissolve into the surface of the silicon carbide coated nickel. Hence the growth of graphene did not occur by participation of dissolved carbon atoms as regularly seen at higher temperatures but rather from the slow transformation of the hydrocarbon into graphene. The growth of graphene on not only copper films but also and on nickel films highlights the potential that using films as growth surfaces offer.

5.1.3 Transfer of graphene from thin films

A study published in a letter to nature by Gao et al. in 2014 [144] demonstrated a technique for transferring graphene onto silica in process that they referred to as face to face transfer. The method involved, treating the Si/SiO_2 with a nitrogen plasma, sputtering a 700 nm copper film onto the substrate, growing graphene with an inductively coupled plasma CVD reactor, then coating the sample with PMMA before etching the copper film.

The group cited numerous reasons for why this method for transferring graphene is advantageous to other transfer processes such as dry and wet etching. While dry etching is capable of transferring a 30 inch graphene film [99], the process commonly results in plenty of cracks, folds and wrinkles [143]. Furthermore, wet etching is difficult to scale up and also often results in the warping, rippling and rolling of the graphene film.

In contrast the face to face method does not need to be done by hand and is therefore not manually intensive. The transfer size is only limited by the size of the underlying wafer. During the transfer, the graphene film spontaneously attaches to the underlying substrate, thus making the transfer process fast. Furthermore the copper film is much thinner than copper foil; hence the etching time is much shorter.

The group noted the follow observations about their transfer process. It was found that if the copper layer became too thick; than the PMMA coated graphene would be delaminate during the transfer process. The PMMA graphene layer is not necessarily damaged during the transfer process, as it acts as a soft membrane which is capable of elastic deformation as is it pulled closer to the substrate. As in wet etching, water can exert forces on the transferred graphene resulting in ripples and folds. The water tension can be mitigated by adding isopropyl alcohol or by increasing the water temperature to 80 ^{o}C. In the Raman spectrum of the as deposited graphene film the D peak was not present. After the transfer of the graphene film a D peak was observed, indicating that damaged had occurred.

5.1.4 Copper films deposited by filtered cathodic vaccum arc

FCVA has been used to deposit a range of films, including copper films. FCVA deposited copper films could be ideal growth surfaces for graphene. Previously FCVA deposited copper

films have been grown mainly for the purpose of electronic inter connects, not for the growth of graphene.

In a study by Lau et al. [151], the structural and electrical properties of copper films deposited by FCVA with a bias between 0 to -600 V was investigated. The motivation for the investigation was inspired by the extreme likelihood that copper is quickly becoming the main on-chip conductor, replacing the use of aluminium. Copper is advantageous to aluminium for several reasons. First copper has a lower resistance than aluminium. Furthermore copper has a higher mass and melting point making it less susceptible to electro migration. However, copper is known to be a fast diffuser. Thus it is important to make a diffusion barrier to prevent the contamination. Prior to this study the FCVA had been shown to be capable of depositing diffusion barriers from tantalum and tantalum nitride [150].

The deposited films were between 25 nm to 400 nm to thick, the resistance was highest for the thinnest copper film, with a value of 3.6 μΩ.cm. Above 135 nm thick, the resistivity of the copper films found to be ~1.8 μΩ. The higher resistivity was in part due to the smaller copper grain size which were present in thinner copper films. As the thickness of the copper film increased so did the copper grain size. For a film 365 nm thick copper film the copper grain sized varied between 250 – 600 nm. The increase in the grains size was due the island growth mechanism of the film.

The group found that all the deposited films had a polycrystalline structure and a preferably oriented to (111). The (111) orientation of the copper films was enhanced by applied bias. The films' internal stress alternated from tensile to compressive stress as the bias is increased from 0 to -600 V, with the film being stress free for a bias about -300 V.

More work was published by the same group which provide further analysis on the FCVA deposited copper film grown without a bias. The roughness of the films was found to increase from 0.36 to 2.75 nm as the film thickness increased from 60 to 365 nm. The XRD note that intensity of the (220) peak in the polycrystalline films increased with film thickness.

The fact that FCVA can be used to grow reasonably smooth films with (111) orientation, which is the preferred orientation for graphene growth by CVD [152], is promising for the use of these films for the growth of graphene using FCVA.

5.2 Experimental

The schematic in Figure 37 shows the steps involved in synthesis of the carbon films. (a) Silicon <100> and silica (thermal oxide 1000 nm thickness on Si) substrates were placed in the FCVA system (see reference [68] for details) and copper under-layers ~200 nm thick were deposited with a range of substrate biases at room temperature using a 99.99% pure copper cathode. (b) Carbon films were then deposited on the copper under-layers at floating substrate potential (20 V) and at a temperature of 750 ^{o}C. (c) In a similar fashion to that discussed in section 5.1.3, relocation of the carbon film to the underlying silica substrate was achieved by etching the copper with ammonium persulfate ($(NH_4)_2S_2O_8$), 0.1 M). The microstructure of the copper films was examined before and after the deposition of the carbon films using SEM, AFM, and Raman spectroscopy.

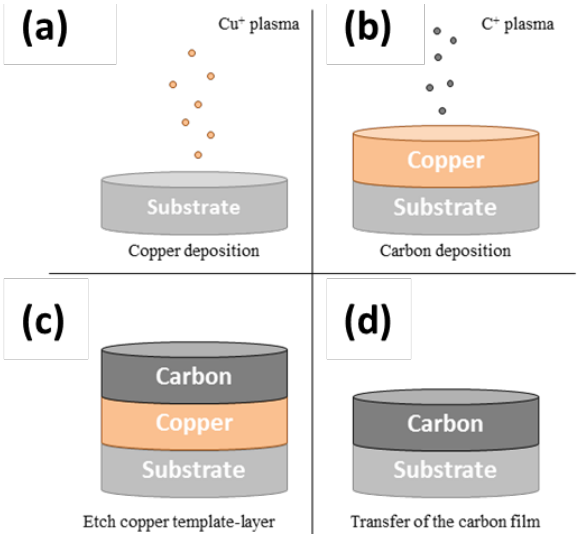

Figure 37: Schematic showing the growth sequence and transfer process employed to fabricate carbon films on silicon/silica substrates.

5.3 Results and discussion

The results and discussion for this section is broken into three parts, the deposition of copper film, synthesis of graphene and the transfer of the graphene film.

5.3.1 Deposition of copper film

Copper films ~50 nm and ~200 nm were deposited by FCVA system with an earthed holder, and at a bias of -25 V and -50 V. Figure 38 shows copper films (~50 nm and ~200 nm) deposited with a -50 V before and after annealing at 750 ^{o}C, the growth temperature used for the subsequent carbon deposition. The ~50 nm thick films showed large copper crystallites on the surface which increased in size following annealing by Ostwald ripening Figure 38a, c. Copper films which were ~200 nm thick (Figure 38b, d) were found to be less susceptible to Ostwald ripening caused by annealing at 750 ^{o}C and appeared relatively uniform. Hence, copper films ~200 nm thick were used in this study.

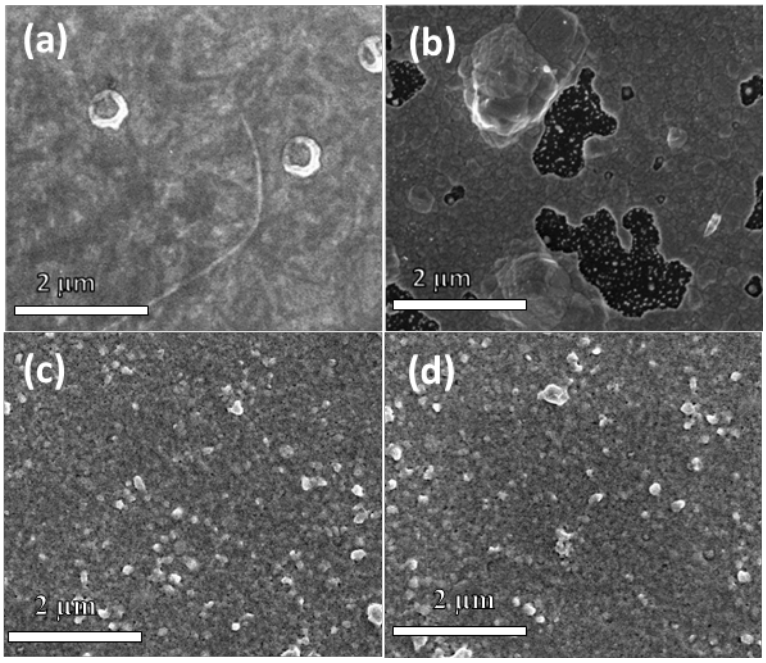

Figure 38: SEM images of copper films deposited onto silica with a -50 V bias. Copper film ~50 nm thick, (a) before and (b) after annealing at 750 ^{o}C. Copper film ~200 nm thick (c) before and (d) after annealing at 750 ^{o}C.

The relationship between the substrate bias (determining the average incident ion energy [89]) and the roughness of the deposited copper films was investigated using AFM (see section 2.2.4 for details). Figure 39 compares the surface morphology of copper films grown on silicon and silica with an earthed substrate holder (Figure 39 (a) and (c)) with films grown with a substrate bias of -50 V. The copper films deposited on silicon at 0 V (earthed) have an RMS roughness of 99 nm. An earthed substrate holder attracts electrons from the plasma leading to increasing temperature during deposition. The increase in deposition temperature resulted in the formation of larger agglomerates, as observed in Figure 39a. The copper film deposited on silicon with a bias of 25 V applied had a lower roughness. As bias was applied to the substrate holder, electrons were repelled and ions were accelerated towards the growing film. The increase in the kinetic energy of the incoming ions promoted

densification and reduced agglomeration, leading to smoother films. As the bias was increased to 50 V, a further reduction in the roughness was observed Figure 39(c).

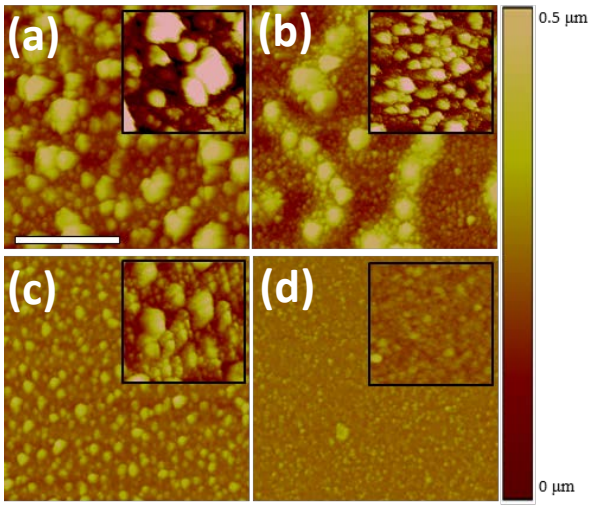

Figure 39: Atomic force micrographs of copper template layers energetically deposited onto silicon (top row) and silica (bottom row) with the substrate holder earthed ((a) and(c)) and biased at -50 V ((b) and (d)). Insets show the morphology of the films after annealing at 750 ^{o}C for 10 minutes. The scale bar is 3 µm in length.

Figure 40 shows the relationship between substrate bias and RMS roughness, measured by AFM. The roughness of films deposited onto silica wafers followed a similar trend to that observed in the films deposited on silicon. The film deposited with an earthed substrate holder was again the roughest and contained the largest copper agglomerates (Figure 39a). As the substrate bias was increased, a reduction in the roughness of the deposited copper films was observed. In general, films deposited on silica were smoother than those deposited on silicon. Before depositing graphene, the copper films were annealed in vacuum at 750 ^{o}C as this temperature was found to be required for the growth of graphene by FCVA [68]. The insets in Figure 39 show the morphologies of the copper films after

annealing at 750 ^{o}C with enlarged agglomerates caused by Ostwald ripening during annealing.

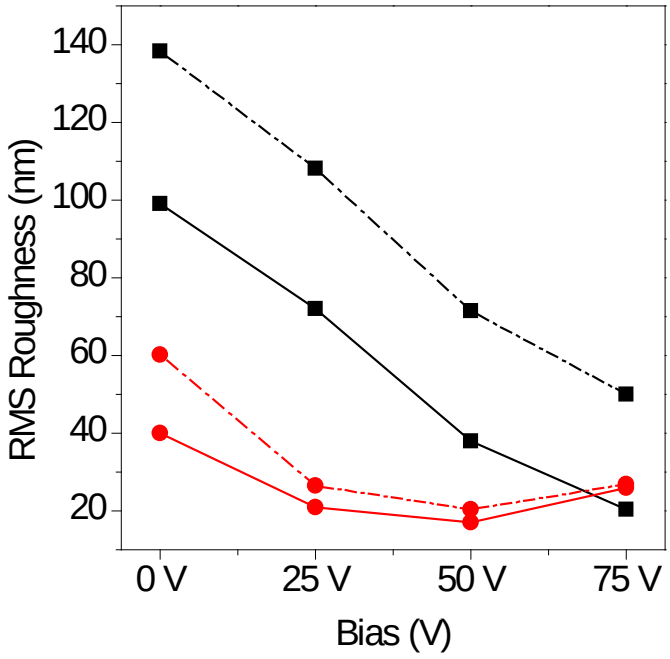

Figure 40: RMS roughness of copper films deposited on silicon and silica by FCVA before and after annealing.

The microstructure of the FCVA deposited copper films was measured before and after annealing using XRD (see section 2.2.3 for details) and was compared against commercial copper foil (Figure 41). Before annealing, the intensity of the (200) peak produced by the copper foil was much greater than that of the (111) peak (Figure 41a). After annealing at 750 ^{o}C, the (111) peak produced by the copper foil was more intense (Figure 41c), consistent with atomic reordering and increased crystallisation. It has been shown that a (111) preferred orientation leads to improved growth of graphene using CVD [153].

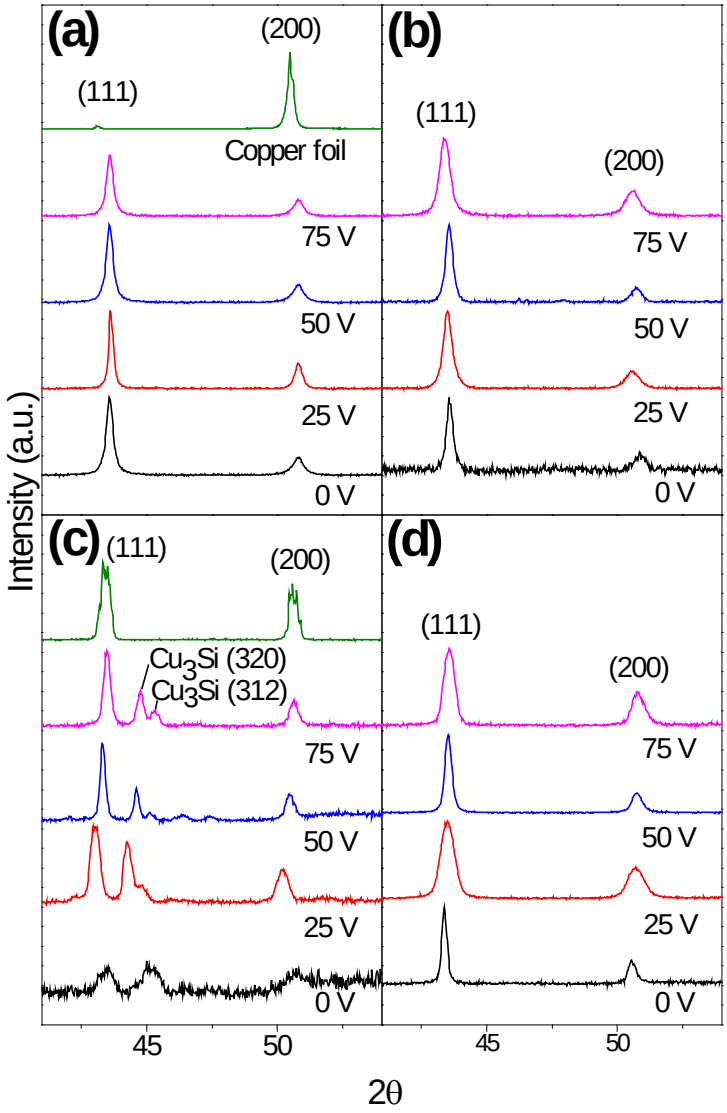

Figure 41: X-ray diffractograms from copper films supported at room temperature on (a) silicon and (b) silica at the substrate bias voltages indicated. (c) and (d) show the corresponding diffractograms after annealing at 750 ^{o}C. Also shown for comparison in (a) and (c) are diffractograms from copper foil.

The copper films deposited onto silicon and silica wafers all produced a more intense (111) peak relative to the (200) peak prior to annealing (Figure 41a, b). This preferred (111) orientation has be reported to provide fewer domain boundaries which contributes to improved growth of graphene [153].

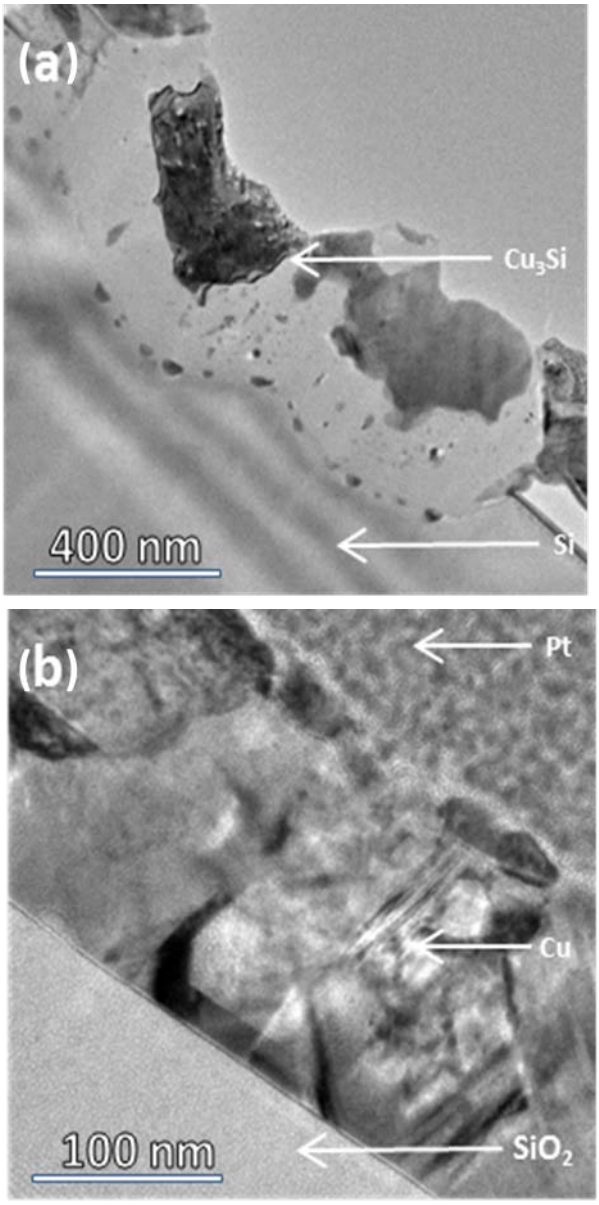

Figure 42: Cross-sectional TEM images showing the copper grown with a 50 V substrate bias on (a) silicon and (b) silica. Various features are labelled.

After annealing, the copper films deposited on silicon retained the more intense (111) peak (Figure 41c). However, peaks attributed to copper silicide (Cu_3Si) were observed, showing that the copper reacted with the underlying silicon during annealing. By contrast, the intensities of the (111) and (200) peaks in the diffractograms from the copper films grown on silica did not change markedly following annealing and no Cu_3Si peaks were produced

(Figure 41d). Hence, we assert that the copper layer did not react with silica due to the thermal stability of the latter [154].

A cross-sectional TEM image (see section 2.2.6 for details) of the copper film deposited onto silicon with 50 V bias applied is shown in Figure 42(a). This confirms the presence of copper silicide and supports the AFM measurements showing higher roughness in the copper films on silicon post annealing. The corresponding TEM image of the copper film deposited onto silica with a 50 V bias (Figure 42b) confirms the lack of copper silicide formation. Unlike the copper film on silicon, the copper film on silica appears continuous and homogenous.

5.3.2 Deposition of graphene

The microstructure of the carbon deposited using FCVA onto the annealed copper/silicon and copper/silica substrates was examined with Raman spectroscopy and the results are shown in Figure 43. Peaks in the Raman spectra located at ~1350 cm^{-1} and ~1580 cm^{-1} are often observed in nano and micro crystalline graphitic materials and are referred to as the D and G peaks. These peaks can be attributed to the defective edges and defect-free centre of graphene layers respectively [110]. The formation of graphene is indicated when the D and G peaks are observed in conjunction with the 2D peak located at ~2700 cm^{-1}. Both the intensity (2D/G) and defect (D/G) ratio, are common methods for indicating the number of layers and quality [110]. All spectra from carbon films deposited on copper/silicon feature a prominent ‘D’ peak, indicating a significant defect density (Figure 43a). A well resolved ‘G’ peak was visible in all spectra. None of the carbon films exhibited intense 2D peaks, indicating that ordered graphene was not produced on copper/silicon. The lack of graphene growth is likely caused by the presence of copper silicide and/or high surface roughness

(Figure 39 and Figure 40). Rather, the spectra resemble those from disordered microcrystalline graphitic material [155].

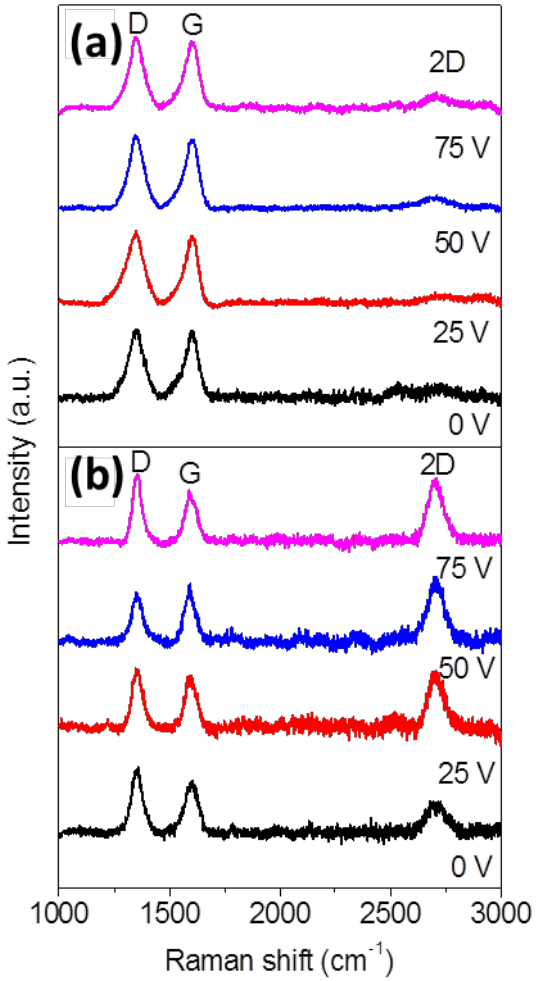

Figure 43: Raman spectra from carbon deposited onto (a) copper/silicon and (b) copper/silica. The bias voltages shown are those used for the deposition of the copper under-layer.

The Raman spectra from the carbon films deposited at 750 °C onto copper/silica feature well resolved, D, G and 2D peaks (Figure 43b). The carbon film deposited on the copper film grown "earthed" has the largest D:G peak, defect ratio (I_D/I_G) and the smallest intensity ratio (I_{2D}/I_G), most likely a consequence of the increased roughness of the copper. A decrease in the defect ratio and an increase in the intensity ratio is observed in the spectra from the film

grown on copper deposited with 25 V bias. The defect ratio decreases and the intensity ratio increases further in the spectra from the carbon films deposited with 50 V and 75 V bias. The presence of the intense 2D peak in all spectra are indicative of ordered graphene. The I_{2D}/I_G for the carbon film deposited on copper/silica biased at 50 V was 1.2, which corresponds to approximately 10 layers of graphene.

5.4 Transfer of graphene

It is clear from Figure 43, that graphene was only grown on the copper/silica substrates. The graphene grown on the copper deposited onto silica using -50 V substrate bias was transferred to the underlying silica by sacrificially etching the copper under-layer (as described in section 5.2). Figure 44 shows (a) the optical and (b) SEM images of the transferred multilayer graphene. The carbon film is continuous over a large area (~1 mm^2). A sheet resistance value of 14.1 kΩ/□ was measured from the transferred graphene film using the four point probe. This value is similar to values reported previously for FCVA deposited graphene grown on and transferred from copper foil [68].

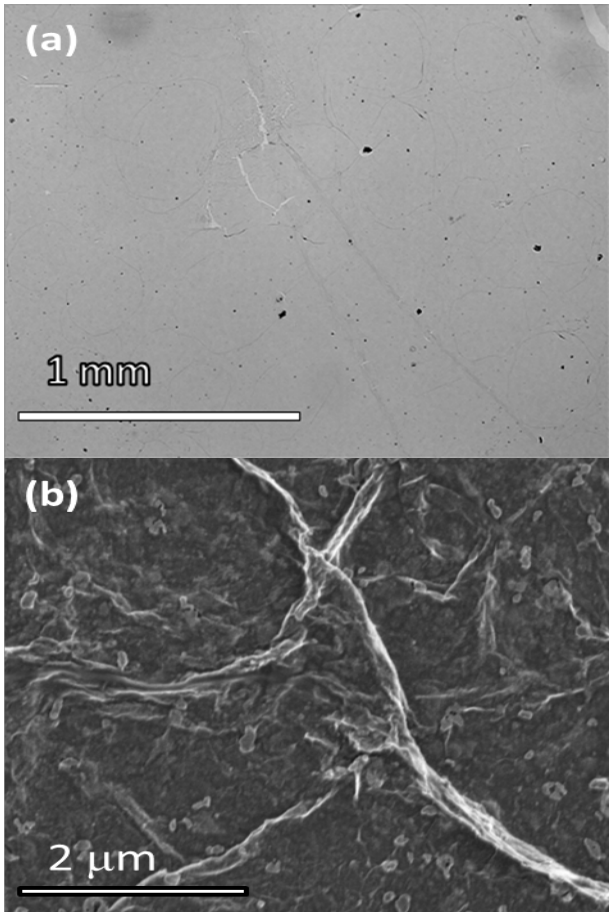

Figure 44: (a) Optical and (b) SEM images of a FCVA deposited multilayer graphene film after sacrificial etching of the copper under-layer (deposited using -50 V substrate bias) and transfer to silica.

Raman spectra were used to assess the quality of the multilayer graphene before and after transfer to the underlying silica substrate *Figure 45*a (achieved by etching the ~200 nm thick copper film). After the transfer, an increase in the D peak and a reduction in the 2D peak were observed. These changes indicate an increase in the number of defects and an increase in the number of layers. This is consistent with the bending and folding visible in Figure 44(b). Also included in *Figure 45*a is the Raman spectrum of multilayer graphene; grown on a copper ~50 nm film deposited with a -50 V bias. This graphene has a larger D peak and smaller 2D peak than that observed for graphene grown on the ~200 nm thick

copper. The increase in defects for the graphene grown on the thinner copper can be explained by the increased Ostwald Ripening, as seen in Figure 38.

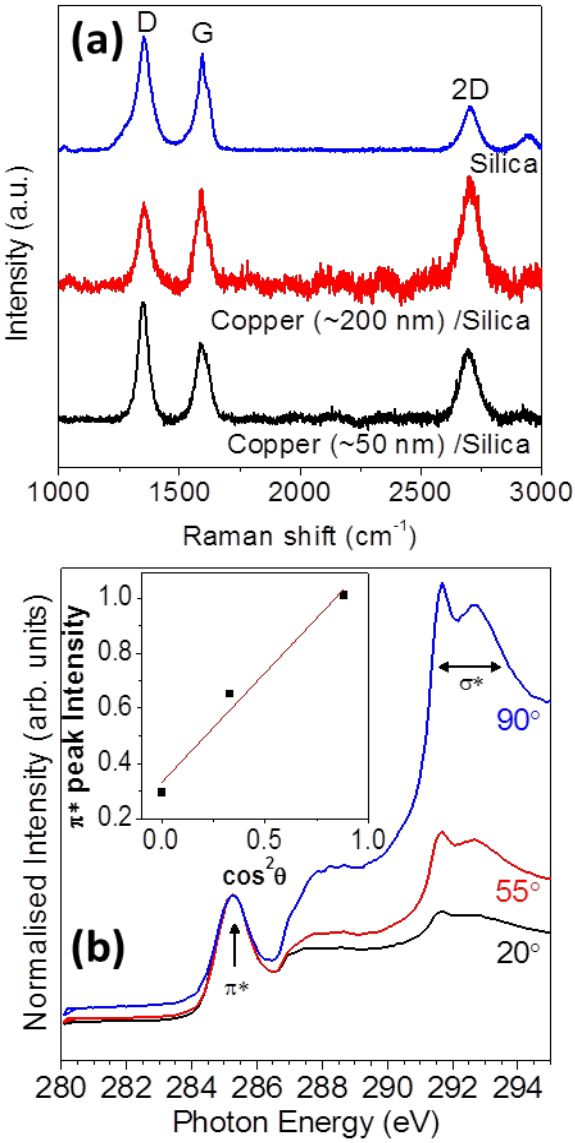

Figure 45: (a) Raman spectra from multilayer graphene before on copper (~200 nm) /silica and after transfer onto the silica by removing the copper. Also included is the Raman spectrum of multilayer graphene grown on a copper ~50 nm film. (b) Angle dependent XANES from a multilayer graphene film grown on copper/silica and subsequently transferred to the underlying silica. The inset shows the angular dependence of the 1s - π resonance with the spectra normalised to the 1s - σ* peak.*

Figure 45b shows carbon K-edges from the transferred multilayer graphene supported on silica (after sacrificial etching of the copper) at varying incident angles. The XANES shows two main features: the 1s - π* peak at ~285 eV (indicated by an arrow) and the 1s – σ* peak at ~ 292 eV. The doublet in the 1s – σ* peak indicates that well-ordered graphitic layers are present [93]. In addition, there is a strong angular dependence of the ratio of intensities of the 1s - π* and 1s – σ* peaks. This is a result of the interaction of the polarised x-ray beam and the highly directional bonds in graphene-like materials [93] . Furthermore, the inset in *Figure 45* shows that there is a linear dependence of the 1s - π* peak intensity (when the spectra are normalised to the 1s – σ* peak) as a function of $\cos^2\theta$. This is as expected for ordered graphene oriented parallel to the substrate [93].

5.5 Conclusion

Energetic deposition has been used to produce copper template layers on silicon and silica substrates. Subsequent energetic deposition of carbon onto these template layers at 750 ^{o}C produced films with structural properties that strongly depend on the structure of the copper templates. Multilayer graphene was deposited onto copper/silica. Formation of the copper silicides prevented this material growing on copper/silicon. The ability to produce high quality copper template under-layers and multilayer graphene using a single deposition method enables simplified fabrication of this technologically important material. A reduction in the temperature required to grow gaphene was oberved with a decrease in the copper film thickness. However, AFM and SEM analysis also showed that the thinner copper film were more sensitive to Ostweld ripening caused by the deposition temperature.

6 Conclusion

To replace existing materials in electronic and other devices, efficient methods are needed to grow high quality graphene directly on a range of substrates. Currently there are several existing techniques which are capable of producing graphene. Each method for graphene production has its strengths and weakness. The different production methods produce varying quantities and qualities of graphene, which make them suitable for a varying array of applications. CVD has proven to be capable of producing large quantities of high quality graphene, however there are several drawbacks. CVD entails high temperatures (~1000 °C), the method is substrate dependent, it is not CMOS compatible, and requires a transfer process to relocate graphene to a desirable substrate.

To address the issues surrounding the production of CVD grown graphene, this thesis investigated the deposition of graphene by PVD in a FCVA. Carbon films were deposited onto different substrates and the effect of changing the deposition conditions was also investigated.

In chapter 3, graphene films were synthesised on copper foil using the FCVA. The effect of deposition parameters on the microstructure of the carbon films was investigated using electron microscopy and spectroscopic techniques. It was found that the energetic deposition from a FCVA onto copper substrates heated to 750 ^{o}C with a carbon dose of $3.4x10^{16}$ atoms/cm^{2} produced ordered graphene layers. Raman spectroscopy and TEM analysis showed that graphene layers were comparable in quality to that grown by CVD at 1050^{o}C. Whereas CVD depends upon high temperatures of ~1000 ˚C [98] and labile organic gases to ensure correct arrangement of the carbon, the FCVA achieves this at a lower

temperature using carbon ions alone. This outcome is attributed to dynamic annealing which occurs during the energetic deposition of carbon. Floating substrate holder i.e. sitting at the plasma potential of 21 V, the incoming carbon ions will have an average energy of ~45 eV [58]. This energy enables the carbon atoms to rearrange into lower energy bonding configurations and the formation of graphene layers [116] templated by the underlying copper. While the difference in growth temperature is not that great, there are other considerable advantages to growing graphene by FCVA; such as short deposition times.

Hydrogen gas was not required to deposit graphene by FCVA, H_2 gas is routinely employed to removing the surface oxide layer from the copper substrate before depositing graphene by CVD. In the FCVA the energetic carbon ions were attributed to removing the oxide layer from the copper substrate, allowing the growth of graphene. Further the introduction of a processing gas in the FCVA was found to inhibit the growth of graphene due to increased ion bombardment.

The observations above, lead to the proposed growth model for FCVA deposited graphene on copper foil. Similar to CVD, a templating substrate is required for synthesis of graphene in a FCVA system. The energetic carbon ions remove oxygen from the surface copper. SRIM calculations showed that the energetic carbon ions have an average implantation depth of 5 Å. A H_2 processing gas is not required, as the native oxide layer on the substrate is removed by the energetic carbon ions. As the substrate temperature is elevated from room temperature to 750 ^{o}C greater mobility allows the deposited carbon to rearrange into graphene layers. Like CVD, the thickness of the carbon film is limited due to a loss of the templating effect of the copper substrate, which reduces as a function of film thickness. Intrinsic stresses in the film may also limit the thickness of graphene growth.

In chapter 4, graphene films were synthesised onto substrates other than copper using the FCVA system. The type of substrate was found to influence the microstructure of the deposited carbon films. Carbon films were deposited onto CVD graphene. It was observed that the energetic flux introduced defects into the underlying graphene layers.

Multilayer was successfully deposited onto nickel at 750 ^{o}C with a carbon dose of 4.6x10^{17} atoms/cm^{2}. The increase in the required dose to deposit graphene, compared to copper, was attributed to the carbon dissolving in the hot nickel. Films deposited with a higher or lower dose than 4.6x10^{17} atoms/cm^{2} were shown to be highly defective. This is due to a build-up of disordered carbon accumulates on the surface for the higher doses, and to discontinuous film growth for the lower doses.

A model for the synthesis of graphene on nickel by FCVA was developed. At room temperature, the carbon ions are directly incorporated into a film on the surface of the substrate and do not absorb into the surface of the nickel foil and the deposited film has an amorphous structure. As the temperature is elevated to 750 ^{o}C the carbon atoms are absorbed into the nickel substrate. Upon cooling the carbon atoms precipitate back to the surface. A change in deposited dose was found to affect the amount of carbon atoms which precipitated to the surface. The morphology of nickel substrate was found to affect the precipitation of the carbon atoms, resulting in a variation in the thickness of the graphene film, as has been reported for graphene prepared by CVD.

Graphene layers were deposited by FCVA at 750 ^{o}C onto CVD grown hBN. This is a promising result, however future work is required using TEM to analyse the atomic arrangement of graphene on hBN in more detail. Finally it was found that it is not possible to prepare graphene on SiC and YSC substrates at 750 ^{o}C.

In chapter 5, FCVA was employed to deposit both the copper growth surface and graphene. Copper templating layers in the form of FCVA deposited copper films ~200 nm and ~50 nm thick were compared before and after annealing at 750 ^{o}C. Copper films which were ~200 nm thick were shown to be less susceptible to Ostwald ripening, caused by annealing. FCVA copper films (~200nm thick) were also found to have a naturally occurring (111) orientation on silica wafers, ideal for graphene growth.

Multilayer graphene comparable to that grown by CVD, was deposited onto the copper templating layers prepared on silica wafers. Copper films deposited on SiO_2 were found to form copper silicide during annealing, which inhibited the growth of graphene on the substrate layer. In the case of multilayer graphene on copper/silica, the graphene could be directly transferred to the silica by etching the copper film. The ability to produce high quality copper template under-layers and multilayer graphene using a single deposition method enables simplified fabrication of this technologically important material.

7 References

[1]. A Nagashima, N Tejima, Y Gamou, T Kawai, and C Oshima. Electronic structure of monolayer hexagonal boron nitride physisorbed on metal surfaces. Physical Review Letters, 1995. 75(21): p. 3918.

[2]. RF Frindt. Superconductivity in Ultrathin $NbSe_2$ Layers. Physical Review Letters, 1972. 28(5): p. 299.

[3]. RF Frindt. Single crystals of MoS_2 several molecular layers thick. Journal of Applied Physics, 1966. 37(4): p. 1928-1929.

[4]. W Divigalpitiya, RF Frindt, and SR Morrison. Inclusion systems of organic molecules in restacked single-layer molybdenum disulfide. Science, 1989. 246(4928): p. 369-371.

[5]. B Radisavljevic, A Radenovic, J Brivio, V Giacometti, and A Kis, Single-layer MoS_2 transistors. Nature Nanotechnology, 2011. 6(3): p. 147-150.

[6]. T Georgiou, R Jalil, BD Belle, L Britnell, RV Gorbachev, SV Morozov, YJ Kim, A Gholinia, SJ Haigh, O Makarovsky, L Eaves, LA Ponomarenko, AK Geim, KS Novoselov, and A Mishchenko. Vertical field-effect transistor based on graphene-WS_2 heterostructures for flexible and transparent electronics. Nature Nanotechnology, 2013. 8(2): p. 100-103.

[7]. H Zhang, CX Liu, XL Qi, X Dai, Z Fang, and SC Zhang. Topological insulators in Bi_2Se_3, Bi_2Te_3 and Sb_2Te_3 with a single Dirac cone on the surface. Nature Physics, 2009. 5(6): p. 438-442.

[8]. L Li, Y Yu, GJ Ye, Q Ge, X Ou, H Wu, D Feng, XH Chen, and Y Zhang. Black phosphorus field-effect transistors. Nature Nanotechnology, 2014. 9(5): p. 372-377.

[9]. A Castellanos-Gomez. Black phosphorus: narrow gap, wide applications. The Journal of Physical Chemistry Letters, 2015. 6(21), 4280-4291.

[10]. HO Churchill, and P Jarillo-Herrero. Two-dimensional crystals: Phosphorus joins the family. Nature Nanotechnology, 2014. 9(5): p. 330-331.

[11]. KS Novoselov, AK Geim, SV Morozov, D Jiang, Y Zhang, SV Dubonos, IV Grigorieva, and AA Firsov. Electric field effect in atomically thin carbon films. Science, 2004. 306(5696): p. 666-669.

[12]. AK Geim and KS Novoselov. The rise of graphene. Nature Materials, 2007. 6(3): p. 183-191.

[13]. KI Bolotin, KJ Sikes, J Hone, HL Stormer, and P Kim. Temperature-dependent transport in suspended graphene. Physical Review Letters, 2008. 101(9): p. 096802.

[14]. KI Bolotin, KJ Sikes, Z Jiang, M Klima, G Fudenberg, J Hone, P Kim, and HL Stormer. Ultrahigh electron mobility in suspended graphene. Solid State Communications, 2008. 146(9): p. 351-355.

[15]. RR Nair, P Blake, AN Grigorenko, KS Novoselov, TJ Booth, T Stauber, NMR Peres, and AK Geim. Fine structure constant defines visual transparency of graphene. Science, 2008. 320(5881): p. 1308-1308.

[16]. AA Balandin, S Ghosh, W Bao, I Calizo, D Teweldebrhan, F Miao, and CN Lau. Superior thermal conductivity of single-layer graphene. Nano Letters, 2008. 8(3): p. 902-907.

[17]. C Lee, X Wei, JW Kysar, and J Hone. Measurement of the elastic properties and intrinsic strength of monolayer graphene. Science, 2008. 321(5887): p. 385-388.

[18]. Y Nishi. Lithium ion secondary batteries; past 10 years and the future. Journal of Power Sources, 2001. 100(1): p. 101-106.

[19]. G Kucinskis, G Bajars, and J Kleperis. Graphene in lithium ion battery cathode materials: A review. Journal of Power Sources, 2013. 240: p. 66-79.

[20]. B Pei, H Yao, W Zhang, and Z Yang. Hydrothermal synthesis of morphology-controlled $LiFePO_4$ cathode material for lithium-ion batteries. Journal of Power Sources, 2012. 220: p. 317-323.

[21]. FFC Bazito and RM Torresi. Cathodes for lithium ion batteries: the benefits of using nanostructured materials. Journal of the Brazilian Chemical Society, 2006. 17(4): p. 627-642.

[22]. X Sun, J Li, C Shi, Z Wang, E Liu, C He, X Du, and N Zhao. Enhanced electrochemical performance of $LiFePO_4$ cathode with in-situ chemical vapor deposition synthesized carbon nanotubes as conductor. Journal of Power Sources, 2012. 220: p. 264-268.

[23]. XM Liu, ZD Huang, SW Oh, B Zhang, PC Ma, MMF Yuen, and JK Kim. Carbon nanotube (CNT)-based composites as electrode material for rechargeable Li-ion batteries: a review. Composites Science and Technology, 2012. 72(2): p. 121-144.

[24]. L Chen, M Zhang, and W Wei. Graphene-based composites as cathode materials for lithium ion batteries. Journal of Nanomaterials, 2013. 2013: p. 2.

[25]. FY Su, YB He, B Li, XC Chen, CH You, W Wei, W Lv, QH Yang, and F Kang. Could graphene construct an effective conducting network in a high-power lithium ion battery? Nano Energy, 2012. 1(3): p. 429-439.

[26]. DR Cooper, B D'Anjou, N Ghattamaneni, B Harack, M Hilke, A Horth, N Majlis, M Massicotte, L Vandsburger, E Whiteway, V Yu. Experimental review of graphene. ISRN Condensed Matter Physics, 2012.

[27]. AR Schlatmann, DW Floet, A Hilberer, F Garten, PJM Smulders, TM Klapwijk, and G Hadziioannou. Indium contamination from the indium–tin–oxide electrode in polymer light-emitting diodes. Applied Physics Letters, 1996. 69(12): p. 1764-1766.

[28]. G Gustafsson, Y Cao, G Treacy, F Klavetter, N Colaneri, and A Heeger. Flexible light-emitting diodes made from soluble conducting polymers. Nature, 1992. 357(6378): p. 477-479.

[29]. X Wang, L Zhi, and K Müllen. Transparent, conductive graphene electrodes for dye-sensitized solar cells. Nano Letters, 2008. 8(1): p. 323-327.

[30]. A Aghigh, V Alizadeh, H Wong, MS Islam, N Amin, and M Zaman. Recent advances in utilization of graphene for filtration and desalination of water: A review. Desalination, 2015. 365: p. 389-397.

[31]. Z Wang, B Dou, L Zheng, G Zhang, Z Liu, and Z Hao. Effective desalination by capacitive deionization with functional graphene nanocomposite as novel electrode material. Desalination, 2012. 299: p. 96-102.

[32]. F Fornasiero, JB In, S Kim, HG Park, Y Wang, CP Grigoropoulos, A Noy, and O Bakajin. pH-tunable ion selectivity in carbon nanotube pores. Langmuir, 2010. 26(18): p. 14848-14853.

[33]. Z Hu, Y Chen, and J Jiang. Zeolitic imidazolate framework-8 as a reverse osmosis membrane for water desalination: Insight from molecular simulation. The Journal of Chemical Physics, 2011. 134(13): p. 134705.

[34]. GH Lee, YJ Yu, X Cui, N Petrone, CH Lee, MS Choi, DY Lee, C Lee, WJ Yoo, K Watanabe, T Taniguchi, C Nuckolls, P Kim, and J Hone. Flexible and transparent MoS_2 field-effect transistors on hexagonal boron nitride-graphene heterostructures. ACS Nano, 2013. 7(9): p. 7931-7936.

[35]. J Lee, TJ Ha, H Li, KN Parrish, M Holt, A Dodabalapur, RS Ruoff, and D Akinwande. 25 GHz embedded-gate graphene transistors with high-k dielectrics on extremely flexible plastic sheets. ACS Nano, 2013. 7(9): p. 7744-7750.

[36]. A Nathan, A Ahnood, MT Cole, S Lee, Y Suzuki, P Hiralal, F Bonaccorso, T Hasan, L Garcia-Gancedo, A Dyadyusha, S Haque, P Andrew, S Hofmann, J Moultrie, D Chu, AJ Flewitt, AC Ferrari, MJ Kelly, J Robertson, GAJ Amaratunga, and WI Milne. Flexible electronics: the next ubiquitous platform. Proceedings of the IEEE, 2012. 100(Special Centennial Issue): p. 1486-1517.

[37]. B Lang. A LEED study of the deposition of carbon on platinum crystal surfaces. Surface Science, 1975. 53(1): p. 317-329.

[38]. E Rokuta, Y Hasegawa, A Itoh, K Yamashita, T Tanaka, S Otani, and C Oshima. Vibrational spectra of the monolayer films of hexagonal boron nitride and graphite on faceted Ni(755). Surface Science, 1999. 427: p. 97-101.

[39]. H Shioyama. Cleavage of graphite to graphene. Journal of Materials Science Letters, 2001. 20(6): p. 499-500.

[40]. DV Kosynkin, AL Higginbotham, A Sinitskii, JR Lomeda, A Dimiev, BK Price, and JM Tour. Longitudinal unzipping of carbon nanotubes to form graphene nanoribbons. Nature, 2009. 458(7240): p. 872-876.

[41]. F Cataldo, G Compagnini, G Patané, O Ursini, G Angelini, PR Ribic, G Margaritondo, A Cricenti, G Palleschi, and F Valentini. Graphene nanoribbons produced by the oxidative unzipping of single-wall carbon nanotubes. Carbon, 2010. 48(9): p. 2596-2602.

[42]. G Cravotto, and P Cintas. Sonication-assisted fabrication and post-synthetic modifications of graphene-like materials. Chemistry – A European Journal, 2010. 16(18): p. 5246-5259.

[43]. G Zheng, J Wu, W Wang, and C Pan. Characterizations of expanded graphite/polymer composites prepared by in situ polymerization. Carbon, 2004. 42(14): p. 2839-2847.

[44]. MJ McAllister, JL Li, DH Adamson, HC Schniepp, AA Abdala, J Liu, M Herrera-Alonso, DL Milius, R Car, RK Prud'homme, and IA Aksay. Single sheet functionalized graphene by oxidation and thermal expansion of graphite. Chemistry of Materials, 2007. 19(18): p. 4396-4404.

[45]. KV Emtsev, A Bostwick, K Horn, J Jobst, GL Kellogg, L Ley, JL McChesney, T Ohta, SA Reshanov, J Röhrl, E Rotenberg, AK Schmid, D Waldmann, HB Weber and T Seyller. Towards wafer-size graphene layers by atmospheric pressure graphitization of silicon carbide. Nature Materials, 2009. 8(3): p. 203-207.

[46]. ZY Juang, CY Wu, CW Lo, WY Chen, CF Huang, JC Hwang, FR Chen, KC Leou, and CH Tsai. Synthesis of graphene on silicon carbide substrates at low temperature. Carbon, 2009. 47(8): p. 2026-2031.

[47]. S Stankovich, DA Dikin, RD Piner, KA Kohlhaas, A Kleinhammes, Y Jia, Y Wu, ST Nguyen, and RS Ruoff. Synthesis of graphene-based nanosheets via chemical reduction of exfoliated graphite oxide. Carbon, 2007. 45(7): p. 1558-1565.

[48]. X Fan, W Peng, Y Li, X Li, S Wang, G Zhang, and F Zhang. Deoxygenation of exfoliated graphite oxide under alkaline conditions: a green route to graphene preparation. Advanced Materials, 2008. 20(23): p. 4490-4493.

[49]. D Wei, B Wu, Y Guo, G Yu, and Y Liu. Controllable chemical vapor deposition growth of few layer graphene for electronic devices. Accounts of Chemical Research, 2012. 46(1): p. 106-115.

[50]. HJ Park, JC Meyer, S Roth, and V Skákalová. Growth and properties of few-layer graphene prepared by chemical vapor deposition. Carbon, 2010. 48(4): p. 1088-1094.

[51]. A Malesevic, R Vitchev, K Schouteden, A Volodin, L Zhang, G Van Tendeloo, A Vanhulsel, and CV Haesendonck. Synthesis of few-layer graphene via microwave plasma-enhanced chemical vapour deposition. Nanotechnology, 2008. 19(30): p. 305604.

[52]. KS Novoselov, VI Fal, L Colombo, PR Gellert, MG Schwab, and K. Kim. A roadmap for graphene. Nature, 2012. 490(7419): p. 192-200.

[53]. Vlassiouk, I., M. Regmi, P. Fulvio, S. Dai, P. Datskos, G. Eres, and S. Smirnov, Role of hydrogen in chemical vapor deposition growth of large single-crystal graphene. ACS Nano, 2011. 5(7): p. 6069-6076.

[54]. L Tao, J Lee, H Chou, M Holt, RS Ruoff, and D Akinwande. Synthesis of high quality monolayer graphene at reduced temperature on hydrogen-enriched evaporated copper (111) films. ACS Nano, 2012. 6(3): p. 2319-2325.

[55]. Y Lee, S Bae, H Jang, S Jang, SE Zhu, SH Sim, YI Song, BH Hong, and JH Ahn. Wafer-scale synthesis and transfer of graphene films. Nano Letters, 2010. 10(2): p. 490-493.

[56]. ZY Juang, CY Wu, AY Lu, CY Su, KC Leou, FR Chen, and CH Tsai. Graphene synthesis by chemical vapor deposition and transfer by a roll-to-roll process. Carbon, 2010. 48(11): p. 3169-3174.

[57]. MC Polo, JL Andújar, A Hart, J Robertson, and WI Milne. Preparation of tetrahedral amorphous carbon films by filtered cathodic vacuum arc deposition. Diamond and Related Materials, 2000. 9(3–6): p. 663-667.

[58]. DWM Lau, A Moafi, MB Taylor, JG Partridge, DG McCulloch, RC Powles, and DR McKenzie. The structural phases of non-crystalline carbon prepared by physical vapour deposition. Carbon, 2009. 47(14): p. 3263-3270.

[59]. P Wang, X Wang, Y Chen, G Zhang, W Liu, and J Zhang. The effect of applied negative bias voltage on the structure of Ti-doped aC: H films deposited by FCVA. Applied Surface Science, 2007. 253(7): p. 3722-3726.

[60]. DW Lau. Characterisation of novel carbonaceous materials synthesised using plasmas. 2009, RMIT University Melbourne, Australia.

[61]. OS Panwar, AK Kesarwani, SR Dhakate, BP Singh, RK Rakshit, A Bisht, and S Chockalingam. Few layer graphene synthesized by filtered cathodic vacuum arc technique. Journal of Vacuum Science & Technology B, 2013. 31(4): p. 040602.

[62]. O Panwar, A Kesarwani, A Bisht, S Chockalingam, S Dhakate, B Singh, and R Rakshit. Synthesis of multilayer graphene by filtered cathodic vacuum arc technique. Physics of Semiconductor Devices. 2014, Springer. p. 651-654.

[63]. AK Kesarwani, O Panwar, S Chockalingam, A Bisht, S Dhakate, B Singh, A Srivastava, and R Rakshit. Graphene synthesized from solid carbon source using filtered cathodic vacuum arc technique for transparent conducting and field effect transistor devices. Science of Advanced Materials, 2014. 6(10): p. 2124-2133.

[64]. A Anders, Cathodic arcs: from fractal spots to energetic condensation. 2008, Springer. p. 429-490.

[65]. PR Somani, SP Somani, and M Umeno. Planer nano-graphenes from camphor by CVD. Chemical Physics Letters, 2006. 430(1): p. 56-59.

[66]. T Ohta, FE Gabaly, A Bostwick, JL McChesney, KV Emtsev, AK Schmid, T Seyller, K Horn, and E Rotenberg. Morphology of graphene thin film growth on SiC(0001). New Journal of Physics, 2008. 10(2): p. 023034.

[67]. E Rollings, GH Gweon, S Zhou, B Mun, J McChesney, B Hussain, A Fedorov, P First, W De Heer, and A Lanzara. Synthesis and characterization of atomically thin graphite films on a silicon carbide substrate. Journal of Physics and Chemistry of Solids, 2006. 67(9): p. 2172-2177.

[68]. DT Oldfield, DG McCulloch, CP Huynh, K Sears, and SC Hawkins. Multilayered graphene films prepared at moderate temperatures using energetic physical vapour deposition. Carbon, 2015. 94: p. 378-385.

[69]. RK Vijayaraghavan, C Gaman, B Jose, AP McCoy, T Cafolla, PJ McNally, and S Daniels. Pulsed-Plasma Physical Vapor Deposition Approach Toward the Facile Synthesis of Multilayer and Monolayer Graphene for Anticoagulation Applications. ACS Applied Materials & Interfaces, 2016. 8(7): p. 4878-4886.

[70]. LM Viculis, JJ Mack, and RB Kaner. A chemical route to carbon nanoscrolls. Science, 2003. 299(5611): p. 1361-1361.

[71]. KS Novoselov, D Jiang, F Schedin, TJ Booth, VV Khotkevich, SV Morozov, and AK Geim. Two-dimensional atomic crystals. Proceedings of the National Academy of Sciences of the United States of America, 2005. 102(30): p. 10451-10453.

[72]. AN Obraztsov, EA Obraztsova, AV Tyurnina, and AA Zolotukhin. Chemical vapor deposition of thin graphite films of nanometer thickness. Carbon, 2007. 45(10): p. 2017-2021.

[73]. Q Yu, J Lian, S Siriponglert, H Li, YP Chen, and SS Pei. Graphene segregated on Ni surfaces and transferred to insulators. Applied Physics Letters, 2008. 93(11): p. 113103.

[74]. A Reina, X Jia, J Ho, D Nezich, H Son, V Bulovic, MS Dresselhaus, and J Kong. Large area, few-layer graphene films on arbitrary substrates by chemical vapor deposition. Nano Letters, 2008. 9(1): p. 30-35.

[75]. M Losurdo, MM Giangregorio, P Capezzuto, and G Bruno. Graphene CVD growth on copper and nickel: role of hydrogen in kinetics and structure. Physical Chemistry Chemical Physics, 2011. 13(46): p. 20836-20843.

[76]. AN Obraztsov, AA Zolotukhin, AO Ustinov, AP Volkov, Y. Svirko, and K. Jefimovs. DC discharge plasma studies for nanostructured carbon CVD. Diamond and Related Materials, 2003. 12(3): p. 917-920.

[77]. J Wang, M Zhu, R Outlaw, X Zhao, D Manos, B Holloway, and V Mammana. Free-standing subnanometer graphite sheets. Applied Physics Letters, 2004. 85(7): p. 1265-1267.

[78]. S Mao, K Yu, J Chang, DA Steeber, LE Ocola, and J Chen. Direct growth of vertically-oriented graphene for field-effect transistor biosensor. Scientific Reports, 2013. 3.

[79]. L Tao, J Lee, H Li, RD Piner, RS Ruoff, and D. Akinwande. Inductively heated synthesized graphene with record transistor mobility on oxidized silicon substrates at room temperature. Applied Physics Letters, 2013. 103(18): p. 183115.

[80]. L Huang, QH Chang, GL Guo, Y Liu, YQ Xie, T Wang, B Ling, and HF Yang. Synthesis of high-quality graphene films on nickel foils by rapid thermal chemical vapor deposition. Carbon, 2012. 50(2): p. 551-556.

[81]. JM Lee, HY Jeong, and WI Park. Large-scale synthesis of graphene films by Joule-heating-induced chemical vapor deposition. Journal of electronic materials, 2010. 39(10): p. 2190-2195.

[82]. W Cai, RD Piner, Y Zhu, X Li, Z Tan, HC Floresca, C Yang, L Lu, MJ Kim, and RS Ruoff. Synthesis of isotopically-labeled graphite films by cold-wall chemical vapor deposition and electronic properties of graphene obtained from such films. Nano Research, 2009. 2(11): p. 851-856.

[83]. TH Bointon, MD Barnes, S Russo, and MF Craciun. High quality monolayer graphene synthesized by resistive heating cold wall chemical vapor deposition. Advanced Materials, 2015. 27(28): p. 4200-4206.

[84]. AV De Parga, F Calleja, B Borca, MCG Passeggi Jr, JJ Hinarejos, F Guinea, and R Miranda. Periodically rippled graphene: growth and spatially resolved electronic structure. Physical Review Letters, 2008. 100(5): p. 056807.

[85]. AG Cano-Márquez, FJ Rodríguez-Macías, J Campos-Delgado, CG Espinosa-González, F Tristán-López, D Ramírez-González, DA Cullen, DJ Smith, M Terrones, and YI Vega-Cantú. Ex-MWNTs: graphene sheets and ribbons produced by lithium intercalation and exfoliation of carbon nanotubes. Nano Letters, 2009. 9(4): p. 1527-1533.

[86]. M Qian, YS Zhou, Y Gao, JB Park, T Feng, SM Huang, Z Sun, L Jiang, and YF Lu. Formation of graphene sheets through laser exfoliation of highly ordered pyrolytic graphite. Applied Physics Letters, 2011. 98(17): p. 173108.

[87]. H Zhang, and PX Feng. Fabrication and characterization of few-layer graphene. Carbon, 2010. 48(2): p. 359-364.

[88]. I Kumar, and A Khare. Multi-and few-layer graphene on insulating substrate via pulsed laser deposition technique. Applied Surface Science, 2014. 317: p. 1004-1009

[89]. A Anders. Energetic deposition using filtered cathodic arc plasmas. Vacuum, 2002. 67(3): p. 673-686.

[90]. DWM Lau, A Moafi, MB Taylor, JG Partridge, DG McCulloch, RC Powles, and DR McKenzie. The structural phases of non-crystalline carbon prepared by physical vapour deposition. Carbon, 2009. 47(14): p. 3263-3270.

[91]. A Anders. A structure zone diagram including plasma-based deposition and ion etching. Thin Solid Films, 2010. 518(15): p. 4087-4090.

[92]. LM Malard, MA Pimenta, G Dresselhaus, and MS Dresselhaus. Raman spectroscopy in graphene. Physics Reports, 2009 473(5), 51-87.

[93]. J Stöhr. NEXAFS spectroscopy. Vol. 25. 2013: Springer Science & Business Media.

[94]. KS Kim, Y Zhao, H Jang, SY Lee, JM Kim, KS Kim, JH Ahn, P Kim, JY Choi, and BH Hong. Large-scale pattern growth of graphene films for stretchable transparent electrodes. Nature, 2009. 457(7230): p. 706-710.

[95]. SY Kwon, CV Ciobanu, V Petrova, VB Shenoy, J Bareno, V Gambin, I Petrov, and S Kodambaka. Growth of semiconducting graphene on palladium. Nano Letters, 2009. 9(12): p. 3985-3990.

[96]. PW Sutter, JI Flege, and EA Sutter. Epitaxial graphene on ruthenium. Nature Materials, 2008. 7(5): p. 406-411.

[97]. J Coraux, AT N'Diaye, C Busse, and T Michely. Structural coherency of graphene on Ir(111). Nano Letters, 2008. 8(2): p. 565-570.

[98]. X Li , W Cai, J An, S Kim, J Nah, D Yang, R Piner, A Velamakanni, I Jung, E Tutuc, SK Banerjee, L Colombo and RS Ruoff. Large-area synthesis of high-quality and uniform graphene films on copper foils. Science, 2009. 324(5932): p. 1312-1314.

[99]. S Bae, H Kim, Y Lee, X Xu, JS Park, Y Zheng, J Balakrishnan, T Lei, HR Kim, and YI Song, YJ Kim, KS Kim, B Özyilmaz, JH Ahn, BH Hong and S Iijima. Roll-to-roll production of 30-inch graphene films for transparent electrodes. Nature Nanotechnology, 2010. 5(8): p. 574-578.

[100]. TP Ong, F Xiong, RPH Chang, and CW White. Nucleation and growth of diamond on carbon-implanted single crystal copper surfaces. Journal of Materials Research, 1992. 7(09): p. 2429-2439.

[101]. L Constant, C Speisser, and F. Le Normand. HFCVD diamond growth on Cu(111). Evidence for carbon phase transformations by in situ AES and XPS. Surface Science, 1997. 387(1): p. 28-43.

[102]. W Zhou, Z Han, J Wang, Y Zhang, Z Jin, X Sun, Y Zhang, C Yan, and Y Li. Copper catalyzing growth of single-walled carbon nanotubes on substrates. Nano Letters, 2006. 6(12): p. 2987-2990.

[103]. ST Lee, S Chen, G Braunstein, X Feng, I Bello, and W. Lau. Heteroepitaxy of carbon on copper by high-temperature ion implantation. Applied Physics Letters, 1991. 59(7): p. 785-787.

[104]. MZ Butt. Effect of hydrogen attack on the strength of high purity copper. Journal of Materials Science Letters, 1983. 2(1): p. 1-2.

[105]. Y Trehan. The reduction of copper oxides by molecular hydrogen. Zeitschrift für anorganische und allgemeine Chemie, 1962. 318(1-2): p. 107-112.

[106]. GH Han, F Gunes, JJ Bae, ES Kim, SJ Chae, HJ Shin, JY Choi, D Pribat, and YH Lee. Influence of copper morphology in forming nucleation seeds for graphene growth. Nano letters, 2011. 11(10): p. 4144-4148.

[107]. X Li, W Cai, L Colombo, and RS Ruoff. Evolution of graphene growth on Ni and Cu by carbon isotope labeling. Nano Letters, 2009. 9(12): p. 4268-4272.

[108]. EB Saubestre. Copper etching in ferric chloride. Industrial & Engineering Chemistry, 1959. 51(3): p. 288-290.

[109]. J Schwan, S Ulrich, V Batori, H Ehrhardt, and SRP Silva. Raman spectroscopy on amorphous carbon films. Journal of Applied Physics, 1996. 80(1): p. 440-447.

[110]. AC Ferrari, JC Meyer, V Scardaci, C Casiraghi, M Lazzeri, F Mauri, S Piscanec, D Jiang, KS Novoselov, S Roth, and AK Geim. Raman spectrum of graphene and graphene layers. Physical Review Letters, 2006. 97(18), 187401.

[111]. X Li, Y Zhu, W Cai, M Borysiak, B Han, D Chen, RD Piner, L Colombo, and RS Ruoff. Transfer of large-area graphene films for high-performance transparent conductive electrodes. Nano Letters, 2009. 9(12): p. 4359-4363.

[112]. X Liang, BA Sperling, I Calizo, G Cheng, CA Hacker, Q Zhang, Y Obeng, K Yan, H Peng, Q Li, X Zhu, H Yuan, ARH Walker, Z Liu, LM Peng, and CA Richter. Toward clean and crackless transfer of graphene. ACS Nano, 2011. 5(11): p. 9144-9153.

[113]. B Deng, Z Pang, S Chen, X Li, C Meng, J Li, M Liu, J Wu, Y Qi, and W. Dang. Wrinkle-Free Single-Crystal Graphene Wafer Grown on Strain-Engineered Substrates. ACS Nano, 2017. 11(12): p. 12337-12345.

[114]. JG Zhou, J Wang, CL Sun, JM Maley, R Sammynaiken, TK Sham, and WF Pong. Nano-scale chemical imaging of a single sheet of reduced graphene oxide. Journal of Materials Chemistry, 2011. 21(38): p. 14622-14630.

[115]. JA Brandes, GD Cody, D Rumble, P Haberstroh, S Wirick, and Y Gelinas. Carbon K-edge XANES spectromicroscopy of natural graphite. Carbon, 2008. 46(11): p. 1424-1434.

[116]. JS Williams, KT Short, RG Elliman, MC Ridgway, and R Goldberg. Ion-beam-induced amorphization and dynamic annealing processes in silicon. Nuclear Instruments and Methods in Physics Research Section B: Beam Interactions with Materials and Atoms, 1990. 48(1): p. 431-434.

[117]. SE Zhu, S Yuan and GCAM Janssen. Optical transmittance of multilayer graphene. EPL (Europhysics Letters), 2014. 108(1): p. 17007.

[118]. AK Geim, and IV Grigorieva. Van der Waals heterostructures. Nature, 2013. 499(7459): p. 419-425.

[119]. LA Ponomarenko, AK Geim, AA Zhukov, R Jalil, SV Morozov, KS. Novoselov, IV Grigorieva, EH Hill, VV Cheianov, and VI Fal'Ko, K. Watanabe, T Taniguchi, RV Gorbachev. Tunable metal-insulator transition in double-layer graphene heterostructures. Nature Physics, 2011. 7(12): p. 958-961.

[120]. L Britnell, RV Gorbachev, R Jalil, BD Belle, F Schedin, A Mishchenko, T Georgiou, MI Katsnelson, L. Eaves, S. Morozov, NMR Peres, J Leist, AK Geim, KS Novoselov, LA Ponomarenko. Field-effect tunneling transistor based on vertical graphene heterostructures. Science, 2012. 335(6071): p. 947-950.

[121]. SJ Haigh, A Gholinia, R Jalil, S Romani, L Britnell, DC Elias, KS Novoselov, LA Ponomarenko, AK Geim, and R Gorbachev. Cross-sectional imaging of individual layers and buried interfaces of graphene-based heterostructures and superlattices. Nature Materials, 2012. 11(9): p. 764-767.

[122]. C Dean, AF Young, L Wang, I Meric, GH Lee, K Watanabe, T Taniguchi, K Shepard, P Kim, and J Hone. Graphene based heterostructures. Solid State Communications, 2012. 152(15): p. 1275-1282.

[123]. RV Gorbachev, AK Geim, MI Katsnelson, KS Novoselov, T Tudorovskiy, IV Grigorieva, AH MacDonald, K Watanabe, and T Taniguchi. Strong Coulomb drag and broken symmetry in double-layer graphene. Nature Physics, 2012. 8(12): p. 896-901.

[124]. AJ Pollard, EW Perkins, NA Smith, A Saywell, G Goretzki, AG Phillips, SP Argent, H Sachdev, F Müller, S. Hüfner, S Gsell, M Fischer, M Schreck, J Osterwalder, T Greber, S Berner, NR Champness, PH Beton. Supramolecular assemblies formed on an epitaxial graphene superstructure. Angewandte Chemie International Edition, 2010. 49(10): p. 1794-1799.

[125]. P Zeller, S Dänhardt, S Gsell, M Schreck, and J Wintterlin. Scalable synthesis of graphene on single crystal Ir(111) films. Surface Science, 2012. 606(19): p. 1475-1480.

[126]. SK Jerng, DS Yu, JH Lee, C Kim, S Yoon, and SH Chun. Graphitic carbon growth on crystalline and amorphous oxide substrates using molecular beam epitaxy. Nanoscale Research Letters, 2011. 6(1): p. 1-6.

[127]. C Berger, Z Song, T Li, X Li, AY Ogbazghi, R Feng, Z Dai, AN Marchenkov, EH Conrad, and PN First and WA. de Heer. Ultrathin epitaxial graphite: 2D electron gas properties and a route toward graphene-based nanoelectronics. The Journal of Physical Chemistry B, 2004. 108(52): p. 19912-19916.

[128]. C Berger, Z Song, X Li, X Wu, N Brown, C Naud, D Mayou, T Li, J Hass, AN Marchenkov, EH Conrad, PN First, WA de Heer. Electronic confinement and coherence in patterned epitaxial graphene. Science, 2006. 312(5777): p. 1191-1196.

[129]. J Hass, R Feng, T Li, X Li, Z Zong, W De Heer, PN First, EH Conrad, CA Jeffrey, and C Berger. Highly ordered graphene for two dimensional electronics. Applied Physics Letters, 2006. 89(14): p. 143106-143106-3.

[130]. H Hibino, H Kageshima, F Maeda, M Nagase, Y Kobayashi, and H Yamaguchi. Microscopic thickness determination of thin graphite films formed on SiC from quantized oscillation in reflectivity of low-energy electrons. Physical Review B, 2008. 77(7): p. 075413.

[131]. A Reina, S Thiele, X Jia, S Bhaviripudi, MS Dresselhaus, JA Schaefer, and J Kong. Growth of large-area single-and bi-layer graphene by controlled carbon precipitation on polycrystalline Ni surfaces. Nano Research, 2009. 2(6): p. 509-516.

[132]. JJ Lander, HE Kern, and AL Beach. Solubility and diffusion coefficient of carbon in nickel: Reaction rates of Nickel-Carbon alloys with barium oxide. Journal of Applied Physics, 1952. 23(12): p. 1305-1309.

[133]. RY Tay, MH Griep, G Mallick, SH Tsang, RS Singh, T Tumlin, EHT Teo, and SP Karna. Growth of large single-crystalline two-dimensional boron nitride hexagons on electropolished copper. Nano letters, 2014. 14(2): p. 839-846.

[134]. RV Gorbachev, I Riaz, RR Nair, R Jalil, L Britnell, BD Belle, EW Hill, KS Novoselov, K Watanabe, T Taniguchi, AK Geim, P Blake. Hunting for monolayer boron nitride: optical and Raman signatures. Small, 2011. 7(4), 465-468.

[135]. G Veerappan, K Bojan, and SW Rhee. Sub-micrometer-sized graphite as a conducting and catalytic counter electrode for dye-sensitized solar cells. ACS Applied Materials & Interfaces, 2011. 3(3): p. 857-862.

[136]. MF El-Kady, and RB Kaner. Scalable fabrication of high-power graphene micro-supercapacitors for flexible and on-chip energy storage. Nature Communications, 2013. 4: p. 1475.

[137]. BY Lee, SM Seo, DJ Lee, M Lee, J Lee, JH Cheon, E Cho, H Lee, IY Chung, YJ Park, S Kim and S Hong. Biosensor system-on-a-chip including CMOS-based signal processing circuits and 64 carbon nanotube-based sensors for the detection of a neurotransmitter. Lab on a Chip, 2010. 10(7): p. 894-898.

[138]. SH Jo, T Chang, I Ebong, BB Bhadviya, P Mazumder, and W Lu. Nanoscale memristor device as synapse in neuromorphic systems. Nano Letters, 2010. 10(4): p. 1297-1301.

[139]. E Yoo, J Kim, E Hosono, Hs Zhou, T Kudo, and I Honma. Large reversible Li storage of graphene nanosheet families for use in rechargeable lithium ion batteries. Nano Letters, 2008. 8(8): p. 2277-2282.

[140]. J Sun, Y Chen, MK Priydarshi, Z Chen, A Bachmatiuk, Z Zou, Z Chen, X Song, Y Gao, MH Rümmeli, Y Zhang, and Z Liu. Direct chemical vapor deposition-derived graphene glasses targeting wide ranged applications. Nano Letters, 2015. 15(9): p. 5846-5854.

[141]. J Pang, RG Mendes, PS Wrobel, MD Wlodarski, HQ Ta, L Zhao, L Giebeler, B Trzebicka, T Gemming, L Fu, Z Liu, J Eckert, A Bachmatiuk, and MH Rümmeli. Self-terminating confinement approach for large-area uniform monolayer graphene directly over Si/SiO_x by chemical vapor deposition. ACS Nano, 2017. 11(2): p. 1946-1956.

[142]. DH Chua, WI Milne, D Sheeja, BK Tay, and D. Schneider. Fabrication of diamond-like amorphous carbon cantilever resonators. Journal of Vacuum Science & Technology B: Microelectronics and Nanometer Structures Processing, Measurement, and Phenomena, 2004. 22(6): p. 2680-2684.

[143]. J Kang, S Hwang, JH Kim, MH Kim, J Ryu, SJ Seo, BH Hong, MK Kim, and JB Choi. Efficient transfer of large-area graphene films onto rigid substrates by hot pressing. ACS Nano, 2012. 6(6): p. 5360-5365.

[144]. L Gao, GX Ni, Y Liu, B Liu, AHC Neto, and KP Loh. Face-to-face transfer of wafer-scale graphene films. Nature, 2014. 505(7482): p. 190-194.

[145]. AM Pagon, ED Doyle, and DG McCulloch. The microstructure and mechanical properties of TiN-Ni nanocomposite thin films. Surface and Coatings Technology, 2013. 235: p. 394-400.

[146]. BK Tay, ZW Zhao, and DHC Chua. Review of metal oxide films deposited by filtered cathodic vacuum arc technique. Materials Science and Engineering: R: Reports, 2006. 52(1): p. 1-48.

[147]. JR Shi, SP Lau, Z Sun, X Shi, BK Tay, and HS Tan. Structural and electrical properties of copper thin films prepared by filtered cathodic vacuum arc technique. Surface and Coatings Technology, 2001. 138(2): p. 250-255.

[148]. J Strömquist, L Bengtsson, M Persson, and B Hammer. The dynamics of H absorption in and adsorption on Cu (111). Surface science, 1998. 397(1): p. 382-394.

[149]. L Thomsen, J Onsgaard, PJ Godowski, P Møller, and SV Hoffmann. Adsorption of hydrogen on clean and potassium modified low index copper surfaces: Cu (100) and Cu (110). Journal of Vacuum Science & Technology A, 2001. 19(4): p. 1988-1992.

[150]. J Lahiri, T Miller, L Adamska, II Oleynik, and M Batzill. Graphene growth on Ni (111) by transformation of a surface carbide. Nano letters, 2010. 11(2): p. 518-522.

[151]. SP Lau, YH Cheng, JR Shi, P Cao, BK Tay, and X Shi. Filtered cathodic vacuum arc deposition of thin film copper. Thin Solid Films, 2001. 398: p. 539-543.

[152]. RM Jacobberger, and MS Arnold. Graphene growth dynamics on epitaxial copper thin films. Chemistry of Materials, 2013. 25(6): p. 871-877.

[153]. L Gao, L, JR Guest, and NP Guisinger. Epitaxial graphene on Cu (111). Nano letters, 2010. 10(9): p. 3512-3516.

[154]. W Schröter, V Kveder, M Seibt, H Ewe, H Hedemann, F Riedel, and A Sattler. Atomic structure and electronic states of nickel and copper silicides in silicon. Materials Science and Engineering: B, 2000. 72(2): p. 80-86.

[155]. A Cuesta, P Dhamelincourt, J Laureyns, A Martinez-Alonso, and JMD Tascón. Raman microprobe studies on carbon materials. Carbon, 1994. 32(8): p. 1523-1532.